UNIVERSITEIT•STELLENBOSCH•UNIVERSITY
jou kennisvennoot • your knowledge partner

Design of a Hexapod Mount for a Radio Telescope

by

Frank Janse van Vuuren

Thesis presented in partial fulfilment of the requirements for the degree Master of Science in Engineering (Mechatronic) at the University of Stellenbosch

Supervisor: Dr. Yoonsoo Kim
Co-supervisor: Prof. Kristiaan Schreve
Faculty of Engineering
Department of Mechanical an Mechatronic Engineering

March 2011

Departement Meganiese en Megatroniese Ingenieurswese

Department of Mechanical and Mechatronic Engineering

DECLARATION

By submitting this thesis electronically, I declare that the entirety of the work contained therein is my own, original work, that I am the owner of the copyright thereof (unless to the extent explicitly otherwise stated) and that I have not previously in its entirety or in part submitted it for obtaining any qualification.

November 2010

SUMMARY

The world's astronomy community is working together to build the largest and most sensitive radio telescope in the world namely: the SKA (Square Kilometre Array). It will consist of approximately three thousand dishes which will each require accurate positioning. The Square Kilometer Array has a testbed called the Phased Experimental Demonstrator (PED) in Observatory, Cape Town. A hexapod positioning mechanism is required to position a 3.7 m radio telescope which forms part of an array of seven radio telescopes.

This thesis details the design process of the hexapod system. The design consists of the mechanical design of the joints and linear actuators, a kinematic and dynamic model, a controller and a user interface.

In order to verify the design for the PED hexapod a scaled prototype was designed, built and tested. The hexapod's repeatability as well as ability to track a path was tested using an inclinometer. The tests confirmed the design feasibility of the PED hexapod and also highlight issues that require care when constructing the full scale hexapod, such as the amount of play in the platform joints.

The designed full scale hexapod will have an error angle less than 0.13°, a payload capacity of 45 kg, withstand wind speeds of 110 km/h and cost R160 000.

OPSOMMING

Die wêreld se sterrekundige gemeenskap is besig om saam te werk om die grootste en mees sensitiewe radioteleskoop in die wêreld te bou, naamlik: die SKA (Square *Kilometre Array*). Dit sal uit ongeveer drie duisend skottels bestaan wat elkeen akkurate posisionering benodig. Die SKA het ‘n toetssentrum, genaamd die “*Phased Experimental Demonstrator*” in Observatory, Kaapstad. ‘n Sespoot posisionering meganisme word benodig om die 3.7 m radioteleskoop te posisioneer, wat deel vorm van ‘n stelsel van sewe radioteleskope.

Hierdie tesis beskryf die proses om die sespoot stelsel te ontwerp. Die ontwerp bestaan uit die meganiese komponent van die koppelings en lineêre aktueerders, ‘n kinematiese en dinamiese model, ‘n beheerder, asook ‘n gebruikersintervlak.

‘n Geskaleerde prototipe is ontwerp, gebou en getoets om die ontwerp te verifieer. Die platform se herhaalbaarheid sowel as akkuraatheid om ‘n pad te volg was getoets met ‘n oriëntasie sensor. Die toetse het probleme uitgelig wat versigtig hanteer moet word gedurende die konstruksie van die volskaalse sespoot, veral die hoeveelheid speling in die koppelings.

Die volskaalse sespoot ontwerp het ‘n hoek fout van minder as 0.13°, ‘n ladingsvermoë van 45 kg en kan ‘n windspoed van 110 km/h weerstaan en kos R160 000.

ACKNOWLEDGMENTS

Square Kilometer Array (SKA) South Africa for funding this research.

My wife Jeanette, for her enduring support and motivation.

Dr. Yoonsoo Kim for his sound advice, patience and guidance.

Prof. Kristiaan Schreve for his support and vast mechanical experience.

The workshop staff, especially Graham Harmse, for his help, ideas and service.

Pieter Greeff for his invaluable advice.

Edward Ehlers for use of his tilt sensor and gyrometer knowledge.

Prof. C. Scheffer who kindly allowed me access to his valuable orientation measuring apparatus.

Table of Contents

Page

LIST OF FIGURES

Page

LIST OF TABLES

Page

GLOSSARY

Abbreviation	Description
AC	Alternating Current
A/D	Analogue to Digital
alt	Altitude
az	Azimuth
CAD	Computer Aided Drawing
CMM	Coordinate Measuring Machine
DC	Direct current
DOF	Degrees of Freedom
el	Elevation
I/O	Input/ Output
KAT	Karoo Array Telescope
LDDM	Laser Doppler Displacement Meter
LHS	Left Hand Side
LVDT	Linear Variable Displacement Transducer
PED	Phased Experimental Demonstrator
PWM	Pulse Width Modulation
PCB	Printed Circuit Board
RF	Radio Frequency
RHS	Right Hand Side
SKA	Square Kilometre Array
US	United States
USB	Universal Serial Bus
XDM	eXperimental Development Model

NOMENCLATURE

Variable	Description
$\boldsymbol{b}$	Alternating side length of base
$\boldsymbol{b_i}$ $(\boldsymbol{i = 1\ to\ 6})$	Vector from centre of base to joint B_i $(i = 1\ to\ 6)$
$\boldsymbol{B_i}$ $(\boldsymbol{i = 1\ to\ 6})$	Joints on the base
B(x,y,z)	Cartesian coordinate system with origin at centre of hexapod base
$\boldsymbol{d_i}$ $(\boldsymbol{i = 1\ to\ 6})$	Leg lengths
$\boldsymbol{\dot{d}_i}$ $(\boldsymbol{i = 1\ to\ 6})$	Change in the leg lengths
$\boldsymbol{\widehat{F}_i}$	Sum of applied and inertia wrenches about the centre of mass of each link *i*
$\boldsymbol{h_i}$ $(\boldsymbol{i = 1\ to\ 3})$	Height of triangle ($\overrightarrow{B_{2\iota-1}B_{2\iota}}$, $\overrightarrow{B_{2\iota}T_\iota}$, $\overrightarrow{T_\iota B_{2\iota-1}}$)
$\boldsymbol{I}$	Identity matrix
$\boldsymbol{J}$	Jacobian
$\boldsymbol{k_i}$ $(\boldsymbol{i = 1\ to\ 3})$	Distance from B_{2i} to (X_{Pi}, Y_{Pi})
$\boldsymbol{m}$	Vector from the centre of the base to the centre of the top platform
$\boldsymbol{m_t}$	Mass of platform
$\boldsymbol{m_2}$	Mass of piston
$\boldsymbol{m_1}$	Mass of cylinder
$\boldsymbol{p}$	Side length of base
$\boldsymbol{P_i}$ $(\boldsymbol{i = 1\ to\ 3})$	Distance from B_{2i-1} to (X_{Pi}, Y_{Pi})
$\boldsymbol{^B R_T}$	Rotation matrix to convert vectors from platform (*T*) coordinates to base coordinates (*B*)
$\boldsymbol{^B R_i}$	Rotation matrix to convert vectors from leg frame (*i*) to base coordinates (*B*)

$\boldsymbol{s_i}$ $(\boldsymbol{i = 1\ to\ 6})$	Unit vector along the leg d_i $(i = 1\ to\ 6)$
$\boldsymbol{t_i}$ $(\boldsymbol{i = 1\ to\ 6})$	Vector from centre of platform to joint T_i $(i = 1\ to\ 6)$
$\boldsymbol{T_i}$ $(\boldsymbol{i = 1\ to\ 6})$	Joints on the platform
T(x,y,z)	Cartesian coordinate system with origin at centre of hexapod platform
$\boldsymbol{v_p}$	Platform velocity vector
$\boldsymbol{x_p}$	A vector of the location of the platform
$\boldsymbol{(X_{Ti}, Y_{Ti}, Z_{Ti})}$ $(\boldsymbol{i = 1\ to\ 3})$	Coordinates of platform joints
$(\boldsymbol{X_{Bi}, Y_{Bi}, Z_{Bi}})$ $(\boldsymbol{i = 1\ to\ 6})$	Coordinates of base joints
$(\boldsymbol{X_{Pi}, Y_{Pi}})$	Point where h_i meets base of triangle

1 INTRODUCTION

The world astronomy community is working together to build the largest and most sensitive radio telescope in the world: the SKA (Square Kilometre Array). It is likely to consist of thousands of antennae dishes each of which has a diameter of 12 m (SKA, 2009). In total the surface area of the array should be approximately one million square metres. These dishes all require simultaneous accurate positioning. Currently the most common positioning mechanism is the elevation-azimuth (also known as el-azimuth or alt-azimuth) mount, as seen in Figure 1a. The positioning is done by two different motors, one controls the elevation (up/down) and the other the azimuth (left/right). However there is another positioning mechanism that has a number of characteristics that may make it more suitable, a hexapod mount, also known as the Stewart platform, shown below in Figure 1b.

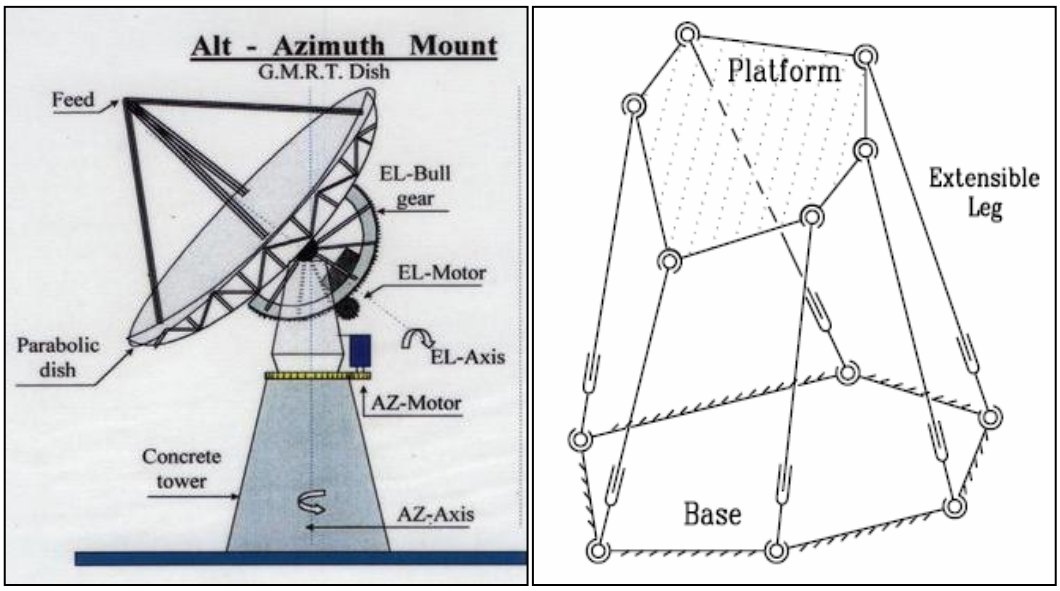

Figure 1:a) An Elevation-Azimuth Mount (Jangan, 2005), (Left).
b) Hexapod (Tsai, 1999), (Right).

The hexapod is a positioning mechanism that consists of two platforms joined by six linear drives. The base plate is stationary while the platform is moved by changing the lengths of the extendable legs.

The main advantages of this positioning mechanism are its high load carrying capacity, stiffness and precise positioning accuracy (Ulacay, 2006).

1.1 The Phased Experimental Demonstrator

A decision will be made in 2012 (SKA, 2009) as to where the telescope will be built. As part of South Africa's bid there are prototypes being built, a single

prototype dish; XDM (eXperimental Development Model), the KAT (Karoo Array Telescope) consisting of 7 dishes and the MeerKAT consisting of 80 dishes of diameter 12 m. Additionally there will be further testing and research. One such test facility is the PED (Phased Experimental Demonstrator).

South Africa and Australia[1] are the final two countries on a shortlist to site the array of telescopes.

The PED, shown in Figure 2, is used primarily as a risk reduction facility for the larger KAT project. It will be a test bed for KAT software to monitor and control the system, perform remote operations, basic scheduling as well as measurement testing.

Currently the PED consists of six steerable dishes with el-azimuth mounts (2.3 m) and one stationary dish (3.7 m). The PED is further used to train and educate students.

Figure 2: The 3.7 m antennae at the PED

1.2 Problem Statement

The main aim of this project is to

- Design a hexapod mount for the 3.7 m antenna at the PED.

In order to illustrate the feasibility of the design a scale model will be designed, built and controlled with the following characteristics. These characteristics were not defined by SKA, but submitted as a proposal at the start of the project.

[1] Both South Africa's and Australia pathfinders (MeerKAT and ASKAP) have used el-azimuth mounts. ASKAP however has a third polarization axis, enabling it to rotate the antenna about its el-axis as defined in Figure 1a). The rotation about the polarization axis eliminates beam rotation.

- Stationary positional accuracy of 0.5°.
- Dynamic accuracy of 1°.
- Load capacity of 1 kg.
- A graphical user interface that allows easy input of the hexapod's orientation.
- A control system to accurately track objects and position the hexapod.

The positioning requirements of the model were relaxed from the requirements of the full scale hexapod as this was a proof of concept with a budget of only R20 000. The proposed requirements are sufficient to track the sun and moon with a radio telescope (Knöchel, 2003).

1.3 Design Approach

Initially a mathematical model was developed in order to choose the physical parameters of the hexapod. Once these parameters were chosen the design proceeded to a range of different design fields, which were, mechanical, electrical, and programming.

Mechanical design procedure:

1. Define the requirements.
2. Generate concepts.
3. Evaluate concepts.
4. Choose concept with the highest score.
5. Perform a detailed design of the chosen concept.
6. Evaluate the model.
7. Perform a detailed design for the PED.

Electronic design procedure:

1. Determine what functionality is required.
2. Identify components able to provide the performance.
3. Design a PCB (Printed Circuit Board) with suitable capability.
4. Program the microcontroller.
5. Verify the performance.

A graphical user interface design procedure:

1. Determine the program flow.
2. Define all the functions required.
3. Program and test each function separately.
4. Add functions together in the program flow order.

Once all three of the designs were completed they could be integrated into the hexapod system. Simulations were then performed to verify the design

requirements. Once the performance of the hexapod system attains the requirements a design for the 3.7 m dish at the PED will be performed.

1.4 Motivation

A hexapod mount specifically designed for a 12 m antenna, Figure 3, proposed by (Kingsley *et al*., 1997), is stiffer, cheaper and lighter than a conventional elevation over azimuth mount.

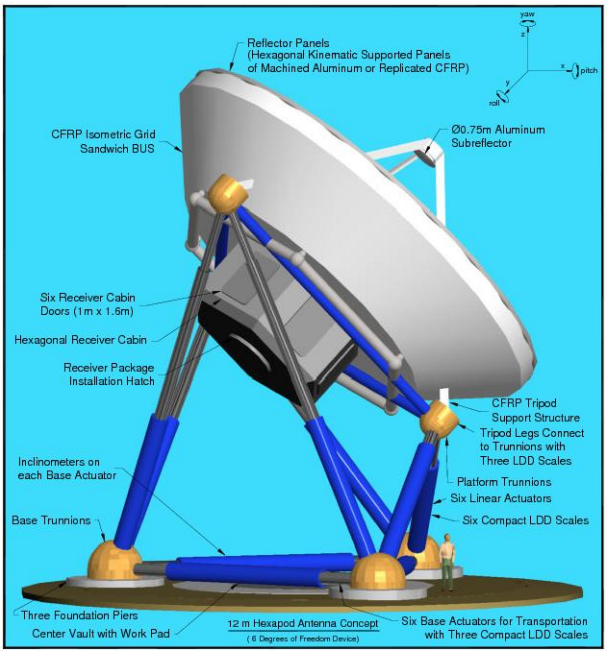

Figure 3: 12 m Hexapod Antenna (Kingsley *et al*., 1997)

The fact that the legs are always axially load is a characteristic which makes it less sensitive to external forces, such as wind, and particularly well suited for precise positioning. Additionally the platform load which is split among each of the legs is a contrast to an el-azimuth mount where the load is carried by the motor controlling the elevation.

The hexapod mount has been used successfully as a flight simulator, in precision machining, vibration absorber, tyre tester, suspension tester, dental simulator (Alemzadeh *et al*., 2007) and surgery robots. The hexapod has also been used as a positioning mechanism for many different applications including telescopes, such as the AMiBA in Hawaii, the UKIRT in Hawaii, Hexapod Telescope at the Cerro Armazones in Chile, Large Zenith Telescope in Vancouver and positions the tracker in the SALT (Southern African Large Telescope), South Africa.

Therefore the technology involved is not completely new and is not accompanied with this inherent risk. Considering all these factors, the hexapod justifies a feasibility study for application to the SKA.

2 LITERATURE STUDY

2.1 History of the Hexapod

The hexapod is also widely known as a Stewart platform, named after D. Stewart due to an article introducing the manipulator as a flight simulator (Stewart,1965). He also provided further applications for which it would be a suitable device. Stewart's paper attracted much attention and sparked further research on the hexapod. Figure 4a is the original Stewart platform as a flight simulator.

Stewart highlighted the advantages that the parallel manipulator has over normal serial manipulators when he mentions that the hexapod will be most suitable for applications where rigidity and response is of greater importance than amplitude of motion. Prior to Stewart's paper and unknown to him Dr. E. Gough built a tyre testing machine (Figure 4b) in 1954 at Dunlop Rubber Co., England.

The machine was designed to test tyres under combined loads. When this became common-knowledge many researchers referred to the hexapod mount as a Stewart-Gough platform and still do.

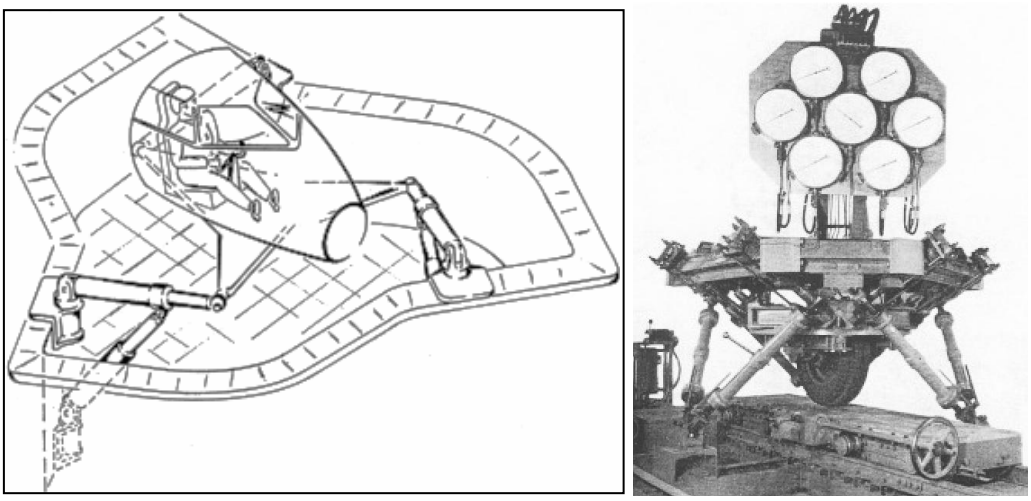

Figure 4 a): Original Stewart Platform (Stewart, 1965), left
4 b): Original Gough Platform (Bonev, 2009), right

In 2009 an additional name was added to the list of people who invented the hexapod, the American Klaus Cappel (Bonev, 2009). Cappel was granted a US patent for the motion simulator of Figure 5 in 1971, after filing it in 1964, before Stewart's paper was published and unaware of Gough's universal tyre tester.

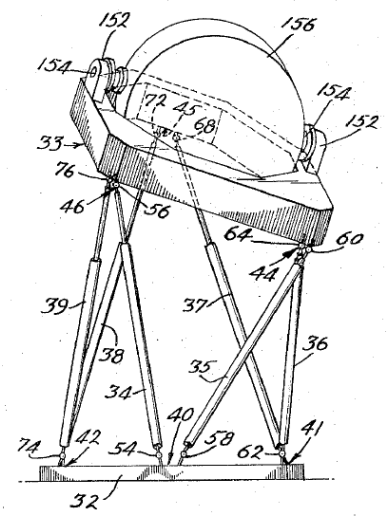

Figure 5: Cappel's 1967 Patent (Cappel, 1967)

With the hexapod's rich history in science and with three different inventors it is difficult to decide whom to credit. Although it is widely referred to as a Stewart platform, a Gough platform, or a Stewart-Gough platform, it will be referred to as a hexapod in the rest of this thesis.

2.2 Hexapod Components

There are three main mechanical components which determine the performance of a hexapod: linear drives, joints and encoders. The linear drives are the hexapod's adjustable legs, the joints connect the linear drives to the base and the platform and the encoders measure the length of the hexapod's legs.

2.2.1 Linear Drives

Linear drives (or linear actuators) which are used in the construction of hexapods are hydraulic, pneumatic or electric. The most common drives are electric drives (Tsai, 1999). Hydraulic drives are commonly used for large loads, over 2500 kg (Koekebakker, 2001) and pneumatic drives when speed is important and the load is small.

Hydraulic and pneumatic drives each have a major drawback: hydraulic drives have the possibility of leaking oil, while pneumatic drives are difficult to control under load, since air is compressible a pneumatic drive's length will vary with its load.

Electric linear drives are also referred to as screw jacks or jack screws. There are two main types of electric linear drives, using either a lead screw or a ball screw. The lead screw operation is similar to a nut being twisted on a bolt to gain linear displacement. A ball screw works in a similar fashion, but contains ball bearings

which move along the threaded shaft, making it much more efficient. Although a ball screw is efficient, it is more expensive and bulky since it needs to re-circulate the ball bearings. Advantages of the lead screw are that it is cheap, more compact as well as usually being self-locking.

Another type of linear drive which is not commonly used in hexapods, but which have some desirable characteristics is a linear motor. Linear motors are electric linear drives which produce linear motion directly, instead of converting rotational to translational movement. The disadvantage of these motors is that they are only able to provide a small force.

A much more innovative concept and an alternative to rigid links is to suspend the hexapod's platform from wires, which are varied in length. This allows a light and fast robot. The control however is made more difficult as the wires must all be kept under tension (Merlet, 2002).

For low force precision applications piezoelectric motors have been used.

Current linear drives used at the PED on the el-azimuth mounts are electric drives with lead screws.

2.2.2 Joints

There are a number of joints that are available and have been used in the construction of a hexapod. Universal and ball joints are the two most common joints used. Universal joints are able to reach a larger angular range than ball joints. Both joints have a range of uses in other industries and can be purchased as standard components.

Standard ball joints rarely offer more than 20° of movement about their axis, as shown in Figure 6. The ball joint of Figure 6 has a small range of motion, but rotates about a single point and is a small, cheap, compact design.

Figure 6: Standard Ball-Joint Range of Motion

Figure 7 illustrates the universal joint's large angular range. Unfortunately the two rotation axes do not intersect, the universal joint if used would thus modelled as

three components which rotate about two axes. This model would be simpler if the rotation axes intersected.

Figure 7: Standard Universal Joint Range of Motion

There is a simple mechanical solution to produce a ball joint with a large range, while mainly using standard components. By adding a small bush to the inner diameter of a plain spherical bearing, which is basically a ball joint, a smaller diameter shaft can be mounted in the bush, to allow a greater range of movement, illustrated in Figure 8.

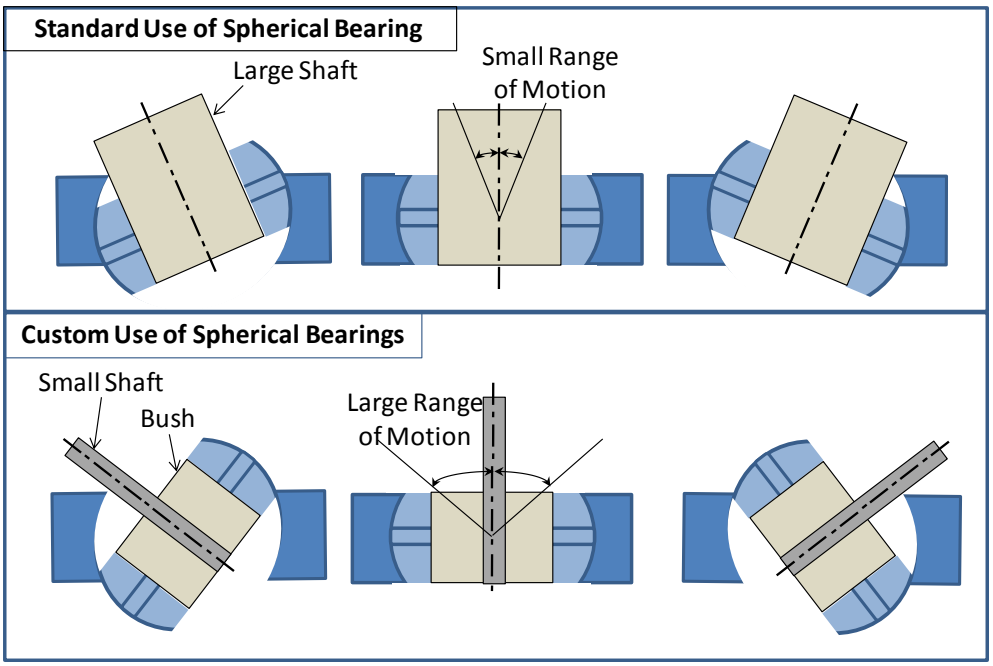

Figure 8: Custom Ball-Joint with Large Range of Motion

Unique ball-joints have also been developed which have the ball screw encased in the ball of the joint. These joints are known as SphereDrive™ and offer a very compact design.

When small scale hexapods are constructed, it is common to use flexure joints. These joints have many advantages since they are compact, have no backlash or

friction and do not require lubrication. Unfortunately they have a limited range of motion since they need to remain out of the plastic deformation range (Ulacay, 2006). These factors generally make them suitable for hexapods with small workspaces and very small payloads.

For some hexapod layouts two legs meet at a single point and require a special type of joint referred to as a 2-1 joint. Since there are very few applications that require such joints, custom joints often need to be manufactured. Two different joints have been found in literature, a custom modified universal joint (Fichter, 1986), as well as range of split ball joints (Youssef & El-Hofy, 2008), which are either solely mechanical or incorporate magnets in their design. The split ball joints were developed by Geodetic Technology International, specifically for machining hexapods. Split ball joints which are also known as bifurcation ball joints, are expensive and difficult to source.

2.2.3 Encoders

Encoders are required to measure the leg lengths. There are two main types of encoders; relative encoders and absolute encoders. Absolute encoders only require an initial calibration after installation and can then immediately measure the required length while relative encoders require calibration prior to every use.

Absolute encoders include LVDT (Linear Variable Displacement Transducer), produced by Macrosensors, LDDMs (Laser Doppler Displacement Meters) produced by Optodyne and optical systems produced by Renishaw. These absolute encoders are very accurate but expensive systems.

Rotary encoders measure the amount of rotation of a shaft. Most rotary encoders are relative encoders; however Fanuc produces relative encoders which act as absolute encoders as they have a battery which keeps count of the number of encoder increments.

The most widely used and most cost effective rotary encoders, which are relative encoders, are optical encoders and potentiometers. While potentiometers measure rotation through resistance variation, optical encoders make use of a light source and a photo detector. An encoder disk has either markings or holes which are detected by the photo detector to measure the rotational motion.

2.3 Hexapod Characteristics

A common robot classification scheme is whether its kinematic structure forms an open-loop or a closed-loop. Common robot arms are an example of an open-loop kinematic structure and are referred to as serial manipulators. A hexapod has a closed-loop kinematic structure and is thus known as a parallel manipulator. If a

mechanism contains both an open and a closed-loop structure it is then defined as a hybrid manipulator.

Table 1 lists the characteristics of a parallel manipulator and is a summary of the points raised in (Tsai,1999) and (Liu *et al*., 1994).

Table 1: Characteristics of a Parallel Manipulator

Advantages	Disadvantages
• The load is shared between the drives, giving them a large load carrying capacity • High stiffness • Low inertia • Drive position errors are not additive	• Small workspace • Difficult direct kinematics

2.3.1 Forward Kinematics of a Hexapod

The forward kinematic problem can be described as follows: *given the leg lengths, find the corresponding position and orientation of the platform.* The forward kinematics is also referred to as the direct kinematics.

Many different mathematical representations of the forward kinematic problem have been suggested, but they are similar in that they end up with three non-linear equations with three unknowns which are solved iteratively. These equations have up to 40 possible solutions. Once these unknowns have been determined, they are used to explicitly solve the rest of the parameters required to fully describe the layout of the hexapod.

The representation in (Zhang & Song, 1994), requires the simultaneous solution of three fourth order equations. Equation variables to be determined are the three values of the rotation matrix. The orthogonal conditions which a rotation matrix must satisfy are used to determine the remaining six inputs of the rotation matrix, which is then used to determine the orientation of the hexapod.

An alternative representation in (Ku, 2000), specifically for a 6-3 hexapod (a special hexapod configuration which simplifies the kinematics; a more detailed explanation is given in section 3.1), provides three highly non-linear equations with trigonometric functions that need to be solved to calculate the inclination angles. The inclination angles are then used to determine the explicit orientation of the hexapod.

A further representation in (Liu *et al*., 1994) also specifically for a 6-3 hexapod, provides non-linear equations which require you to solve for the x-coordinate of the platform. The rest of the coordinates are then determined explicitly.

Since these equations are non-linear, with the same number of equations as unknowns, they all need to be solved with the use of a solver. Solvers are particularly sensitive to the starting points of non-linear equations and therefore if one is able to provide reasonably accurate starting points for the solver, this will greatly improve the probability of achieving quick convergence to the desired solution.

Considering all of these factors, the method by (Liu *et al*., 1994) was used. It is much more cumbersome to calculate the initial conditions for the inclination angles or the variables of the rotation matrix than the x-coordinates of the platform. In addition, since the x-coordinates are known for a specific orientation, excellent starting values can be provided to the solver. In this way, one can speed up the convergence and virtually guarantee obtaining the desired solution.

2.3.2 Inverse Kinematics of a Hexapod

The inverse kinematic problem can be described as follows: *given the position and orientation of the platform find the corresponding leg lengths.* This is a simple problem for parallel manipulators such as the hexapod, although it is difficult for serial manipulators.

2.3.3 Dynamic Model of a Hexapod

The dynamic equations of the hexapod are required to determine the forces in the legs due to the platform load, orientation and acceleration. Once the performance requirements of a hexapod have been determined, dynamic simulations can be performed in order to aid in the selection of linear drives, and joints. Accurate dynamic modelling is crucial for the control of hexapods with high loads and acceleration where precision control is required.

The dynamic equations are complicated by the existence of numerous closed-loop chains as well as kinematic constraints. Various modelling methods have been proposed, such as the Newton Euler formulation, the Lagrangian formulation, the principle of virtual work and Kane's method (Guo & Li, 2006).

The Newton Euler formulation requires the computation of all the constraint forces and moments at all joints, which is unnecessary. This requires a great number of equations and leads to poor computational efficiency.

Although the Lagrangian formulation eliminates the unwanted reaction forces, deriving explicit equations of motion is made tedious due to the numerous

constraints imposed by the closed loops. Lagrangian multipliers as well as additional coordinates are often introduced.

Kane's Method is widely used in robotic systems. The principle characteristics which Kane's method has are that it automatically eliminates unwanted reaction forces from the beginning. Additionally Kane's method allows the use of motion variables which can be any linear combination of their time derivatives. These two qualities of Kane's method allow easy formulation and result in simple equations (Kurfess, 2000).

The characteristics which make Kane's method attractive are similar to those of the principle of virtual work. Dynamic models of hexapods using both these methods were obtained.

A detailed dynamic model using the principle of virtual work was presented by (Tsai, 1999), accompanied with numerical values and simulation results. While a dynamic model using Kane's method is presented by (Koekebakker, 2001), comparison of the equations which needed to be solved, showed no obvious computational advantage for Kane's method. Since the model presented by Tsai has numerical values and simulation results which can be used to verify the dynamic model, it was selected.

2.3.4 Singularities

Singularities are important for both parallel and serial manipulators. At a singular position a serial manipulator loses one or more degrees of freedom and a parallel manipulator gains one or more degrees of freedom.

Singularities are determined by the Jacobian matrix of the kinematics. When the determinant of the Jacobian matrix is zero it indicates a singular position. A slider crank mechanism in Figure 9 is used to illustrate singularities. Since it is a hybrid mechanism it can illustrate the two types of singularities. Figure 9(a) shows the rotational mechanism which rotates about its joints causing the slider to move along the track.

Once the slider moves to the extreme left of the track, Figure 9 (b), and lines up with the other leg, it is able to rotate freely. It no longer has a single possible position, but an array of positions, all located along the circle. In other words, a degree of freedom has been gained.

Once the slider moves back to the extreme right of the track and the two linkages line up, a displacement of the slider is impossible, and the mechanism is stuck Figure 9 (c). Clearly a degree of freedom has been lost.

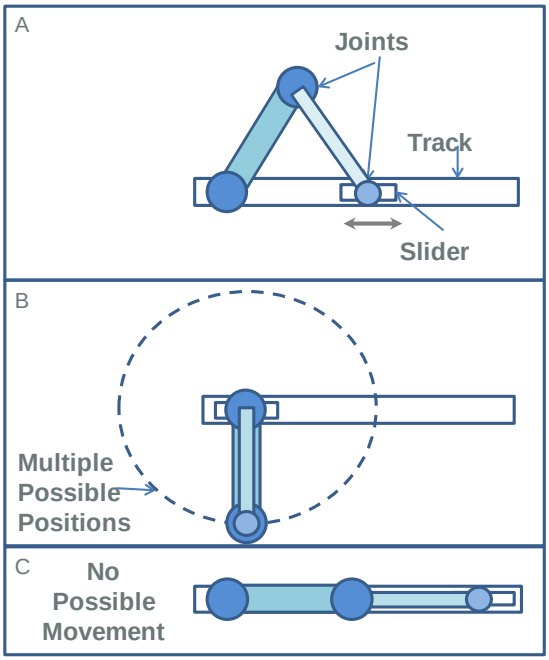

Figure 9: (a) Slider Crank Mechanism; (b) One Degree of Freedom Gained; (c) One Degree of Freedom Lost

2.4 Path Planning

Astronomical objects cross the sky following known paths. In order to track these objects path planning is of great importance.

Unfortunately path planning is complicated due to singularities, which might occur on the path to be tracked. Large forces are required in the legs when a hexapod approaches a singular point. In fact, the forces required to change leg lengths increases significantly as a singular point is approached.

It is thus undesirable to bring the hexapod even close to singular positions, as the large leg forces are undesirable and may cause damage to the hexapod. Although the determinant provides the criterion to determine a singularity, a better measure of ill-conditioning is provided by the condition number (Dasgupta & Mruthyunjaya,1998). For this reason, instead of simply checking the determinant of the Jacobian the condition number is used as this is a much better measurement of the hexapod stability (Chen & Liao, 2008).

When hexapods are used in machining, the path planning of hexapods is about contour planning (Pugazenthi *et al*., 2002). For a telescope the pointing direction is of greater importance than the three dimensional position of the hexapod. Although there are many articles on the calibration of hexapods for telescope applications, no articles have been found on path planning with a telescope, focusing on the pointing direction.

Tracking a physical path is a common problem that has been addressed in literature. However the resolution of encoders (which measure the lengths of the linear drives) has never been taken into account before during this tracking motion. Two different tracking methods were developed by (Nguyen & Antrazi, 1990). One method is used for straight lines in 3D space and the other for curved paths. Specific velocity profiles of the hexapod were also taken into account therein. However, neither of these methods considers singularities or the resolution of encoders which causes the system to be discrete.

The effect of the resolution of the encoders, as well as path planning specifically for a telescope are both issues that will receive some further attention in this thesis.

2.5 Calibration

Calibration is vital for any computer controlled device. Although mathematical modelling is essential, physical systems differ due to manufacturing and assembly errors. These errors are compensated for by calibration. There are two main types of calibration: external calibration and self calibration.

External calibration makes use of independent metrology equipment such as CMM (coordinate measuring machines). However this metrology equipment is very expensive. Further disadvantages are that it is time-consuming, usually small in size, and difficult to ensure accurate measurement.

Self-calibration techniques make use of closed-loop kinematic chains and are therefore well suited to parallel manipulators such as the hexapod. Self-calibration methods can be classified into two categories, the redundant sensor approach (more sensors than DOF) and the mobility constraint approach (constraining DOF) (Chiu & Peng, 2003).

Redundant sensors which have been used for self-calibration include: a ball-bar length measuring device and an inclinometer. The ball-bar device was used as an extra leg by (Patel & Ehmannn, 2000). A very similar method has also been used by (Chiu & Peng, 2004), but with an alternative error modelling approach. An inclinometer with high repeatability has been proposed in (Ren & Su, 2009).

While employing the mobility constraint approach to self-calibration, external mechanical fixtures which impose motion constraints have been used. Unfortunately this presents a challenge in terms of interfacing with an existing machine. Keeping a single leg length fixed, while altering the remaining five legs of the hexapod was suggested by (Zhuang & Roth, 1993), this method will be suitable for all hexapods.

(Zhuang *et al*., 1998) propose an external calibration method, with a model containing 42 error parameters. Three points are measured on the base and platform for 20 different orientations; this is followed by minimization to determine the error parameters. Although the other methods are able to improve the error of the hexapod with cheaper measuring equipment, this method is the only one that is able to determine all 42 error parameters.

It should be noted that before determining the error parameters of a hexapod, repeatability should be tested first, since error parameters of a hexapod that is not repeatable are useless. Aspects which may lead to a hexapod with bad repeatability are: play in joints, play in linear drives, loose joints, loose connections as well as faulty encoders and programming. Only once a hexapod is deemed repeatable can its error parameters be determined and the calibration process completed. Some errors might have a random nature. In this case, those errors could be modelled as a bias plus Gaussian noise.

2.6 Focus and Contributions of this Thesis

The focus of this thesis was the design and testing of a complete hexapod system, which included the hexapod, a controller and a computer interface.

The components designed for the hexapod were the linear drives, base joints and platform joints. The platform joints were similar to a previous hexapod design, but the base joints employed an original way of using a spherical bearing to produce a ball joint.

The dynamics were modelled in Matlab and used to determine the force requirements of the linear drives.

The forward kinematic equations are required to calculate the position and orientation of the platform for given leg lengths and were solved in Matlab.

Using the forward and inverse kinematic equations a basic path planning algorithm was implemented which avoided singularities.

A controller PCB with a microcontroller interfaces with a computer to control the hexapod, by recording the change in leg lengths through the encoders. Once coarsely calibrated the desired orientation of the hexapod can be entered. The hexapod then moves to the desired orientation while avoiding singularities.

In order to test the accuracy of the hexapod tests were performed using an orientation sensor.

It is hoped that this thesis will enable a designer to understand the major issues which must be taken into account when designing a hexapod for a radio telescope.

3 MODELLING THE HEXAPOD

Before modelling the hexapod, the layout that was used in the project was chosen, since many of the models only apply to certain layouts. Once the layout was determined, kinematic and dynamic models were developed.

3.1 Hexapod Layout Evaluations

Although the hexapod mount's design is fixed by definition (six legs connecting the base and platform), there are a few variations in the number of joints. Two extendable legs can share a single joint at the base or at the platform. Allowing two legs to meet at a single point simplifies the kinematic equations of the system by decreasing the number of variables which need to be solved.

A numbering scheme has been developed to represent the various hexapod layouts. The first number refers to the number of points at which the legs are connected to the base, while the second number refers to the number of points at which the legs are connected to the platform. A general hexapod known as a 6-6 hexapod is seen on the left of Figure 10. In the centre a 6-3 hexapod is shown which has six joints at the base and three at the platform. The hexapod on the far right is therefore labelled a 3-3 hexapod.

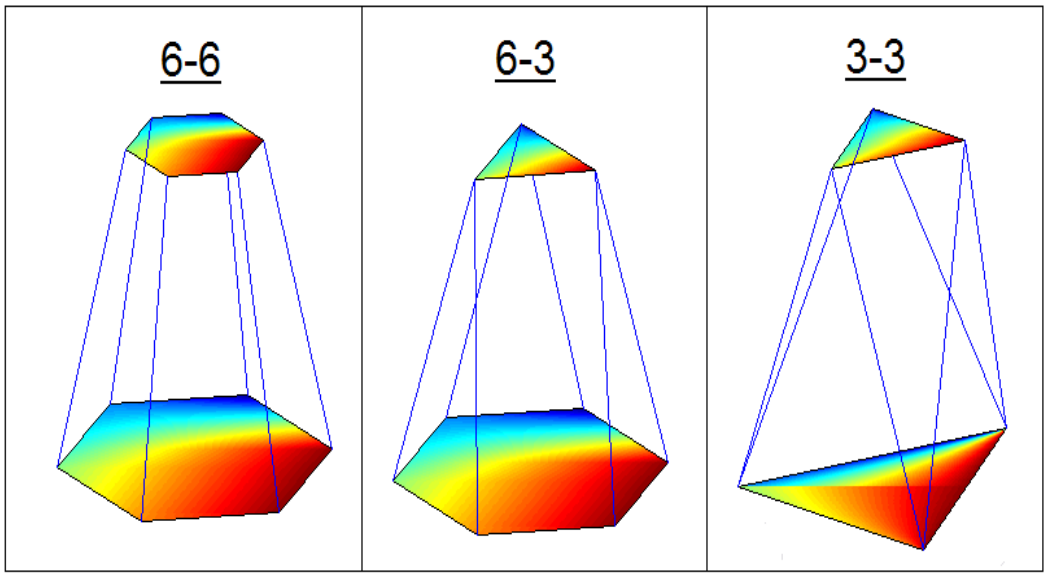

Figure 10: Various Possible Layouts

A brief overview of the characteristics of each of the three layouts is presented in the following sections and the various layouts are evaluated.

3.1.1 The 6-6 Hexapod

Advantages

1. It is the cheapest layout to construct since standard ball joints or universal joints are used to connect the legs to the base and platform.
2. A small change in leg length causes a large change in the orientation of the hexapod, since the legs are more perpendicular to the platform than for other layouts. This means a greater viewing angle can be attained while using the same linear drives in comparison to the other layouts.

Disadvantages

1. Solving the forward kinematic equations is a challenge, since there are up to 40 solutions.

Telescopes with 6-6 Configuration

- AMiBA radio telescope, Hawaii.
- Hexapod Telescope at the Cerro Armazones, Chile.

3.1.2 The 6-3 Hexapod

Advantages

1. Since the legs meet at only three points on the platform, this simplifies the kinematic equations as there are fewer variables which must be solved.
2. As it only has three joints which connect to the platform, this decreases the mass of the platform and allows faster movement and acceleration than the 6-6 hexapod.
3. Since there are only three joints on the platform, there are fewer joints which experience friction.

Disadvantages

1. Three 2-1 joints are required for the construction; a small amount of custom manufacturing is therefore required which increases its cost.

Telescopes with 6-3 Configuration

- SALT, as part of the tracker system, South Africa.

3.1.3 The 3-3 Hexapod

Advantages

1. Since it only has three joints which connect to the platform, this decreases the mass of the platform and allows faster movement and acceleration than the 6-6 hexapod.
2. This is the only form of the hexapod for which the kinematic equations have a closed form solution. Iterations are therefore not required to solve the equations, making the control and positioning considerably easier.
3. As there are only three joints which connect to the platform, there are fewer joints which experience friction.

Disadvantages

1. Since all the joints are 2-1 joints, the high number of custom joints required will make this layout more expensive than the other mounts.
2. A large change in leg length is required to change the orientation of the hexapod in comparison with the other layouts. This is of significant consequence for a telescope positioning device, as a smaller viewing angle is covered while using the same drives.

Telescopes with 3-3 Configuration

- UKIRT telescope, Hawaii.
- Large Zenith Telescope, Vancouver.
- This is also the design proposed by (Kingsley *et al*., 1997) for the SKA shown in Figure 3.

3.1.4 Evaluation Results

The aforementioned three different design alternatives were evaluated by the tabular additive method of (Blanchard *et al*., 2006). This is the evaluation method used throughout the thesis. Once the criteria were defined, a weighting was assigned to each through use of the two pair forced decision method. Thereafter, each design alternative was scored on how well it satisfies the criteria. The scores vary between zero and ten, with ten being the best. The weightings were multiplied by the scores and added for each alternative. The component with the highest total was selected. Evaluation of the three different hexapod design alternatives yields the results presented in Table 2, with the motivation discussed thereafter.

Table 2: Layout Comparison

Characteristic	Weighting	6-6	6-3	3-3
Cost effective construction	0.4	10 (High)	5 (Medium)	0 (Low)
Ease of solving forward kinematic equations	0.2	0 (Low)	10 (High)	10 (High)
Leg actuation to adjustment ratio	0.1	10 (High)	5 (Medium)	0 (Low)
Stiffness	0.3	0 (Low)	5 (Medium)	10 (High)
Total	1	**5**	**6**	**5**

Cost effective construction: It is assumed that the cost of a 2-1 joint is more than a 1-1 joint, since 1-1 joints can be purchased as standard components or manufactured at a lower cost.

Ease of solving forward kinematic equations: The forward kinematic equations of a 6-6 hexapod have up to 40 solutions. Although both the 6-6 and the 6-3 kinematic equations are solved iteratively, the 6-3 kinematic model was found to be much less sensitive to the starting values of the iterations, and could be solved much faster. Although the 3-3 layout has a closed form solution, the 6-3 layout could be solved almost instantaneously motivating their ratings to be equal.

Leg actuation to adjustment ratio: This refers to the amount of degrees a hexapod's orientation will change for the same percentage change in leg lengths. A 3-3 hexapod has the legs at a very low angle to the platform. While a 6-6 hexapod can have its legs completely perpendicular to the base and the platform, which will allow the greatest change in angle.

Stiffness: This refers to the amount of displacement the hexapod will experience as a result of external forces.

From Table 2 it is seen that the highest score is obtained for the 6-3 hexapod layout. The 6-3 hexapod is a fine balance of cost and performance and should be able to attain a suitable range of motion while remaining stiff enough so that wind does not have a major impact on its performance. Consequently, this design is chosen as the focus of this study.

3.2 Inverse Kinematic Model

Figure 11 shows a 6-3 hexapod with the base and platform connected by legs at spherical joints B_i on the base and T_i on the top platform, where $i = 1$ to 6. A Cartesian coordinate system is used with the origin $B(x,y,z)$ located at the centre of the base.

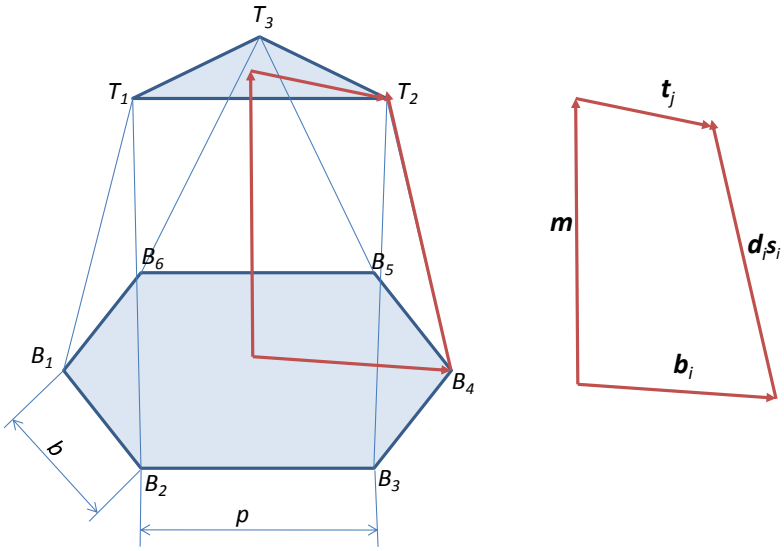

Figure 11: Hexapod Layout with Vector Loop

Taking a vector loop as shown on the right of Figure 11 gives the following:

$$d_i s_i = m + t_j - b_i \quad \text{for } i = 1,2,\ldots 6 \text{ and } j = \lceil i/2 \rceil. \tag{3-1}$$

The length of the legs can be calculated by taking the dot product of the vector $d_i s_i$ with itself,

$$d_i^2 (s_i \cdot s_i) = \left[m + t_j - b_i\right]^T \left[m + t_j - b_i\right] \quad for\ i = 1,2,\ldots 6\ and\ j = \lceil i/2 \rceil. \tag{3-2}$$

Since s_i is a unit vector, the dot product with itself is one. Given that the rest of the vectors are known, this is a simple calculation:

$$d_i = \sqrt{\left[m + t_j - b_i\right]^T \left[m + t_j - b_i\right]} \quad for\ i = 1,2,\ldots 6\ and\ j = \lceil i/2 \rceil. \tag{3-3}$$

Equation (3-3) is the inverse kinematic equation of the hexapod.

3.3 Forward Kinematic Model

In addition to the inverse kinematic equations, it is clearly necessary to describe the forward kinematic equations since the solution of the forward kinematics is useful for calibration and control purposes, because it is easier to measure the lengths of the linear drives than the position and orientation of the platform.

3.3.1 Modelling Parameters

Although the spacing of the hexapod legs is typically symmetrical, the legs are not necessarily equi-spaced on the base. This is illustrated in Figure 12 and taken into consideration in the kinematic model, to allow various design options. Further variables that are used to derive the forward kinematic equations are presented in Figure 13.

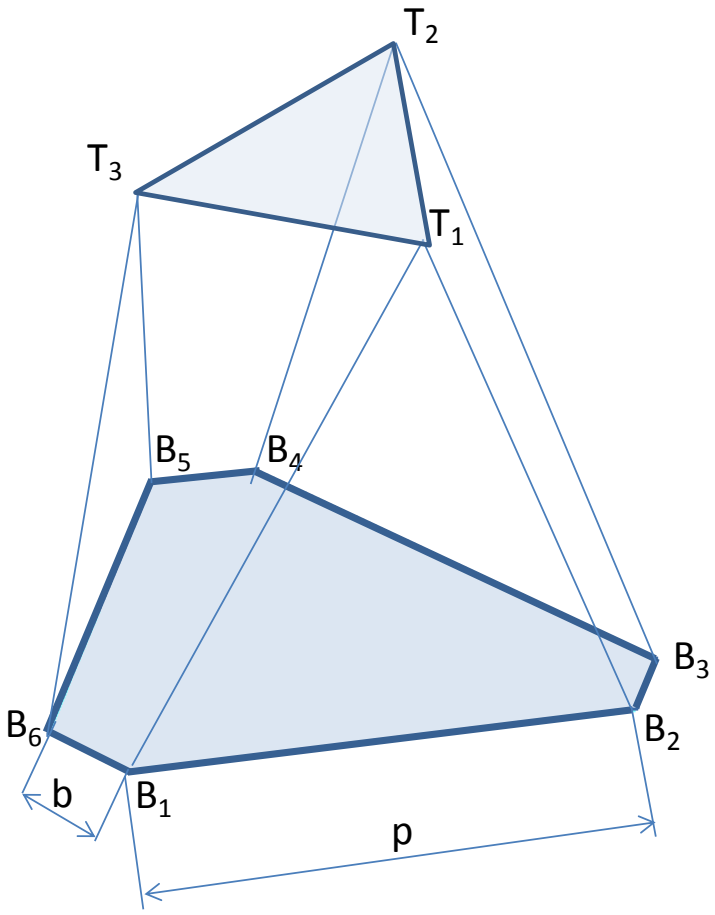

Figure 12: Base with Two Different Side Lengths

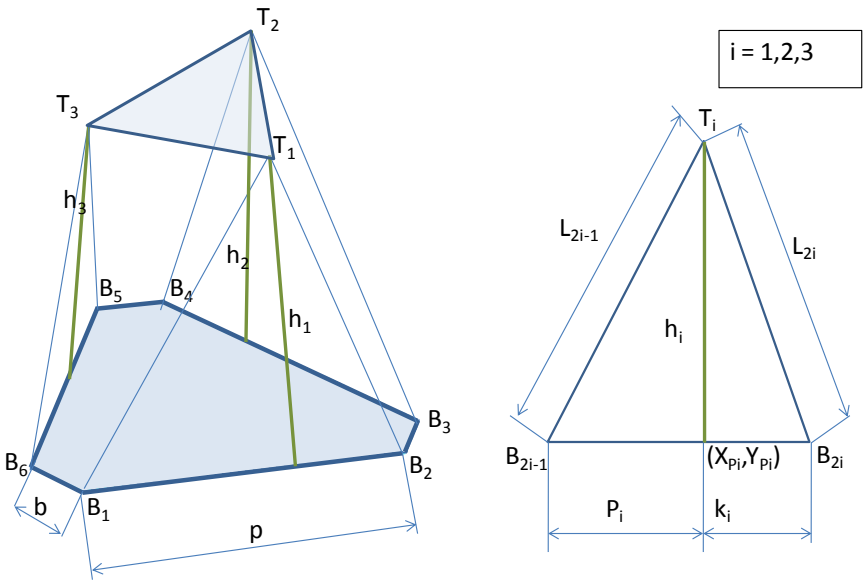

Figure 13: Hexapod Coordinates

From Figure 14 it can be seen that although the sides of the base vary, the platform's sides have a fixed length a.

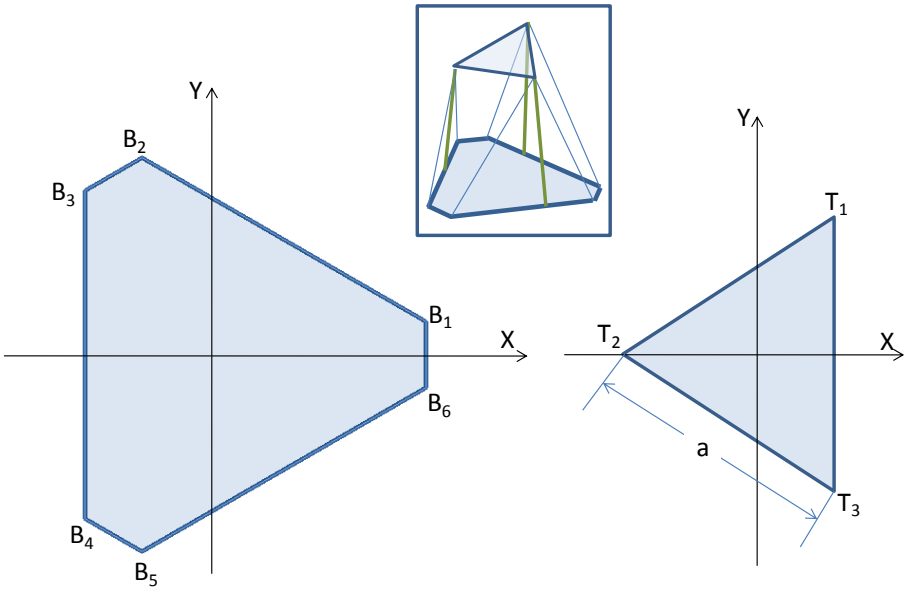

Figure 14: Hexapod Parameters

This is the distance between the corners of the platform and can be expressed as:

$$|T_1 - T_2| = |T_2 - T_3| = |T_3 - T_1| = a. \quad \textbf{(3-4)}$$

Substituting the platform coordinates into the first constraint, $|T_1 - T_2| = a$, yields:

$$\sqrt{(X_{T1}-X_{T2})^2+(Y_{T1}-Y_{T2})^2+(Z_{T1}-Z_{T2})^2}=a. \quad \textbf{(3-5)}$$

Equations which are derived due to the geometry of the hexapod are then substituted into (3-5). The resulting equation is shown below and its proof shown in Appendix A:

$$\begin{aligned} &a^2+2X_{T1}X_{T2}-2X_{T1}\left(X_{P1}+\sqrt{3}(Y_{P1}-Y_{P2})\right)-2X_{P2}X_{T2}\\ &-((\sqrt{3}X_{P1}-Y_{P1}+Y_{P2})^2+(h_1^2+h_2^2)-4X_{P1}^2-X_{P2}^2)\\ &+2\sqrt{(h_1^2-4(X_{T1}-X_{P1})^2)(h_2^2-(X_{T2}-X_{P2})^2)}=0. \end{aligned} \quad \textbf{(3-6)}$$

In a similar fashion, the following two equations are also derived:

$$\begin{aligned} &a^2-4X_{T1}X_{T3}-2X_{T1}\left(X_{P1}+3X_{P3}+\sqrt{3}(Y_{P1}-Y_{P2})\right)\\ &-2X_{T3}\left(-3X_{P1}+X_{P3}+\sqrt{3}(Y_{P1}-Y_{P3}\right)\\ &-(\left(\sqrt{3}(X_{P1}+X_{P3}\right)-Y_{P1}+Y_{P3})^2+\ (h_1^2+h_3^2)-4X_{P1}^2-4X_{P3}^2)\\ &+2\sqrt{(h_1^2-4(X_{T1}-X_{P1})^2)(h_3^2-4(X_{T3}-X_{P3})^2)}=0, \end{aligned} \quad \textbf{(3-7)}$$

and

$$\begin{aligned} &a^2+2X_{T2}X_{T3}-2X_{T3}\left(X_{P3}+\sqrt{3}(Y_{P2}-Y_{P3})\right)-2X_{P2}X_{T2}\\ &-((\sqrt{3}X_{P3}-Y_{P2}+Y_{P3})^2+(h_2^2+h_3^2)-X_{P2}^2-4X_{P3}^2)\\ &+2\sqrt{(h_2^2-(X_{T2}-X_{P2})^2)(h_3^2-(X_{T3}-X_{P3})^2)}=0. \end{aligned} \quad \textbf{(3-8)}$$

The previous three equations have only three unknowns: X_{T1}, X_{T2} and X_{T3}. Solving these equations is the key step in solving the forward kinematic equations. Simultaneously solving the equations is complicated. Since they are highly non-linear and cannot be explicitly solved, a numerical method is required to obtain a solution.

Once equations (3-6), (3-7) and (3-8) are solved, they are used to obtain the platform's y and z coordinates. The platform's position and orientation is then completely described and the solution of the forward kinematic equations is complete.

3.3.2 Numerical Solution of the Forward Kinematic Equations

There are numerous solvers available which employ numerical methods to solve the derived equations (3-6), (3-7) and (3-8). Although Matlab was used, the solver toolbox was not incorporated due to expensive licensing fees. Instead, open source solvers were sourced from the Matlab user's website.

A numerical method employed in one such open-source solver is a Fletcher version of the Levenberg-Marquardt algorithm for minimization of the sum of squares of equation residuals developed by (Balda, 2007). Another numerical method used is the modification of Newton's Method developed in (Hanselman, 2006). Both of these solvers have adjustable parameters, such as the function tolerance and the maximum number of iterations.

The function tolerance (or convergence error) indicates how close the final answer is to the exact answer before the solver stops performing iterations. If the exact answer has been obtained the function is therefore equal to zero.

Starting values required by the solvers are the platform's *x*-coordinates. These can readily be determined and this was the motivation for using the kinematic model developed by (Liu *et al*., 1994), see section 2.3.1.

A numerical example of a hexapod's forward kinematic equations was obtained from (Liu *et al*., 1994) and used to verify the solvers. A three dimensional plot of the hexapods coordinates was illustrated to further verify and visualize the parameters.

The function tolerance parameter was set equal for both solvers to ensure fair evaluation thereof. The two open-source solvers were evaluated against each other and further verification was done by using Microsoft Excel's Solver add-in. The three equations (3-6), (3-7) and (3-8) were entered into the solvers along with starting values. Once the three solvers (the two Matlab solvers and Microsoft Excel's Solver add-in) had converged to solutions, the answers were verified as correct by comparison to the numerical example.

Evaluation criteria for the solvers were defined as the rate at which the solvers converge, as well as the sensitivity to the starting points. Both of the solvers converged at approximately the same rate (0.01s for a function tolerance of 1×10^{-7}). The Levenberg-Marquardt algorithm was found to be less sensitive to the starting values, converging to the desired answer for a broader range of starting points. It was therefore decided to use Balda's Levenberg-Marquadt solver.

3.3.3 Converting Pointing Direction to Position and Orientation

Once a radio telescope is mounted on the hexapod it needs to be pointed in a specific direction in order to observe celestial objects. The ability to adjust the pointing direction accurately is therefore the primary goal of the hexapod.

Once a hexapod is pointing in a specific direction, the same pointing direction can be obtained by rotating the top platform about the pointing direction as shown in Figure 15.

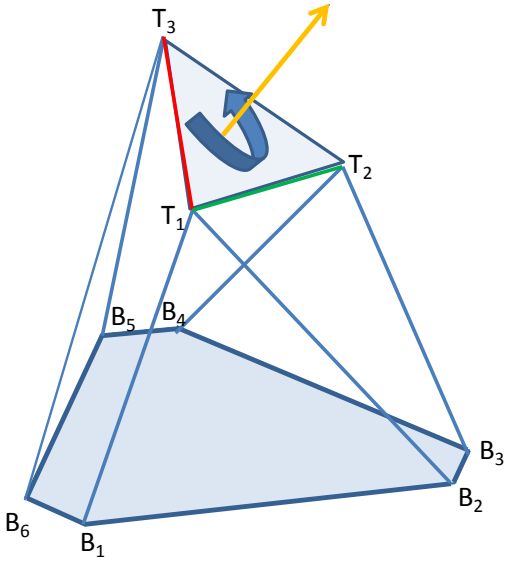

Figure 15: Movement Which Does Not Alter Pointing Direction

The same pointing direction can also be achieved at different heights of the hexapod. Therefore multiple hexapod configurations exist which point the telescope in the same direction. A system is required to select which of these multiple possible positions to use. Previously, this problem has been addressed in ADS INT. S.R.L. (2001). The proposed solution is to:

- Keep the height of the centre of the top platform constant and rotate it about its centre point.

The challenge is to determine how the platform will be rotated. An additional concern will be to ensure that the legs do not collide, or become twisted. Both these problems are elegantly solved by the definition of the rotation matrix. A 3-2-3 rotation matrix was chosen as this enables the rotations to be expressed directly in terms of elevation and azimuth angles (illustrated in Figure 16), which is very convenient. The rotation matrix is defined as:

$$R = \begin{bmatrix} \cos(\psi)\cos(\theta)\cos(\phi) - \sin(\psi)\sin(\phi) & \cos(\psi)\cos(\theta)\sin(\phi) + \sin(\psi)\cos(\phi) & -\cos(\psi)\sin(\theta) \\ -\sin(\psi)\cos(\theta)\cos(\phi) - \cos(\psi)\sin(\phi) & -\sin(\psi)\cos(\theta)\sin(\phi) + \cos(\psi)\cos(\phi) & \sin(\psi)\sin(\theta) \\ \sin(\theta)\cos(\phi) & \sin(\theta)\sin(\phi) & \cos(\theta) \end{bmatrix} \quad \textbf{(3-9)}$$

where φ is the azimuth angle,

θ is the elevation angle and

ψ is the negative of φ.

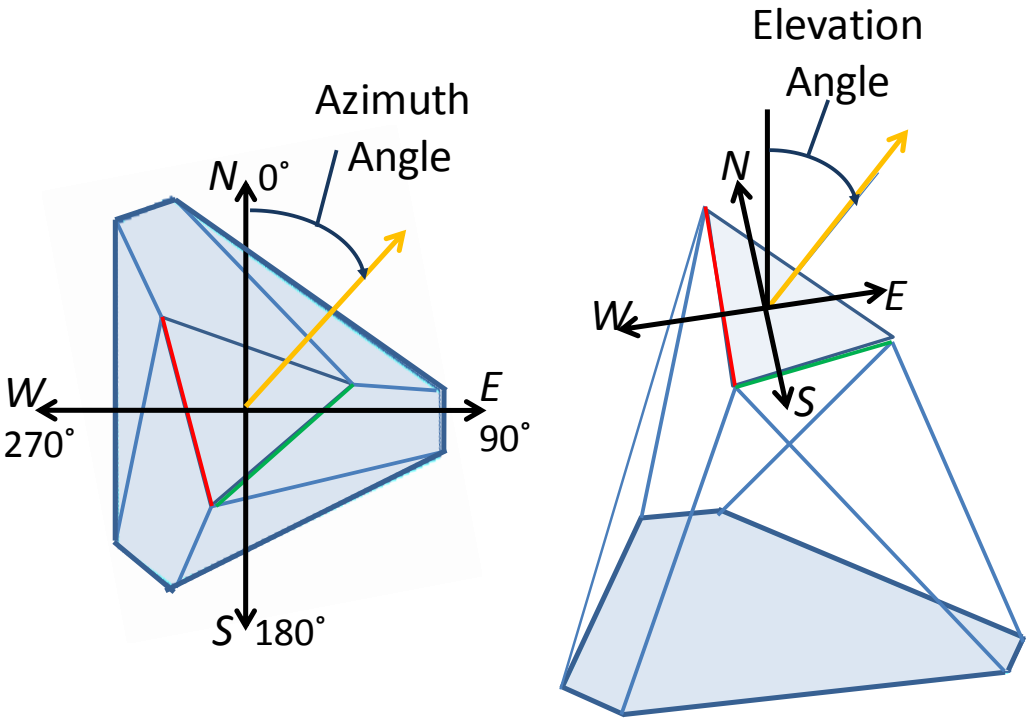

Figure 16: Definition of Elevation and Azimuth Angle

Initially the top platform is rotated about the fixed *z*-axis. Secondly, the top platform is rotated about the rotated *y*-axis. Finally, it is rotated about the rotated *z*-axis at the same angle as the first rotation, but in the reverse direction (this ensures the hexapod does not become twisted and the legs do not collide.

By assuming the platform is rotated about a fixed point, with a rotation matrix of the form R(-az, alt, az), a manipulator with 6 DOF (Degrees of Freedom) is no longer required. It will be possible to position the platform with three legs. However it should be noted that a hexapod still has the following advantages:

1. Stiffness as well as accuracy of the hexapod will be higher assuming the same linear drives are used.
2. Pointing disturbances can be rejected across a broad range of frequencies (McInroy *et al.*, 1999).

3. Various control schemes that make use of all 6 DOF are still available.
4. A larger payload can be carried, assuming the same linear drives.

Therefore using a hexapod, even when all the DOF are not fully utilised, is justified.

3.4 Dynamic Model

The dynamic model basically answers the following question: *given the desired trajectory, speed and acceleration of the platform, what forces are required by the linear drives?*

The general method used to derive the dynamic model is presented here, with the detailed calculations placed in Appendix A.

3.4.1 D'Alemberts Model

Although many dynamic models are found in literature, the model presented in (Tsai, 1999) is more detailed and contains a complete numerical example with four sets of simulation results. This section is based on Tsai's model.

The principle of virtual work is used for static systems which are in equilibrium. D'Alemberts principle is the extension of virtual work to dynamics (Meirovitch, 2001), expressed as:

$$\sum_{i=1}^{N}(F_i - m_i\ddot{r}_i)\delta r_i = 0 \qquad i = 1,2 \dots N. \tag{3-10}$$

where F_i is the applied force,

m_i is the mass of particle,

$m_i\ddot{r}_i$ is the inertia force and

δr_i is the displacement of the system.

The advantage of D'Alemberts procedure over Newton-Euler's method is that all the reaction forces do not need to be calculated.

3.4.2 Derivation of Dynamic Equations

The detailed derivation of the dynamics is shown in Appendix A. Here, only figures which illustrate the assumptions made to derive the dynamics are shown. Although the chosen hexapod layout is a 6-3 hexapod, the dynamics were initially derived for a 6-6 hexapod so that values obtained can be compared with the numerical model in (Tsai, 1999).

Figure 17 below shows the mass distribution in terms of the centres of gravity for the various components, where $\mathbf{m_T}$ denotes the platform, $\mathbf{m_1}$ the cylinder and $\mathbf{m_2}$ the piston.

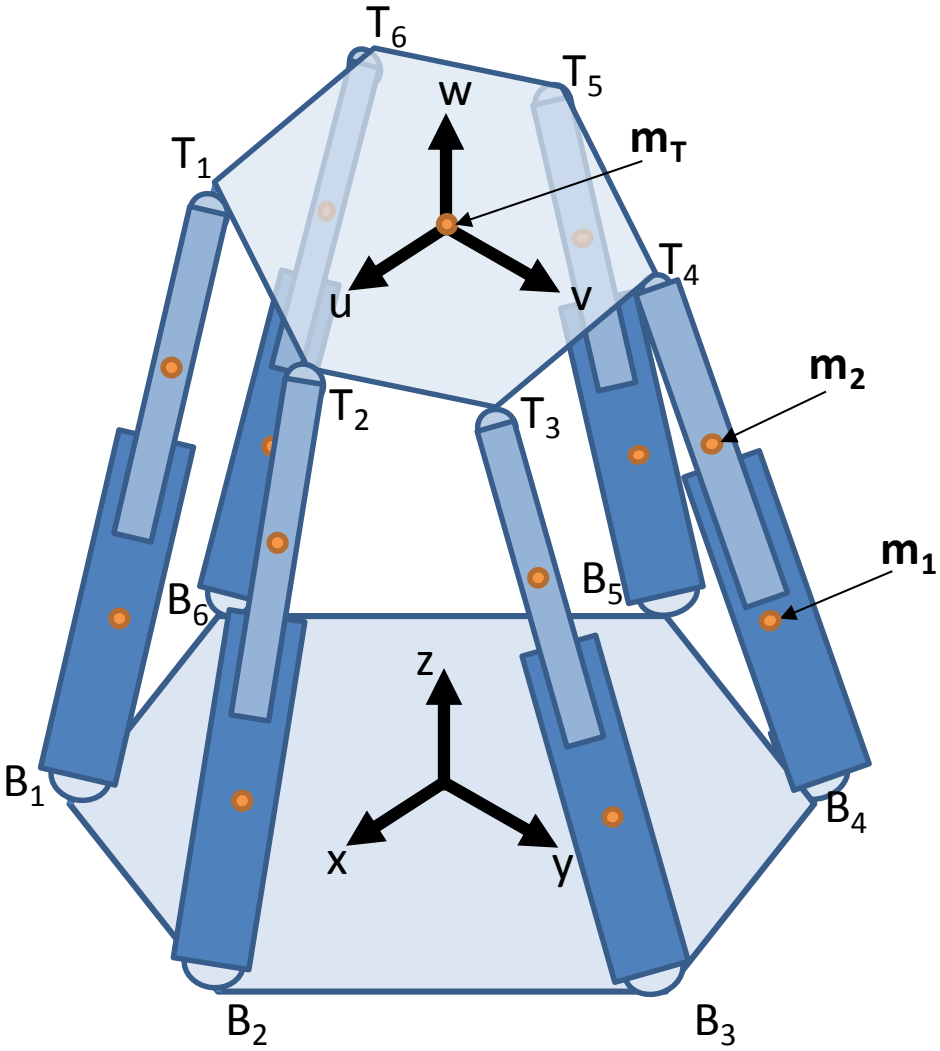

Figure 17: Hexapod Mass Distribution

The derivation of the dynamics is simplified by dividing it into smaller systems: pistons, cylinders and the platform. A moving coordinate system is specified with its origin placed at the centre of the platform. Additional coordinate systems are defined with origins at the base of each leg (B_i where $i = 1$ to 6). To calculate the resultant forces required by each of the legs, the platform movement is converted to the coordinate system of the legs.

The forces acting on each leg are shown in Figure 18. Each leg is made of two main components: a cylinder and a piston. The cylinder is joined to the base at B_i, while the piston is attached to the platform at T_i. Gravity is assumed to act

vertically towards the base. Since the piston moves relative to the cylinder during the operation of the linear drive, this movement is accounted for by measuring the piston's centre of gravity $\mathbf{m_2}$ from the platform and the cylinder's centre of gravity $\mathbf{m_1}$ from the base.

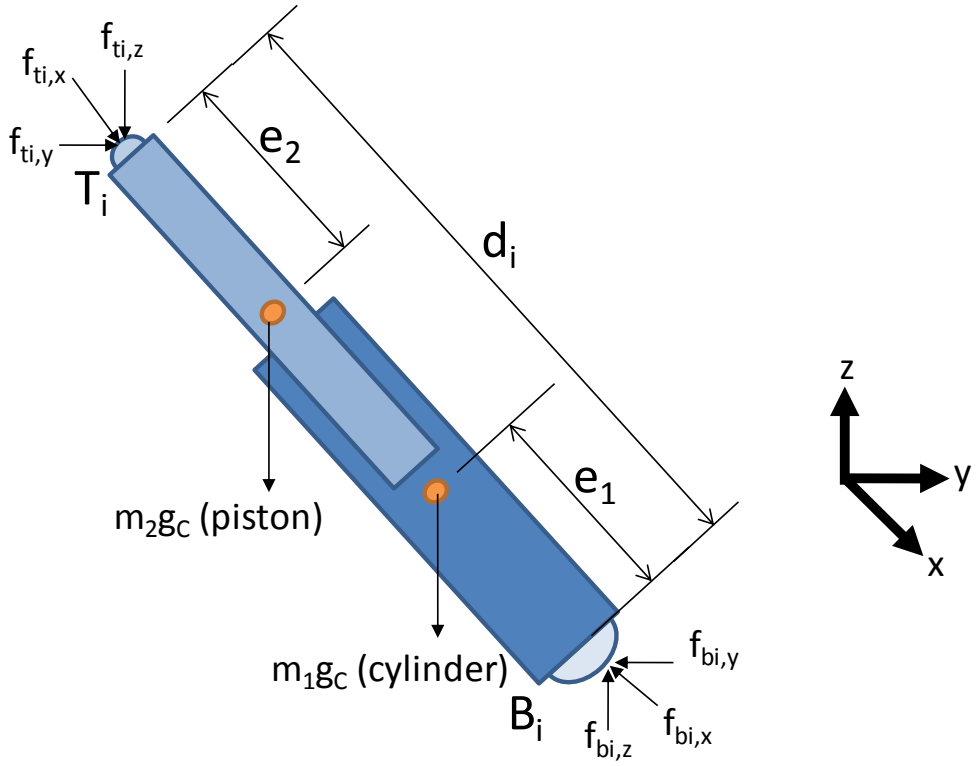

Figure 18: Leg Free-Body Diagram

Each leg is treated individually as a system. All the leg subsystems are combined to form a single equation that needs to be solved:

$$\tau = (J_m^T)^{-1}\left(-\hat{F}_m - J_x^T \hat{F}_x - J_y^T \hat{F}_y\right) - \hat{F}_z \qquad \textbf{(3-11)}$$

where τ is the vector of leg forces,

J_m is the Jacobian matrix of platform,

$\hat{F}_m$ total force on platform,

J_x Jacobian matrix of X components of hexapod legs,

$\hat{F}_x$ total force on hexapod legs in X direction,

J_y Jacobian matrix of Y components of hexapod legs,

$\hat{F}_y$ total force on hexapod legs in Y direction and

$\hat{F}_z$ *total force on hexapod legs Z direction.*

Solving equation (3-11) provides the leg forces required by each leg. The exact calculations are shown in more detail in Appendix A.

A program was written in Matlab to calculate the dynamic response of a hexapod. The results were verified through comparison to the results obtained by (Tsai 1999). After verification, the parameters were adjusted and simulations run to determine the force requirements of the model and full scale hexapod.

3.5 Calculating the Kinematic Jacobian of the Hexapod

As discussed in Chapter 2.3.4, there are positions in a hexapod's workspace for which it loses a DOF. These are known as singularities since the hexapod's Jacobian matrix is singular. If a matrix is singular its determinant is zero. If a singular position is reached during the tracking of an object it would be highly undesirable. It is therefore crucial to be able to predict singularities before path planning can be performed.

Defining the vectors x as

$$x = [x_m\ y_m\ z_m\ \theta_t\ \varphi_t\ \emptyset_t] \quad \textbf{(3-12)}$$

and q as:

$$q = [d_1\ d_2\ d_3\ d_4\ d_5\ d_6]. \quad \textbf{(3-13)}$$

The Jacobian transforms the change in leg rates to the velocity of the hexapod:

$$\dot{q} = J\dot{x}. \quad \textbf{(3-14)}$$

The Jacobian matrix can also be defined as two separate Jacobian matrices.

$$J = {J_q}^{-1} J_x \quad \textbf{(3-15)}$$

Using this definition the type of singulartity can be determined. It has been established that if $\det(J_q) = 0$, there is a loss of DOF. While if $\det(J_x) = 0$, there is a gain in DOF (Tsai, 1999).

Using the equation above (3-14) can be expressed as:

$$J_q\dot{q} = J_x\dot{x}$$

where $\dot{q} = [\dot{d}_1\ \dot{d}_2\ \dot{d}_3\ \dot{d}_4\ \dot{d}_5\ \dot{d}_6]$ and $\quad \textbf{(3-16)}$

$$\dot{x} = [\dot{x_m}\ \dot{y_m}\ \dot{z_m}\ \dot{\theta}_t\ \dot{\varphi}_t\ \dot{\emptyset}_t].$$

This can be expressed in a more compact form as:

$$\dot{x} = [v_m\ \omega_t]. \tag{3-17}$$

Now to determine the Jacobian of a hexapod equation (3-1) is differentiated leading to:

$$d_i\omega_i \times s_i + \dot{d}_\iota s_i = v_m + \omega_T t_i \tag{3-18}$$

where $i = 1,2, \ldots 6$ and $j = \left\lceil \frac{i}{2} \right\rceil$.

Dot multiplying (3-18) by s_i and rearranging gives:

$$\dot{d}_\iota = s_i v_m + (t_i \times s_i)\omega_T \tag{3-19}$$

where $i = 1,2, \ldots 6$ and $j = \left\lceil \frac{i}{2} \right\rceil$.

Equation (3-19) is in the same form as (3-16), therefore $J_x$and J_q are:

$$J_x = \begin{bmatrix} s_1 & (t_1 \times s_1)^T \\ s_2 & (t_1 \times s_2)^T \\ s_3 & (t_2 \times s_3)^T \\ s_4 & (t_2 \times s_4)^T \\ s_5 & (t_3 \times s_5)^T \\ s_6 & (t_3 \times s_6)^T \end{bmatrix} \tag{3-20}$$

$$J_q = I. \tag{3-21}$$

Since J_q is the identity matrix, it will have no singularities at all. It is therefore clear that there is only one type of singularity possible in hexapods. Consequently all singularities cause a gain of degree of freedom in the hexapod mount (Fichter, 1986).

The definition of the Jacobian, as described in this chapter, is used to check for positional singularities. Since the hexapod is a positioning mechanism, it must be designed or controlled such that it can assume desired positions while avoiding singularities. The option of designing the hexapod a singularity free hexapod, (safe hexapod), was explored. However this limited the range which the hexapod could attain. Therefore a hexapod is designed that has singularities in the workspace, but is controlled to avoid them.

4 HEXAPOD MODEL DESIGN

A hexapod system has a large number of components that all need to work together to function properly. Since there are so many components it should clearly be specified how they all function as well as interface with each other. These requirements are considered during the design process.

The total hexapod system consists of three main subsystems: the hexapod mount, controller and computer interface, which all need to be designed separately. Since these three subsystems are from three different engineering fields (mechanical, electronic and computer programming) different design procedures are appropriate for each.

The main hexapod system as well the components of each subsystem is depicted in Figure 19.

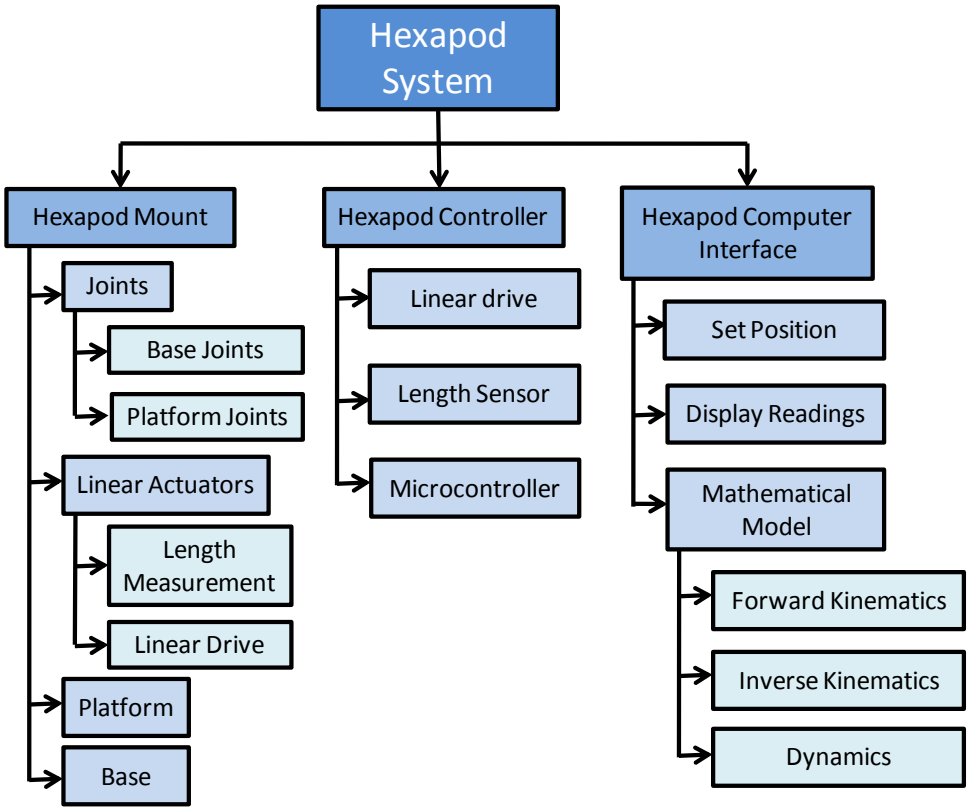

Figure 19: Hexapod Subsystems

4.1 System Operation

The operation modes that the hexapod system requires are presented in Figure 20. The user selects an operation; on completion of that operation the next operation can be selected.

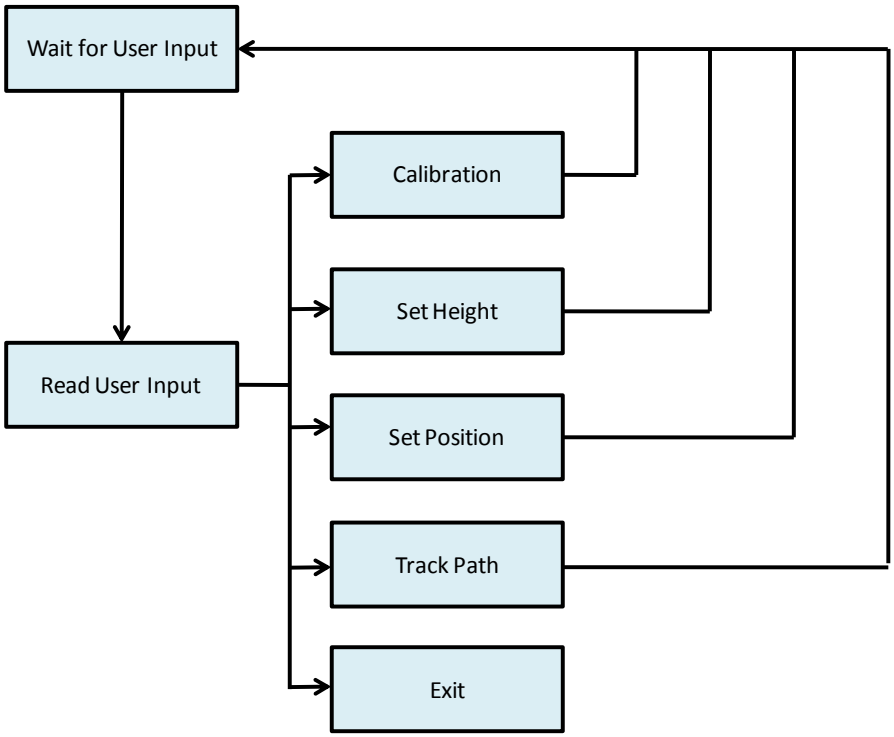

Figure 20: System Operation

The mechanical design procedure used for the Hexapod as well as its subcomponents is shown in Table 3.

Table 3: Mechanical Design Procedure and Method

Design Step	Method
1. Define the requirements.	As specified by SKA. Where requirements were not given explicitly, the problem was researched to generate feasible requirements and added to the project proposal.
2. Generate concepts.	Combination of research and brainstorming.
3. Evaluate concepts.	Table additive method.
4. Choose concept with the highest score.	Table additive method.
5. Perform a detailed design of the chosen concept.	Tools used are Inventor 2009, as well as Matlab.
6. Build and evaluate a prototype.	Simulations are used and calculations made to determine that requirements are met. Performance evaluation of the prototype is done with an inclinometer.
7. Perform a detailed design for the PED.	After analysis of the model, improvements and considerations are suggested for the PED and a full scale CAD model is constructed.

An additional design objective is that all the components can be easily replaced. This is done through use of non-permanent joining methods, such as threads and snap rings.

4.2 Engineering Requirements

The engineering requirements for the model system are:

- Stationary positional accuracy of 0.5°
- Dynamic accuracy of 1°
- Load capacity of 1 kg
- A graphical user interface that allows easy input of the hexapod's orientation
- A control system to accurately track objects and position the hexapod platform

4.3 Mechanical Design

The first step of the mechanical design is to generate concepts. Once the best concept is chosen, detailed designs were performed on each of the components. After the design was completed, a prototype was manufactured. The prototype was tested and changes made as required.

4.3.1 Linear Drive Design

Although linear drives are standard components that are readily available, they are very expensive. Standard components are ideal as they can be replaced if damaged, allowing a longer product lifetime. The linear drives that were available within budget could only be imported from China. This increased the project risk as a considerable time delay is associated with the replacement of damaged linear drives.

The linear drives available also vary in accuracy and strength, with most completely over designed for the hexapod model's requirements, as well as out of budget. The budget to build the scale model was R20 000, and Appendix F shows how this money was spent. In light of the aforementioned risk it was decided to design and build custom linear drives for the model. Custom drives offer the advantage that they can be designed to specifically interface with the required joints, in contrast to standard linear drives which may require some customization.

Since these are custom components there is a risk that they do not work satisfactorily. This risk was minimized by designing, building and testing a prototype linear drive early in the project to determine if another option was required.

The alternative linear drive types that could be designed were evaluated in Table 4. These options were discussed in detail in Chapter 2.2.

Table 4: Comparison of Linear Drives

Characteristic	Weighting	Pneumatic	Hydraulic	Electronic
Load capacity	0.3	5 (Medium)	10 (High)	0 (Low)
Cost efficiency	0.4	5 (Medium)	0 (Low)	10 (High)
Accuracy	0.2	10 (High)	10 (High)	10 (High)
Cost efficiency of encoder	0.1	0 (Low)	0 (Low)	5 (Medium)
Total	**1**	**5.5**	**5**	**6.5**

Load capacity: Assuming actuators of similar sizes the hydraulic linear drives have the highest load capacity, with electronic linear drives the lowest. This is especially true for small linear drives since the power is generated by a small electronic motor, while the power to drive the pneumatic linear drive is a large compressor.

Cost efficiency: Pneumatic actuators require a compressor and hydraulic actuators require a pump as power sources, with a hydraulic linear drive additionally requiring a fluid and better seals, making it more expensive than a pneumatic drive. An electronic drive however only requires an electric motor which is proportionally much cheaper.

Accuracy: It is possible to build all types of actuators with similar accuracies.

Cost efficiency of encoder: Both Pneumatic and Hydraulic drives have no cheap encoder options, with expensive laser based systems available. Electronic drives can also use the accurate laser systems, but alternatively they can also use very cheap rotary encoders such as potentiometers and optical encoders.

The table additive method shows that the electronic linear drive is the most suitable for the design. For the full scale PED hexapod, SKA have a larger budget and thus standard electronic drives will be sourced locally.

Recalling the discussion in Chapter 2.2, a lead screw was chosen over a ball screw since it is cheap, easily manufactured, more compact as well as usually being self-locking. Once a lead screw was selected, a threaded rod of diameter 8 mm was chosen, on which the lead screw would travel.

Motor Selection

For the linear drives there are two possible motors which can be used. The requirements of the motors are:

1. Diameter less than 50 mm; this is to allow more flexibility in the layout of the hexapod since the legs are thinner and less likely to collide.
2. Lift 1 kg when driving a threaded rod (diameter 8 mm, pitch 1.25 mm) through a lead screw.
3. Support a load of 1kg (with 8 mm ball screw) even while its drives are not activated; this will allow the design to change to ball screws if desired.

When a reduction gearbox is added to a motor, the motor is able to produce more torque at a lower speed. Therefore by using geared motors smaller motors can be used which draw less current. Motors that draw low current make the control easier and more cost effective, since low cost standard motor controllers can be used.

Although a DC motor does not have a holding torque, a gearbox with a high gear ratio has much more friction than the motor alone. Since a lead screw is used, it may already be self-locking. However if a motor has sufficient holding torque, this leaves the design flexible to later change to a ball screw.

A stepper motor has a holding torque, but only while it has voltage over its windings. A gearbox is therefore a safer mechanism. A geared stepper motor would be required in order to produce a suitable amount of torque. Although standard controllers are available for stepper motors, these are slightly more expensive than brushed DC motors.

A major advantage of stepper motors is that they move fixed distances when provided with a control pulse. It is therefore possible to calculate the rotational distance and direction that the motor has moved. This characteristic may be used instead of an encoder. Unfortunately, if a motor experiences a large load, and the stepper motor is given a pulse, the motor may not have enough torque to move. The only way to ensure that a stepper motor has moved is through the use of an encoder.

Considering all the above mentioned characteristics, geared stepper and DC motors are evaluated in Table 5, resulting in the selection of geared DC motors.

Table 5: Comparison of Motor Alternatives

Characteristic	Weighting	Geared Stepper Motor	Geared Brushed DC motor
Cost efficiency	0.3	0 (Low)	10 (High)
Ease of control	0.4	5 (Medium)	10 (High)
Possibility of operation without encoder	0.1	5 (Medium)	0 (Low)
Holding torque	0.2	10 (High)	5 (Medium)
Total	**1**	**5.5**	**8**

Cost efficiency: Geared DC motors are approximately 5 times the price of geared stepper motors producing the same amount of torque, while considering the catalogues of Mantech Electronics.

Ease of control: A DC motor has much simpler control than a stepper motor and does not require the adjustment of switching times of the cores.

Possibility of operation without encoder: A stepper motor could possibly be operated without an encoder, as the position of the stepper motor could be determined by keeping track of the number of pulses which have been given to the encoder.

Holding torque: It is common knowledge that stepper motors have a holding torque, and DC motors don't. However a high ratio reduction gearbox also has a high resistance to motion which will be able to hold a load in position.

It should be noted that DC motors produce much less RF (Radio Frequency) noise than AC motors. This should be taken into account during the motor selection process for the hexapod of the PED. Current motors used on the elevation-azimuth mounts of the smaller antenna run off 36 V DC. Suitable controllers have been sourced for these motors; hence using 36 V DC motors would allow use of the same controllers making maintenance easier.

The motor's torque requirement is calculated by considering the forces acting on the lead screw under a load of 1 kg.

The torque, T_R, required by the motor is calculated according to (Shigley *et al*.,2004) as:

$$T_R = \frac{F d_m}{2}\left(\frac{1 + \pi f d_m sec\alpha}{\pi d_m - f l sec\alpha}\right) = 12.32 \times 10^{-3}\ Nm \quad \textbf{(4-1)}$$

where F is the axial compressive force of $9.81\ N$,

d_m is the mean diameter of $7.1881 \times 10^{-3}\ m$,

f is the coefficient of friction of $0.25\ steel\ dry$ (Rothbart, 1985),

$\alpha\ is\ the\ thread\ lead\ angle\ of\ 30°\ or\ 0.5235\ rad$ and

$l\ is\ the\ pitch\ (since\ single\ threaded)\ of 1.25 \times 10^{-3}\ m$.

A DC motor was selected which produces a torque of ($49 \times 10^{-3}\ Nm$; see Appendix C) at maximum efficiency. Therefore the motor will produce enough torque to lift a mass of 3.97 kg. The selected motors are shown in Figure 21.

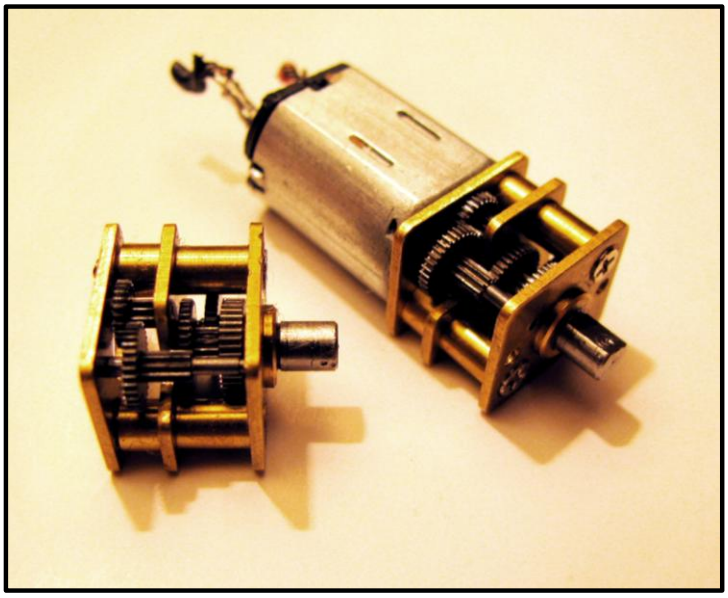

Figure 21: Geared DC Motor with Gearbox

To determine if a lead screw will slip, the following self-locking condition is checked (Shigley *et al*., 2004)

$$\pi f d_m > l \qquad \textbf{(4-2)}$$

$$3.839 \times 10^{-3} m > 1.25 \times 10^{-3} m,$$

proving the lead screw is self-locking. It should be noted that the gears on the motor add an additional force that would also work against the platform's self lowering-force.

Encoder

Given that a DC motor is used, an encoder is required to measure the length of the legs. The requirements of the encoder are that it should:

1. Measure the leg length accurately (within 1 mm)
2. Interface with the controller

Because absolute encoders are too expensive, two main encoder options remained: an optical encoder and a potentiometer.

The main advantage of an optical encoder is that it gives a step output between 0 and 5 V for changes in rotation. The number of steps is counted to determine the angular displacement. The step voltage variation allows interfacing with I/O (input / output) pins on a microcontroller.

In contrast, the potentiometer requires a voltage divider circuit. The voltage over the potentiometer can be measured by an A/D convertor, converted to resistance

and then to rotational displacement. It takes longer to read a value with the A/D convertor than detecting a 0 V or 5 V with an I/O pin. It is not possible to create an interrupt for any change on the A/D convertor and it is consequently not possible to ensure that all changes in the A/D convertor are detected.

Interrupt service routines are sequences of code that execute immediately when an interrupt is triggered, even if a different sequence of code is running. An exception occurs when the programme sequence to be interrupted has a higher priority. Change notification pins can be setup to interrupt once there is a change in the values of a pin between 0 V and 5 V. By using interrupts to measure changes on the encoders, it is ensured that no variation of the leg lengths goes undetected.

Evaluation of the rotary encoders is shown in Table 6.

Table 6: Comparison of Rotary Encoders

Characteristic	Weighting	Potentiometer	Optical Encoder
Accuracy	0.5	5 (Medium)	10 (High)
Ease of interface	0.3	5 (Medium)	10 (High)
Cost efficiency	0.2	10 (High)	5 (Medium)
Total	**1**	**6**	**9**

Accuracy: Potentiometers measure rotary displacement by changes in their resistance, to convert this to angular displacement, a circuit needs to be designed with an A/D convertor which will then be used to determine the position. However optical encoders produce pulses after changes, with low cost encoders available that can produce up to 500 pulses per revolution.

Ease of interface: The circuitry required by a potentiometer will be an amplifier to make the changes in voltage over the range of the A/D convertor. In contrast the requirements of an optical encoder are three resistors and I/O ports which are easy to setup.

Cost efficiency: Although the potentiometer itself is much cheaper than an optical encoder, the extra circuitry that is required to take the reading only makes it marginally more cost effective than an optical encoder.

The preceding evaluation shows that an optical encoder is the most appropriate. Fortunately an affordable optical encoder, with a resolution of 100 counts per revolution, is available locally, and is shown in Figure 22.

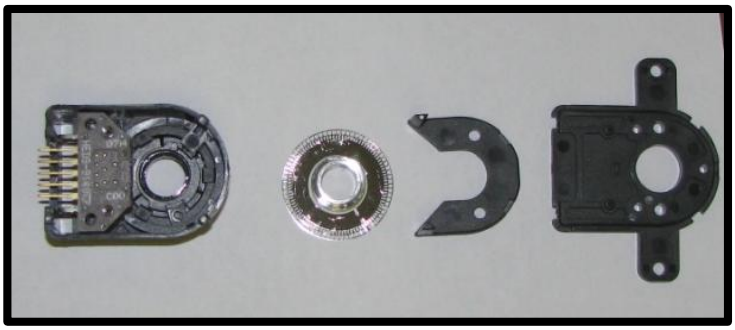

Figure 22: Optical Encoder Disassembled, 100 Steps/Rev

After all the components required for a linear drive had been selected, a detailed design of the linear drive was performed. On completion of the CAD model illustrated in Figure 23, a linear drive was produced.

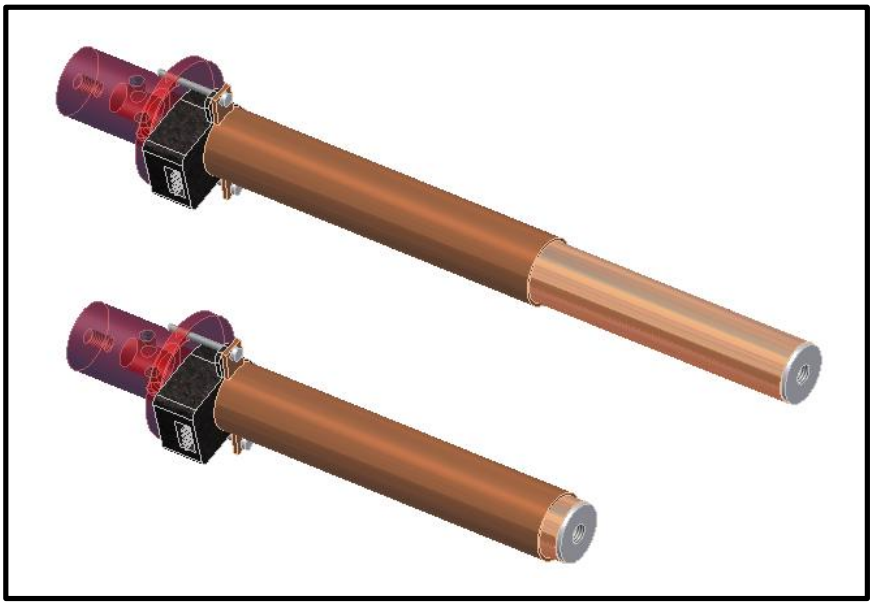

Figure 23: Leg Stroke Length

Since the linear drives need to interface with the base and platform joints, the top and bottom of the linear drive have M6 threaded holes to connect to the joints.

4.3.2 Joint Design

Two different types of joints are required for a 6-3 hexapod. In Section 2.2.2 various possible joints were discussed in detail. The requirements of these joints are that they should provide a connection between the base and the linear drives as well as between the platform and linear drives.

Base Joints

At the base, a joint needs to connect to a single leg (which is referred to as a 1-1 joint), while providing the leg with three rotational DOF. An evaluation of the base joints is presented in Table 7.

Table 7: Alternative 1-1 Base Joints Comparison

Criteria	Weighting	Universal Joint	Spherical Joint	Spherical Plain Bearings	Flexure Joints
Load carrying capacity	0.2	10 (High)	10 (High)	5 (Medium)	0 (Low)
Workspace	0.5	10 (High)	5 (Medium)	10 (High)	5 (Medium)
Standard component	0.3	10 (High)	10 (High)	10 (High)	0 (Low)
Total	**1**	**10**	**7.5**	**9**	**2.5**

Load carrying capacity: Universal joints and spherical joints have high load carrying capacities. Spherical plain bearings have lower load carrying capacity as the load is carried by a smaller percentage of the bearing than the spherical joint. Flexure joints have low load carrying capacity as large forces plastically deform them.

Workspace: The universal joints can attain angles greater than 180°. Spherical joints are limited to less than 180° as the ball needs to be submerged more than half way in the socket. Spherical plain bearings can attain a larger angle than the spherical joint considered as shown in Figure 6 and Figure 8.

Standard component: The only joint which is not standard is the flexure joint.

Although spherical plain bearings are not determined to be the most suitable for the base joints, the universal joints considered for use are from half–inch socket sets. Unfortunately interfacing with the universal joints will prove quite difficult. Additionally the universal joints which are cost effective do not have a single point of rotation, which will add further modelling variables. Due to time constraints the second choice joints are chosen as they can be made quickly and at a similar cost.

Suitable bearings are selected and a CAD model of the joint is constructed. Figure 24 shows the CAD drawings which illustrate the range of motion of the base joints.

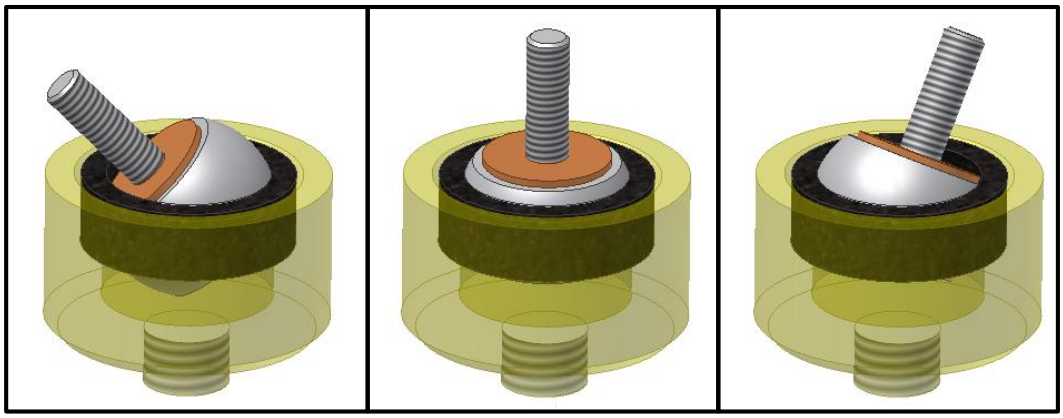

Figure 24: Range of Motion of Base Joint

Platform Joints

At the top of the hexapod, the platform joints need to connect two legs to the platform at a single point, as well as provide 3 DOF. An evaluation of the platform joints is presented in Table 8.

Table 8: Alternative 2-1 Platform Joint Comparison

Characteristic	Weighting	Split Universal Joint	Bifurcation Ball Joint
Load carrying capacity	0.2	5 (Medium)	10 (High)
Workspace	0.4	5 (Medium)	10 (High)
Ease of manufacture	0.3	10 (High)	0 (Low)
Cost efficiency	0.1	10 (High)	0 (Low)
Total	**1**	**7**	**6**

Load carrying capacity: The Bifurcation Ball Joint is able to spread the load over a larger surface than a split universal joint.

Workspace: A bifurcation ball joint is able to produce a range of angles with its two points aligned to 180°. The split Universal Joint is able to achieve 180°, but not for all incident angles.

Ease of manufacture: Bifurcation ball joints will require considerably tighter machining tolerances as well as more difficult assembly procedure, specifically assembling the split ball into the socket.

Cost efficiency: Although the split universal joint consists of more components, the bifurcation ball joint requires more machining time which make it more expensive.

After comparison of the possible platform joints, the split universal joint is chosen. Following this, a detailed design is performed in CAD, similar to other joints in literature. The resultant design as well as its flexibility is shown in Figure 25.

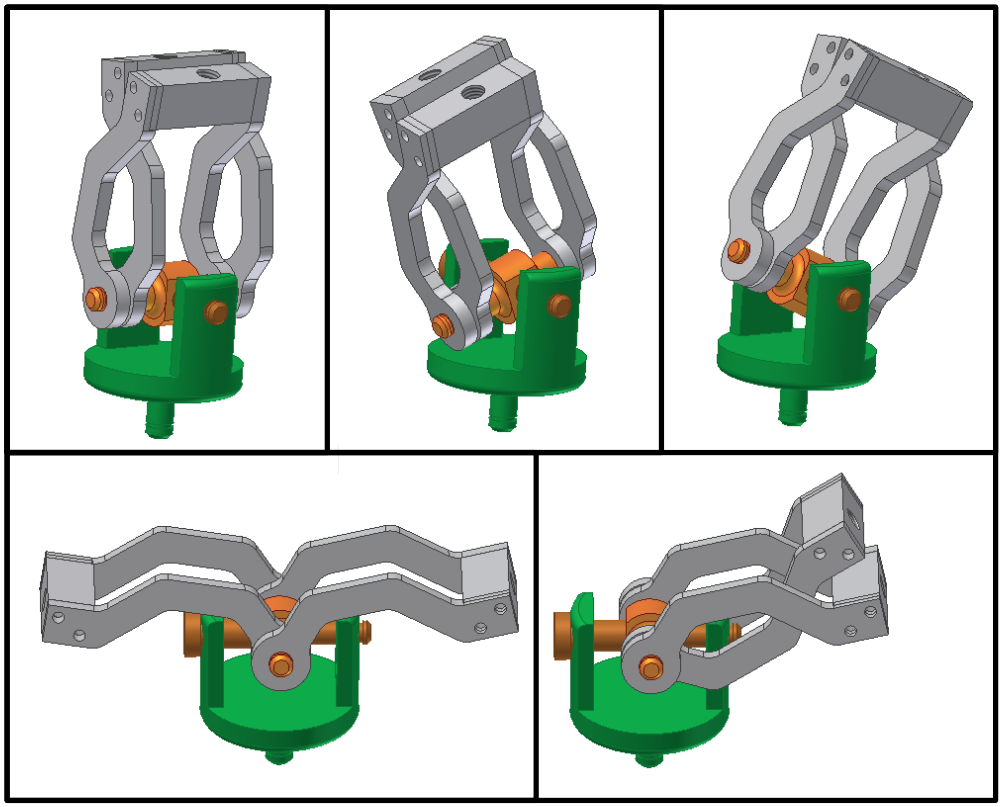

Figure 25: Platform Joint Range of Motion

The two shafts are both made of phosphor bronze. Stainless steel is cheaper and stronger, but stainless steel on stainless steel joints are known to seize, so phosphor bronze is utilized in order to avoid this. Since the joint selected for the platform was a split universal joint there was the possibility of using the same joint for the base with only a single fork. However the plain spherical bearing joint offers the advantages: no rotating surfaces require machining which leads to a joint with less play and only two components require machining in comparison to six, making the joint more cost effective.

4.3.3 Platform and Base Design

With many possible leg lengths and configurations, it is essential to ensure that the various legs do not collide with each other during the operation of the platform. A simulation was performed to check the feasibility of each configuration within the desired range while considering the following constraints, which were due to the components designed for the hexapod model:

- The minimum angle of the 2-1 joint is 14°.
- The leg lengths have a stroke of 120 mm.
- The minimum leg length is 320 mm.

The leg lengths were designed to have an adjustable maximum leg length. This is done by varying the bolt length which connects the legs to the base and platform joints. Therefore the maximum leg length is limited by the longest M6 threaded rod that can be sourced. Originally an 80 mm bolt was chosen.

A complete assembly of the hexapod was designed in Autodesk Inventor. The range of configurations were tested and the dimensions finalised, resulting in the hexapod of Figure 26.

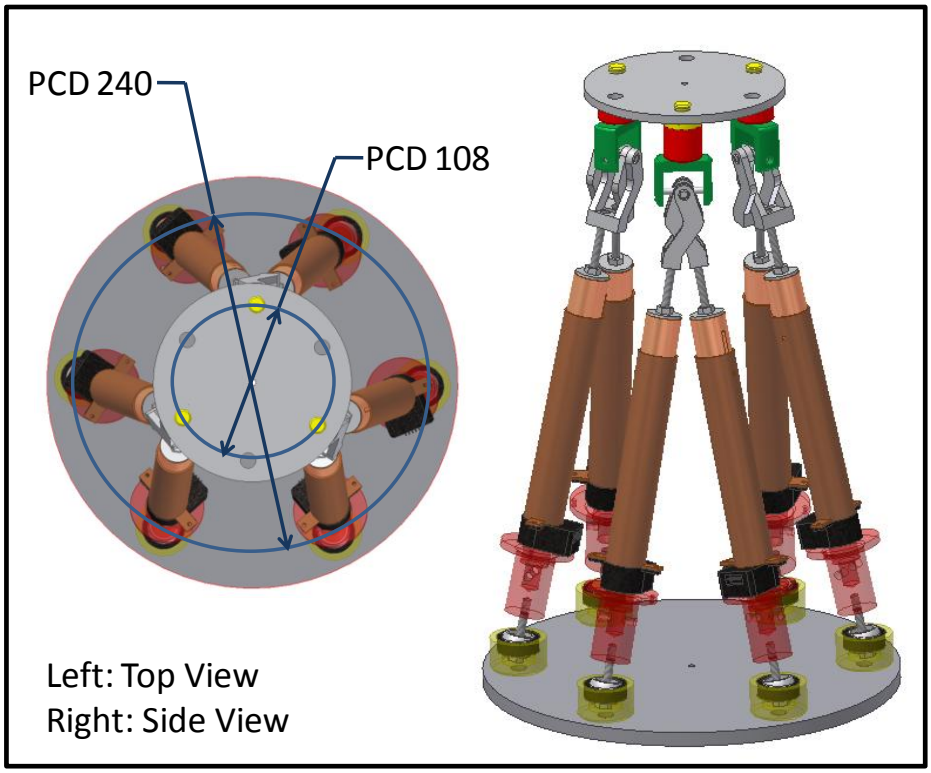

Figure 26: Complete Hexapod Mount

The legs were spaced equally on the base and platform. Both the base and the platform were laser cut from aluminium. Aluminium was selected as it is light and does not corrode in air.

The main assemblies are shown in Appendix D.

4.3.4 Hexapod Improvements

The performance of the hexapod was analysed once assembled and some design adaptations were made.

The legs are connected to the base and platform joints with M6 bolts. These bolts can be screwed in different lengths, since all the holes are not threaded to the exact same depth on the platform joints or the motor housings. Considering these problems, length spacers were added to ensure that all the legs are the same length. This avoided leg length variation due to assembly method. The length spacers are presented in Figure 27.

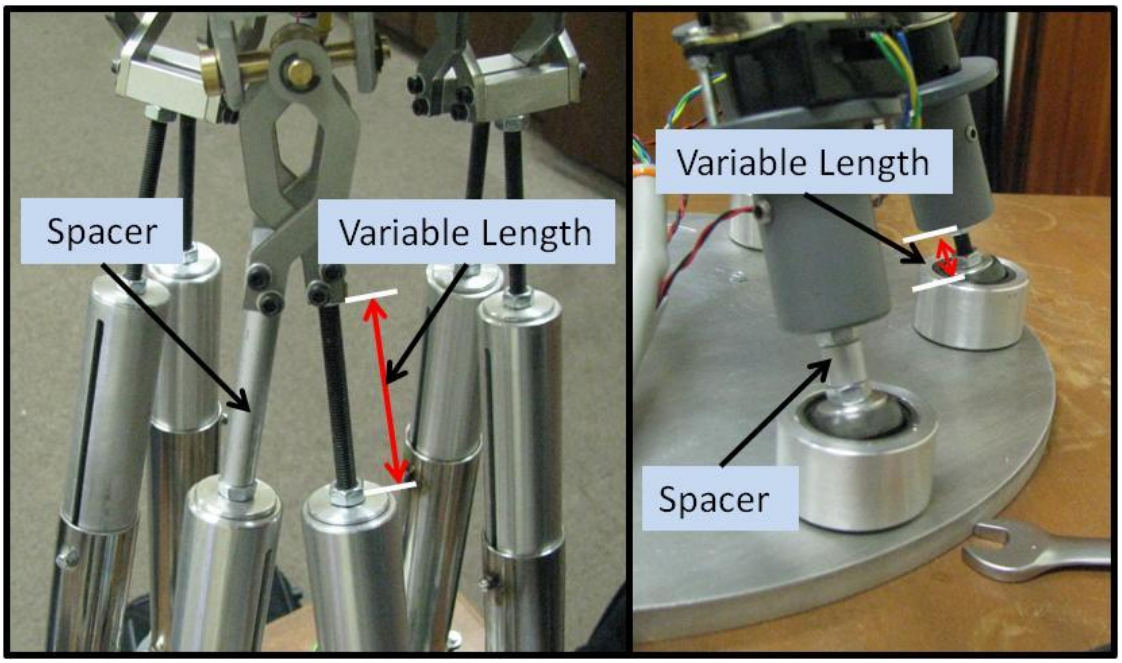

Figure 27: Hexapod with Single Short and Long Spacer Added

4.4 Electronic Design of Controller

The main function of the controller is to manage the operation of the hexapod. The design procedure followed is shown in Table 9:

Table 9: Electronic Design of System

Design Step	Method
1. Determine the required functionality.	Analyse the system requirements and determine the electronic requirements.
2. Identify suitable components.	Read datasheets identifying components which fulfil the requirements.
3. Design a PCB (Printed Circuit Board) with suitable capability	Use a PCB layout programme which connects all the components in the desired fashion, while meeting the electronic specifications of the components.
4. Program the microcontroller.	Write code to perform the required functions in MPlab.
5. Verify the performance.	All commands are tested individually and the output recorded.

The schematics of the PCB layout are shown in Appendix B.

4.4.1 Electronic Requirements

The controller interfaces between the mechanical hardware and computer. It also controls the motors, reads the encoders and communicates with the computer.

The main function of the electronic components is to control the leg lengths. In order to do this, the linear drive lengths must be measured and their speed and direction must be adjusted.

Encoders were used to measure the change in leg lengths. The encoders cannot be directly connected to a computer, and must therefore be read by the controller and transmit the information to the computer in a standard protocol.

In order to receive further feedback from the hexapod, a tilt sensor was used to give an estimation of the hexapod's orientation.

All the components were powered by a standard laboratory power supply. The motivation for not using a fixed power supply was that this allows rapid voltage changes (which change the speed of the platform), as well as a high level of protection in case of short circuits or hexapod collision. By limiting the current, the amount of force that the motors were able to exert is decreased, preventing them from damaging the hexapod.

Control of Linear Drives

The linear drives were powered by brushed DC motors. A standard way of controlling DC motors is H-bridges, which allow both speed and direction control. Although it is possible to construct an H-bridge, low cost packages exist which are compact and easy to interface. These packages enable switching the motor on and off, speed and direction control as well as sensing the current flowing through the motor.

Two Axis Tilt Sensor

Since the leg lengths measured by the rotary encoder are relative measurements, not absolute, a two-axis tilt sensor is used to verify the direction that the hexapod is pointing. A two-axis tilt sensor or gyrometer is able to measure the angle of tilt in a single plane at 90° to each other. By combining this information it is possible to calculate the azimuth angle.

For accurate measurement, the signal produced by the tilt sensor needs to be amplified so that its variation can cover the full range of the A/D (Analogue to Digital) convertor of the microcontroller. Two different types of amplifiers were considered: an operational amplifier and an instrumentation amplifier. An instrumentation amplifier is a single chip which contains three operational amplifiers suitable for accurate low noise data acquisition. The amplifiers are evaluated in Table 10.

Table 10: Comparison of Amplifiers

Characteristic	Weighting	Operational Amplifier	Instrumentation Amplifier
Accuracy	0.4	5 (Medium)	10 (High)
Ease of adjustment	0.1	5 (Medium)	10 (High)
Linearity	0.2	5 (Medium)	10 (High)
Cost efficiency	0.3	10 (High)	0 (Low)
Total	**1**	**6.5**	**7**

Accuracy: An instrumentation amplifier is more accurate than an operational amplifier since it is made up of three operational amplifiers. It also requires less resistors to adjust the amplification. If resistors of the same accuracy were used for both circuits, the operational amplifiers amplification would have a lower accuracy.

Ease of adjustment: An instrumentation amplifier requires a single resistor to set the amplification, while an operational amplifier requires four resistors to set the amplification. Since only a single resistor is required to adjust an instrumentation amplifier it can be adjusted faster.

Linearity: An instrumentation amplifier is more linear over its range than an operational amplifier.

Cost efficiency: An instrumentation amplifier is 20 times the cost of an operational amplifier, but as a percentage of the budget this amount is low.

An instrumentation amplifier was used as it is highly linear, easily adjustable and very stable. Figure 28 presents the amplifier circuit required.

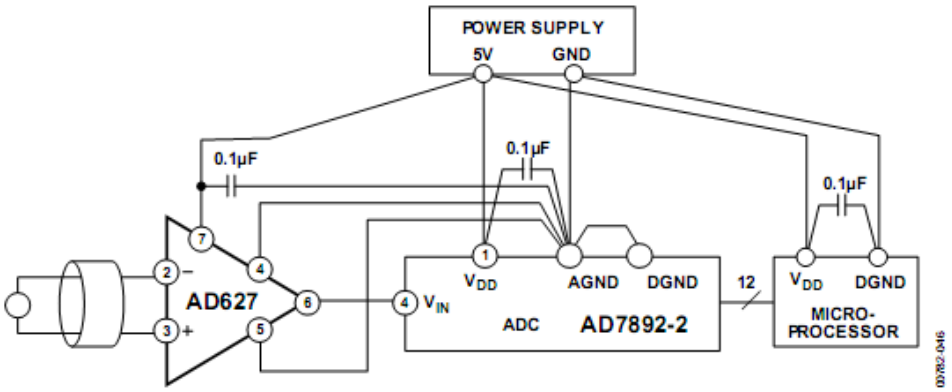

Figure 28: Tilt Axis Circuit (Analogue Devices AD627 datasheet)

The signal from the sensor varied between 0.3 V and 2.3 V for a tilt of 90°. A 2.3 V source was connected to the negative input of the amplifier, and the signal was amplified with a factor of 7. This provided a change from 0.3 V to 4.7 V which was 86% range coverage of the A/D converter. The factor was not further increased as the amplifier loses its linearity close to its rails.

The tilt sensor was not part of the system design or requirements, but added for proof of concept. A more accurate sensor was required for performance measurement of the system.

Small variations were observed in the sensor reading while it was stationary. To counter this effect a passive low-pass filter was added after the amplifier. This significantly reduced the noise in the signal, resulting in a much more stable system.

Figure 29: Tilt Sensor Housing

The readings of the tilt sensor was converted from the pitch and roll angles to elevation and azimuth angles and compared to the calculated values. The tilt sensor was placed in a housing, Figure 29, which was attached to the hexapod platform with double sided tape. The tilt sensor was specifically positioned so the definition of elevation and azimuth would correspond with the GUI definition.

From the previous discussion the complete requirements of the controller was established as:

1. Control six H-bridges
2. Read six encoders
3. Send encoder data to computer.
4. Read tilt sensor.
5. Send tilt sensor data to computer.
6. Receive commands from computer.

4.4.2 Electronic Component Selection

Since previous projects have been performed by the author that required motor control with a microcontroller and reading sensors, familiar components were selected. Risk was therefore reduced and prototyping could be done much faster. The microcontroller selected was Microchip's DSPIC30F4011. The desirable characteristics of this microcontroller are summarized in Table 11.

Table 11: Desirable Characteristics of Microcontroller

Characteristic	Motivation
Flash program memory	Allow a programme to be stored on the microcontroller.
UART module	Standard communication with computer.
Six built in PWM channels	Control three DC motors.
Five 16-bit timers	Control three other DC motors.
10 bit A/D channels	Read tilt sensor.
I/O (Input / Output) ports	Take encoder readings, as well as enable/ disable motors.
External interrupt sources	Used to ensure all encoder steps are detected.

Further standard components selected are voltage regulators, diodes, capacitors and resistors. Low drop diodes were chosen, to increase the effective voltage over the motors.

Through-hole components were selected, as this makes debugging much easier and there was no size constraint for the controller. Once all the components were specified a schematic was drawn and finally a PCB layout was done, resulting in Figure 30.

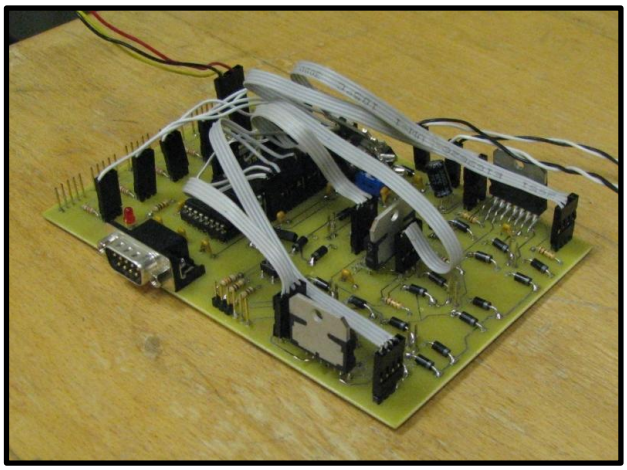

Figure 30: Populated Controller PCB

4.4.3 Microcontroller Program Flow

Once the PCB was assembled and tested, the microcontroller was programmed to perform the commands from the computer interface.

A bootloader was installed on the microcontroller with a programmer. The bootloader allows the microcontroller to be programmed through the serial port, which is faster and more convenient than using the programmer. It also does away with the requirement of an expensive programmer.

After the bootloader was loaded, an open source program, Tiny Bootloader[2] , was used to load the hex files onto the microcontroller through the serial port.

The microcontroller communicates with the computer through the USB at a baud rate of 9600. A standard USB to serial convertor was used for this purpose.

Since the main function of the controller is to perform commands selected by a user on the computer interface, the program flow consists of receiving and executing these commands. The available commands are shown in Appendix E. Once a selected command sequence is performed, the microcontroller waits for the next command. The program flow is shown in Figure 31.

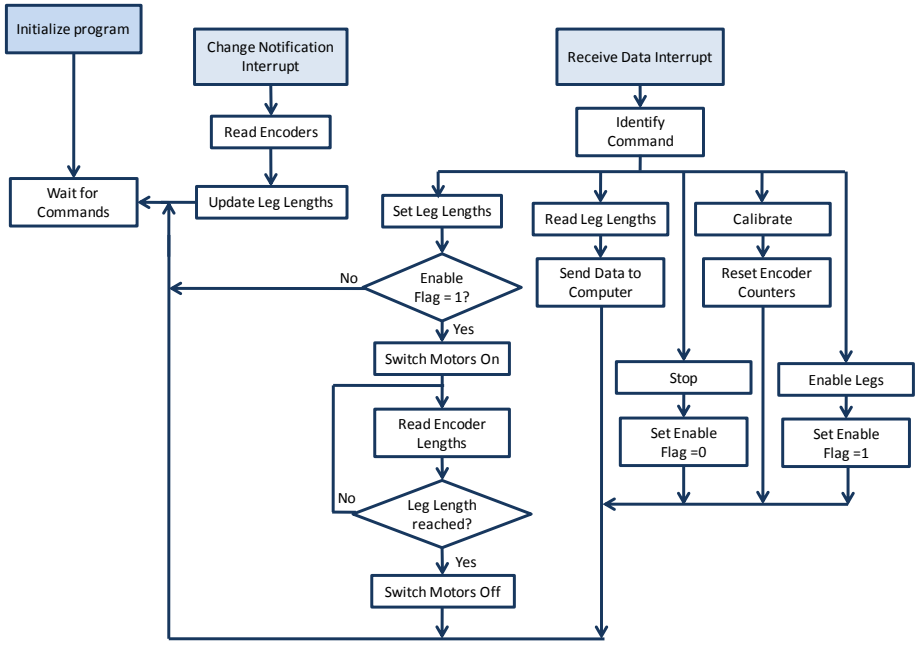

Figure 31: Microcontroller Program Flow

In addition to the commands and actions, the microcontroller was programmed with interrupts. Interrupts stop the current program flow, perform the interrupt service routine and then return to the original point in the program flow.

[2] Available from: http://sourceforge.net/projects/tinybldlin/

Since the encoders produce standard I/O signals, an interrupt service routine is initialised when a change is detected in one of the encoder readings. By using an interrupt instead of reading the encoders after a set time, ensures that no changes in the encoders go undetected.

4.5 Graphical User Interface (GUI)

In order to control the positioning of the hexapod a graphical user interface was programmed. It is more ergonomic to use a graphical interface since it does not require any programming by the user. The GUI design procedure was:

1. Define all the functions required.
2. Determine the program flow.
3. Draw the GUI layout.
4. Program and test each function separately.
5. Add each function to the main program.

4.5.1 GUI Functions

The GUI's main function is to communicate user-selected commands with the microcontroller and display the sensor readings. The main capabilities which the GUI is required to perform are:

1. Communicate with the microcontroller.
2. Calibrate the hexapod.
3. Display current leg lengths.
4. Change leg lengths.
5. Change hexapod orientation.
6. Display tilt sensor's readings.

Calibration

The calibration function is required to ensure that the hexapod is positioned accurately. The function will be performed before hexapod positioning can commence and is discussed further in Chapter 5.

Display Leg Lengths

Once the hexapod has been calibrated the leg lengths are known, and their values displayed. When changes are made to the orientation of the hexapod the encoder readings are used to update the leg lengths.

Change Leg Lengths

It is important to be able to test each leg individually. The direction as well as length change can be specified on the GUI. This verifies the performance of each leg and encoder as well as providing a debugging tool.

Change Hexapod Orientation

Initial and final coordinates of the hexapod are entered to move it between two different points; the details are discussed further in Chapter 6.

The dynamic equations are not integrated with the kinematic model since the speed at which the hexapod needs to move is slow. At low speeds the dynamic forces are miniscule in comparison with the static forces, and therefore not considered during the active control of the system.

Display Orientation Sensor's Readings

A low cost tilt sensor is used which is able to give elevation and azimuth angles to an accuracy of about one degree. This value is also displayed on the interface.

4.5.2 Program Flow

After the interface is initialised, the program waits for the user to select commands. Once an input is received, the command is performed and the interface waits for the next command. The GUI program flow is shown in Figure 32.

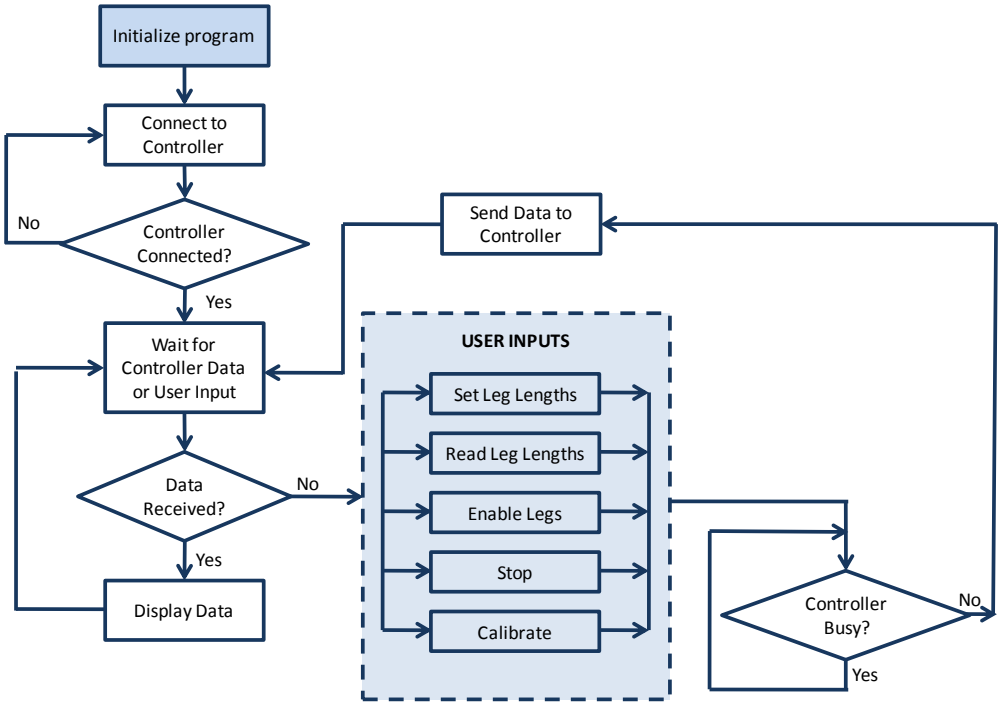

Figure 32: GUI Program Flow

4.5.3 GUI Display

The GUI display, shown in Figure 33, allows the user to operate the hexapod. Desired platform orientation or leg lengths can be entered. Displays include the

current leg lengths, the desired leg lengths, and the elevation and azimuth angles of the hexapod's platform as well as a visual display of the layout.

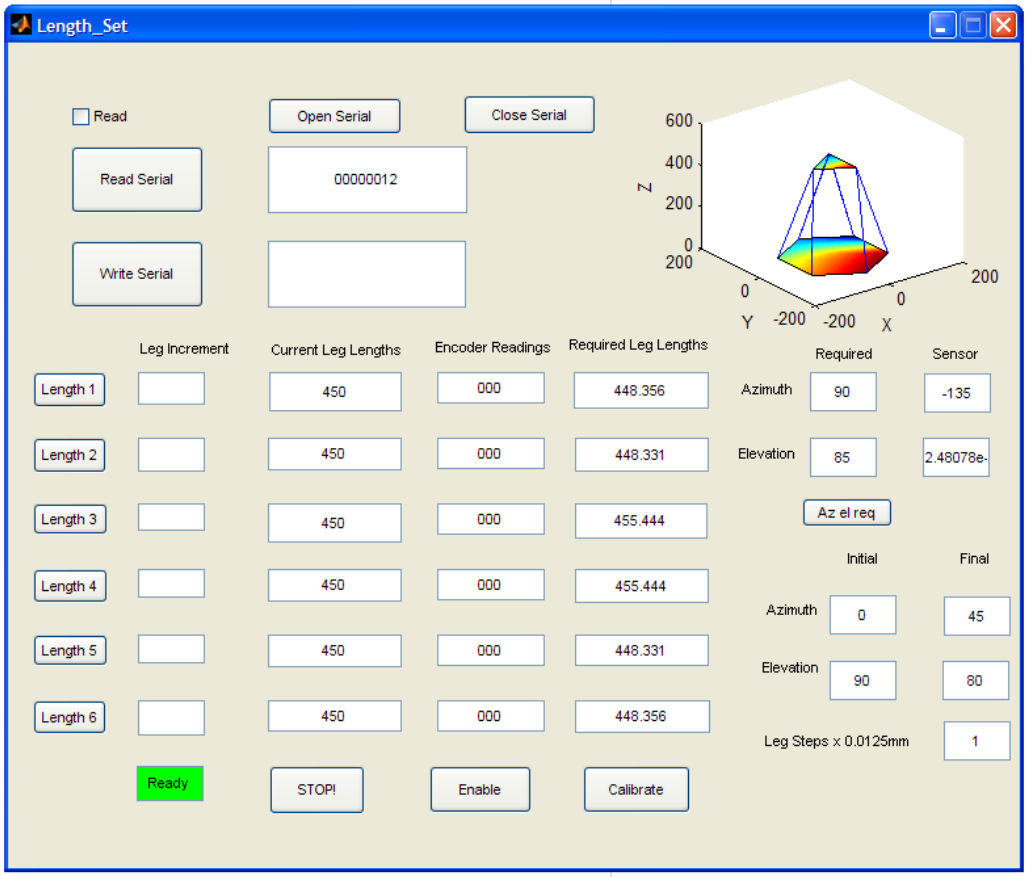

Figure 33: Graphical User Interface

All the components which make up the system of the Hexapod model were completed at this stage. In order to verify that the designed system functions suitably, simulations and tests were performed, which are discussed in the proceeding chapters.

5 SIMULATIONS AND TESTING

Once the hexapod system was built its performance was measured and compared with its predicted performance. The hexapod was calibrated and both computer and physical simulations were run and their results compared.

5.1 Path Planning

Once constructed a hexapod must be controlled to move from one orientation to another. This is not a trivial problem as there are six legs whose lengths may all need to be altered to move from the initial to the final position. Additionally varying the times at which each leg length is changed greatly affects the path tracked by the hexapod.

Although leg lengths are ideally continuous, in reality they are discrete since encoders have a finite resolution. This means that although a specific leg length can be calculated for a specific pointing direction and orientation, the implementation will not be exact since the exact leg lengths cannot be achieved. Although encoders exist with a very high resolution, these encoders are still discrete. This problem is summarised in Figure 34.

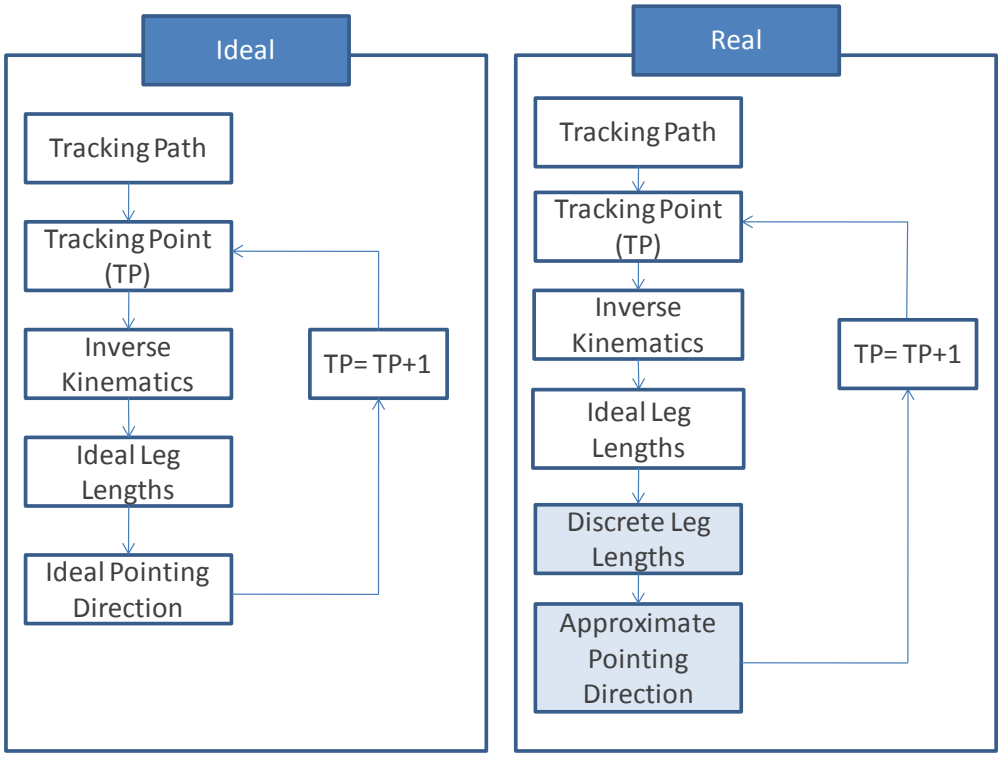

Figure 34: Ideal vs. Real Tracking Sequence

In the end even if the modelling is exact, the final pointing direction of the hexapod's platform remains an approximation. The size of the error due to

discrete leg lengths was calculated for the model and full scale hexapod and presented further on in this thesis.

Figure 35 illustrates the sequence of calculations required to determine a tracking path. It also underlines the need for both an inverse and forward kinematic model.

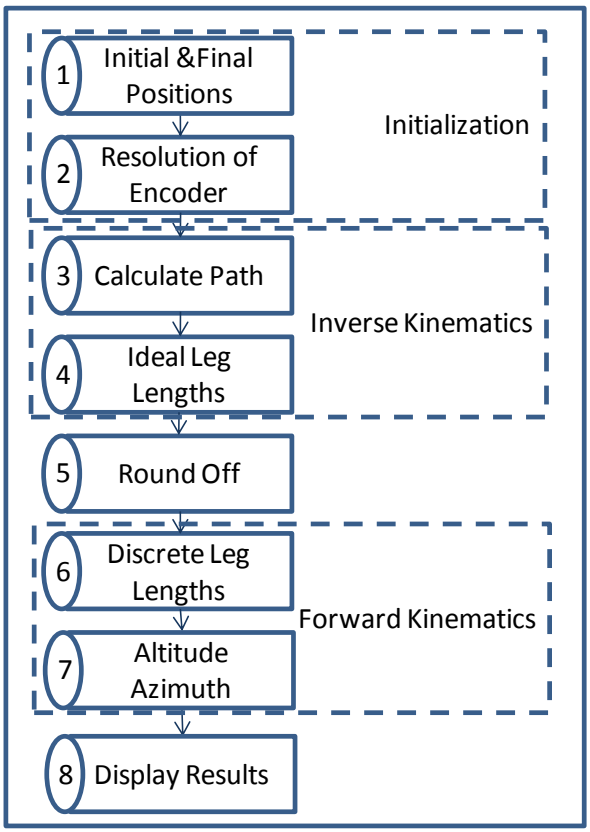

Figure 35: Calculation of Tracking Path

5.2 Tracking

During the operation of the hexapod, the controller is sent a command which specifies the amount that each of the leg lengths should change. This is measured by the encoder and when the encoder detects the required number of pulses the leg is deactivated. Actual leg increments are 0.0125 mm.

5.2.1 Pointing Error

The pointing error is defined as per Figure 36. Generally the pointing accuracy required for an antenna is 10% of the beamwidth (Dydal, 2009). In the case of the Comstar ST-12 which has a beamwidth of 1.3°, therefore an error angle of less than 0.13° is required. This error specification is for the full scale hexapod. For the model hexapod the stationary positional accuracy required is 0.5° and the dynamic positioning angle required is 1° as proposed at the start of the project.

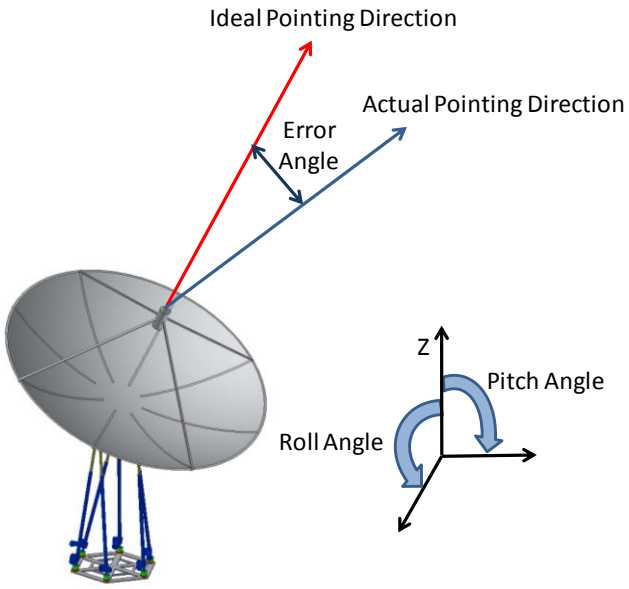

Figure 36: Definition of Error Angle

Although pointing direction is commonly expressed in terms of elevation and azimuth, it is better to calculate the pointing error in terms of pitch and roll. Here the motivation is: when a telescope is pointing vertically, a small variation varies the platform azimuth from 0 to 360°; however if the platform is pointing horizontally, the same variation causes a variation of less than one degree azimuth. Therefore if azimuth is used to measure error, the azimuth error would require a variable weighting, depending on how close to the vertical the telescope is pointing.

In comparison to this complex weighting system, if the error is defined in terms of pitch and roll, the error angle is the combination of the pitch and roll errors.

5.2.2 Computer Simulations

Assuming that the hexapod was perfectly machined and assembled, a simulation was performed of the hexapod model to predict the maximum error of the hexapod, using the sequence illustrated in Figure 34.

The ideal path length was calculated, the attainable positions on that path were then calculated due to the discrete nature of the linear drives. The difference between the ideal path and the discrete path is presented in Figure 37. Assuming no other errors the maximum error angle of the hexapod should be 0.0135°, which far exceeds the engineering requirements.

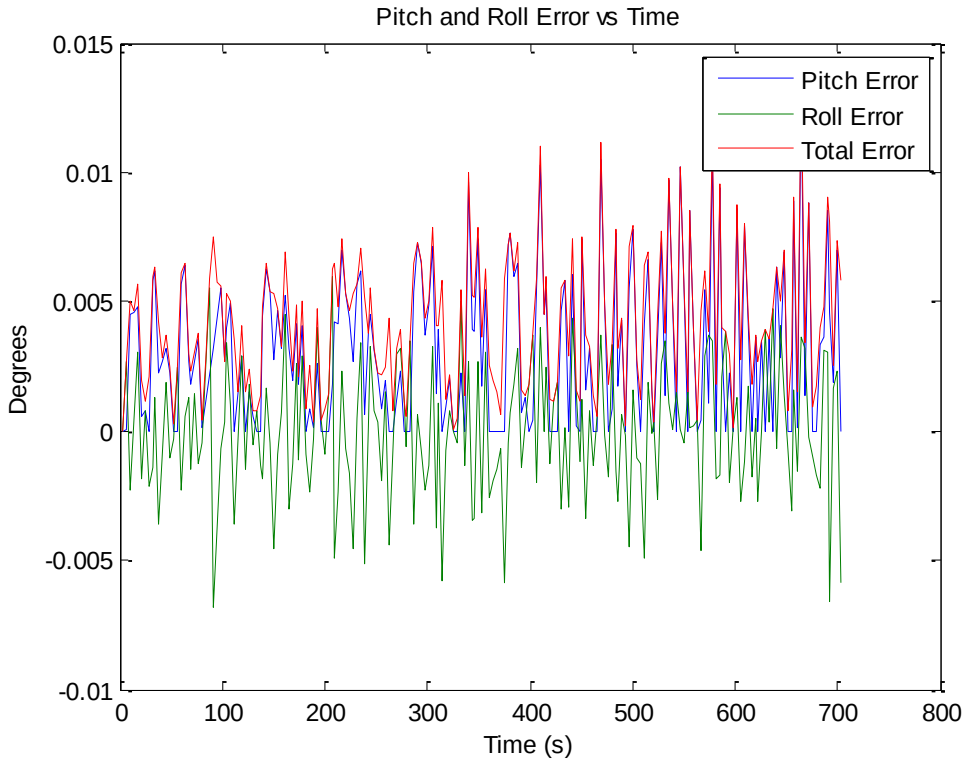

Figure 37: Linear Simulation Errors (Azimuth 0° and Elevation 85° to 90°)

In order to quantify the total error of the hexapod model, physical experiments were performed.

5.3 Physical Experiments

Before performing physical experiments, a coarse calibration method was applied and the hexapod's repeatability tested. Thereafter an orientation sensor was mounted on the hexapod model and simulations done to determine the error angle.

An inclinometer was used to calibrate and test the repeatability of the hexapod. The inclinometer was connected to a computer via the USB port. From Table 12 the inclinometer accuracy is ±0.1° for angles ±30° from the horizontal.

Table 12: ADIS16209 Inclinometer Performance Specification

Table 1.

Parameter	Conditions	Min	Typ	Max	Unit
HORIZONTAL INCLINE	Each axis				
Input Range			±90		Degrees
Relative Accuracy	±30° from horizon, AVG_CNT = 0x08		±0.1		Degrees
Sensitivity	±30° from horizon		0.025		°/LSB

5.3.1 Calibration

Since the rotary encoders only measure relative length of the legs, the hexapod needed to be calibrated as the absolute lengths of the legs are unknown. The following methodology was applied:

1. Adjust all the leg lengths to half their stroke length.
2. Zero the inclinometer for the table, on which the hexapod stands.
3. Adjust the leg lengths individually through the GUI until the pitch and the roll of the inclinometer read zero.
4. Measure the leg lengths with a vernier calliper to verify that they are of equal length. (This ensures that the hexapod is not twisted).
5. Once the platform is level and untwisted, mark the level of each piston in the cylinder of each leg. Otherwise, adjust the hexapod, by repeating steps three and four until the platform is level and untwisted.

Once the marks were made on the hexapod legs, it was adjusted to this configuration manually, by visually lining up the marks and the top of the cylinders. This allows rapid calibration.

5.3.2 Repeatability Test

For the repeatability tests four different movement sequences were selected. Each sequence was performed and reversed (back to the original position). The elevation angle was varied from 90° to 85° while the azimuth was set at 0°, 45°, 90° and then 135°. Each of these sequences was repeated four times. The repeatability was determined for each of the sequences.

Initial results showed the hexapod was not repeatable. By analysing the marks used for calibration during the testing it was seen that the legs became shorter after a few experiments. The origins of this problem were investigated, and various improvements implemented.

The encoders were read by the microcontroller through change notification pins. An interrupt is generated when any of the encoders change in length. This interrupts all other code and updates the leg lengths before returning to executing the previous code. Since this is the best method to detect encoder changes, this was ruled out as the cause of the problem.

It was speculated that the source of the problem was that the legs had too much momentum so they overshot the mark. Since there is less resistance when lowering the platform due to the platform and piston mass working in the lowering direction, the overshoot was worse during the decrease of the leg

lengths. In order to test this, the voltage to the linear drives while they decreased in length was lowered. Lowering the voltage decreased the amount of momentum and allowed the friction of the lead screw as well as the friction in the gearbox to stop the leg faster. Although this drastically improved the hexapod's repeatability it did not solve the problem completely.

The algorithm on the microcontroller which activated the legs, implemented in Figure 31, was checked and an alternative created. Figure 38 shows the two algorithms, their performance is compared in Appendix H.

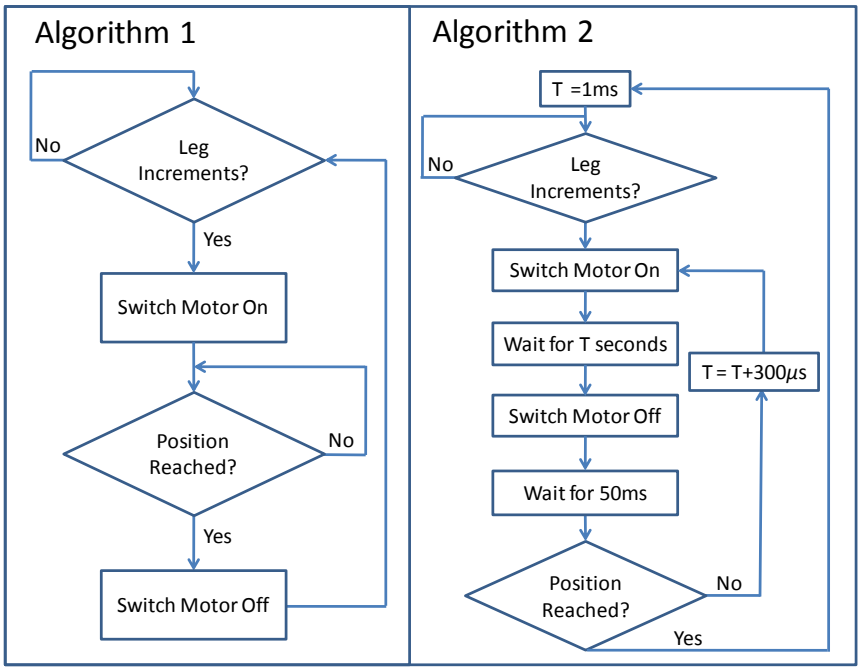

Figure 38: Motor Control Algorithms

Algorithm 1 of Figure 38 was originally used. It was suspected that the momentum of the motors would not allow them to stop immediately and undesired steps would be performed. After the motor is switched off it was determined through experimentation that friction always brought the motor to a standstill within 50 ms. The shortest pulse (T) which allowed any of the legs to increase in position was 1 ms. The pulse length required to change the leg lengths varied at different orientations. Due to this problem Algorithm 2 from Figure 38 was developed. A short pulse is given to the motor; a period of 50 ms is waited for the motor to lose its momentum. If the leg length did not change the pulse length was incremented by 300 µs after each waiting period until it did. Once the leg length changed the pulse length was reset to 1 ms.

When using Algorithm 2 it can be seen that the minimum time that the hexapod could increment one of its legs was 51 ms. It should be noted that since the legs

are changed in single steps (0.0125 mm measured by the encoder), a controller could not be designed to slow down the leg adjustment speed when the legs approached the desired length. To change the orientation of the hexapod by a single degree requires around 70 leg increments. After implementing Algorithm 2 the platform was repeatable to 0.05°, taking the accuracy of the sensor into account this was 0.05° ±0.1°.

Once the platform was found to be repeatable a 0.5 kg then 1 kg weight was loaded on the platform as shown in Figure 39. Unloaded the hexapod moved at 0.014°/s, with a load of 0.5 kg the hexapod moved 0.0135°/s and with 1 kg it moved 0.013°/s. When loaded the hexapods repeatability remained unchanged. This experiment was performed to demonstrate that the hexapod satisfies the requirement of a load capacity of 1kg. Although these angular speeds seem slow, the sun is one of the fastest moving celestial objects that will be tracked, but only moves at 0.00417 °/s these speeds are therefore fast enough to track the sun. The fastest speed at which the custom linear drives can be adjusted is 1 mm/s.

Figure 39: Hexapod with Load

5.3.3 Linear Tracking Tests

From the engineering requirements the hexapod had two different positioning requirements, stationary positioning, where it pointed in a specific direction, and dynamic positioning, where it tracked an object, for instance the sun.

Once the repeatability of the hexapod was satisfactory, tests were performed to determine the error angle of the hexapod. Initial and final orientations were selected and the hexapod followed a linear path between the two points as shown in Figure 40.

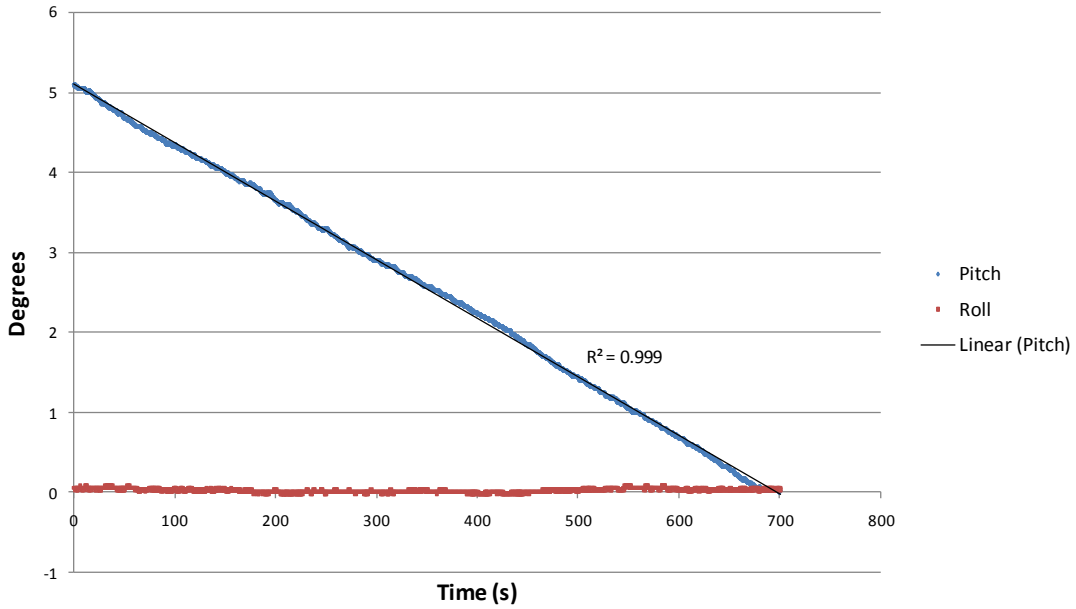

Figure 40: Linear Change of Pitch with Time (Azimuth 0°, Elevation 85° to 90°)

The R^2 value , known as the coefficient of determination, is a measure of how well the data fits the desired path. For a perfect fit the R^2 value is one. Figure 40 shows a R^2 value of 0.999. Since the line is not followed smoothly there are tracking errors as expected, shown in more detail in Figure 41.

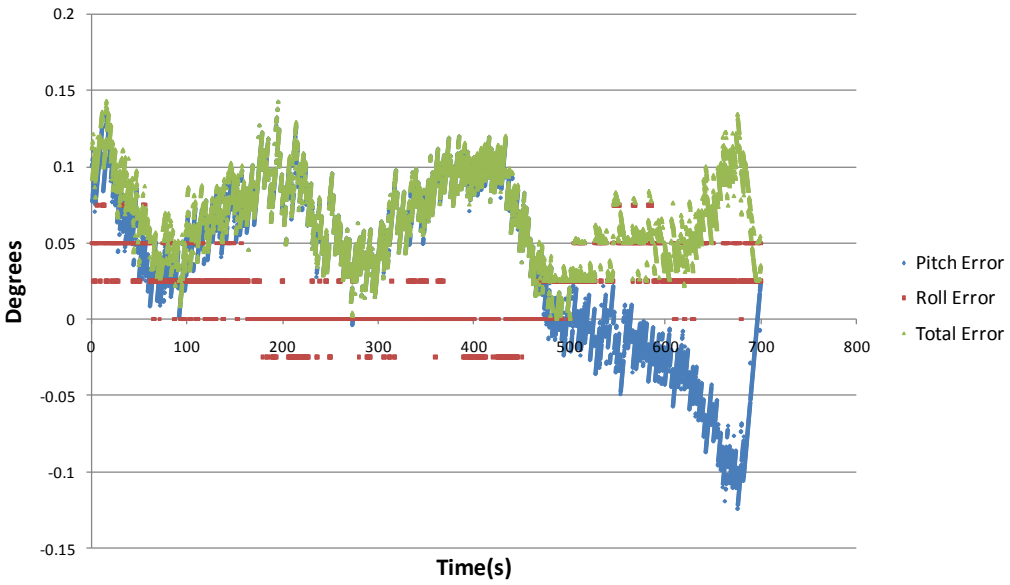

Figure 41: Pitch and Roll Errors of Linear Change of Pitch with Time

From the parallel lines of the roll error, the resolution of the inclinometer can be seen as 0.0025°. The error band of the pitch error is also due to the encoder's resolution, but the pitch error is not divided into parallel lines as the pitch varies with time.

The predicted accuracy was 0.0135° as shown in Figure 37 while the measured accuracy of Figure 41 is 0.14°. The causes of the additional errors may be play in the joints, machining variations in the linear drives and the coarse calibration method.

Figure 42 and Figure 43 shows a test to show that the pitch and roll can be varied simultaneously during tracking. This is proven by the high R^2 values of 0.999 and the low maximum error of 0.21°.

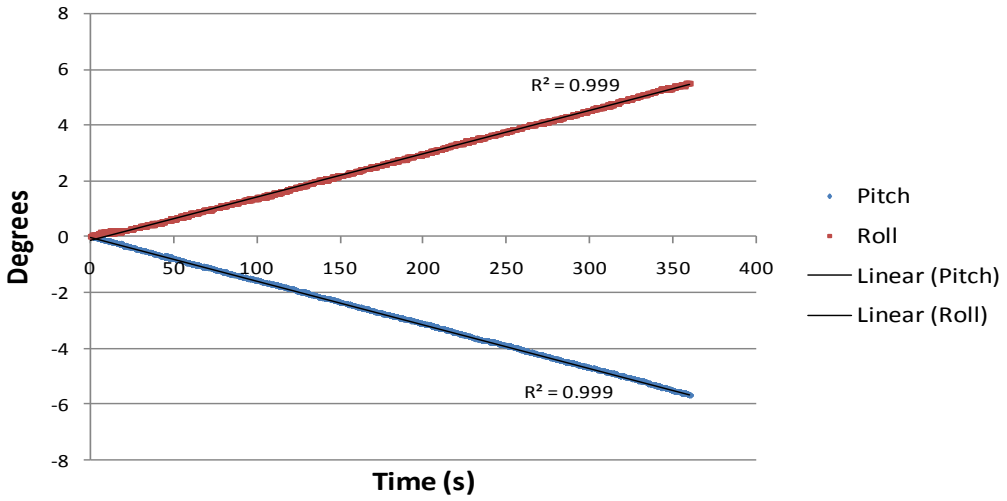

Figure 42: Hexapod Linear Test (Azimuth 135° and Elevation 90° to 82°)

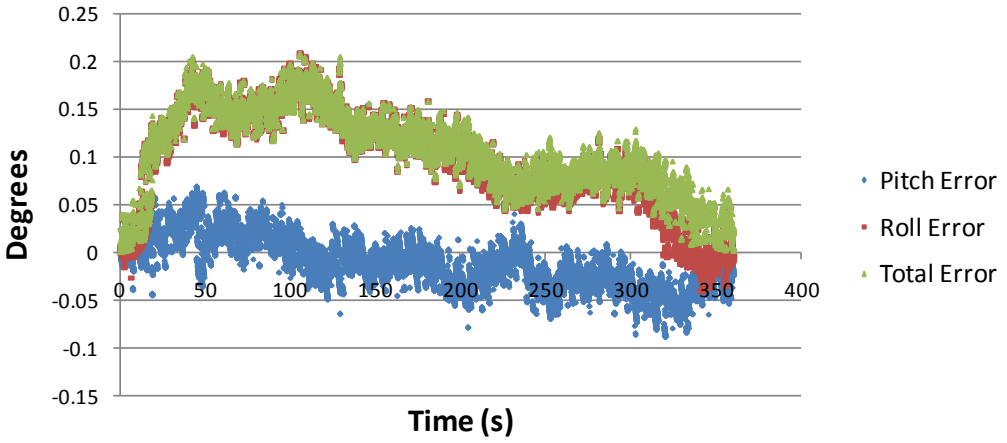

Figure 43: Hexapod Linear Test Errors

5.3.4 Sun Tracking Tests

A conventional el-azimuth mount has a problem with tracking celestial objects which are directly overhead. This is because an el-azimuth mount typically has a range from 0 to 90°. When a celestial object passes directly overhead, it loses sight of the object while it rotates 180° about its z-axis and then continues to track the object. The ability of a hexapod to continually track objects directly overhead is another advantage which a hexapod offers above an el-azimuth mount. A test was performed to illustrate this. The path that the sun would follow was simulated using a sun positioning programme by (Vincent, 2009). The path that the hexapod followed was compared with the desired tracking path. The sun's path was determined for the 30/9/2010 from 12:00 until 13:00 at coordinates 19.26.00E, 2.32.00S, and altitude 136 m and is presented in Figure 44.

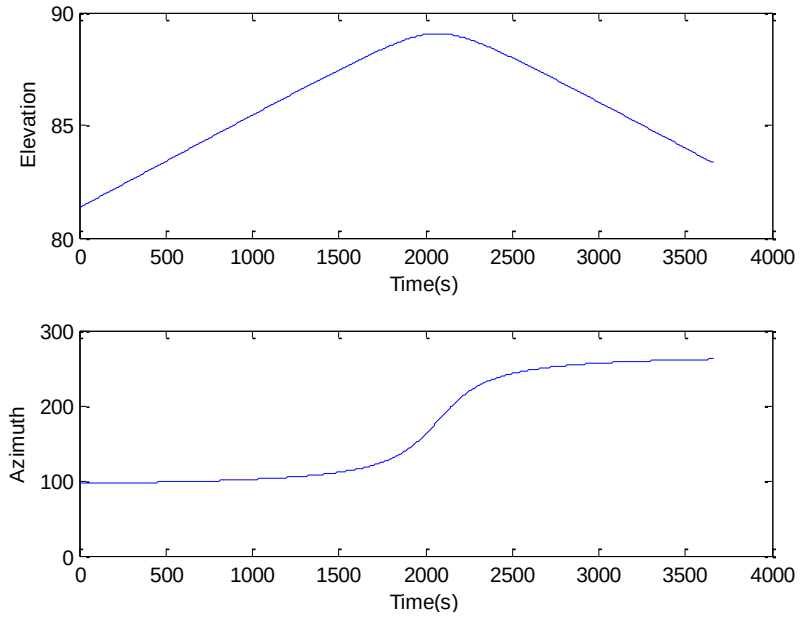

Figure 44: Azimuth and Elevation Angles along the Sun's Path

In order to compare the required angles with the inclinometer output, the angles are converted to pitch and roll in Figure 45. The roll angle varies much more than the pitch angle, and the hexapod points passes within 1° of the vertical.

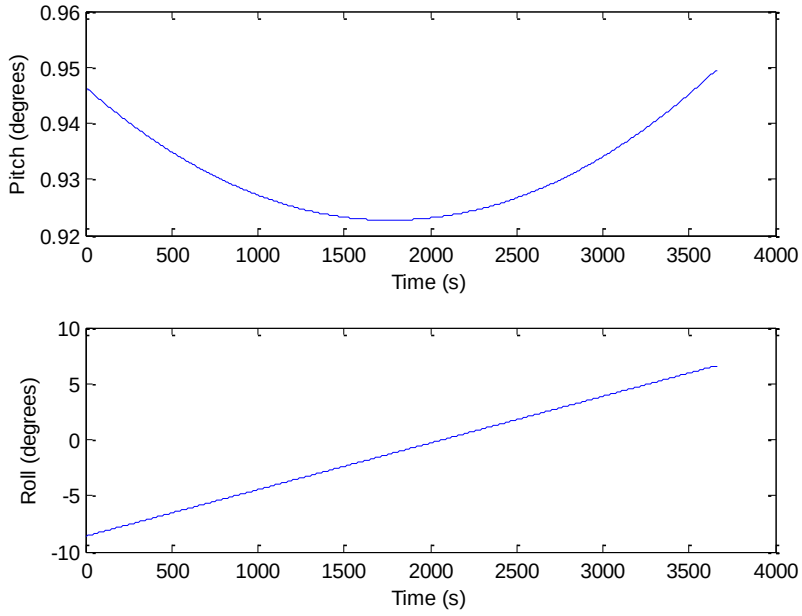

Figure 45: Sun's Pitch and Roll Corresponding to Azimuth and Elevation

Figure 46 and Figure 47 illustrate that the hexapod was able to track the sun within an accuracy of 0.3° ±0.1°.

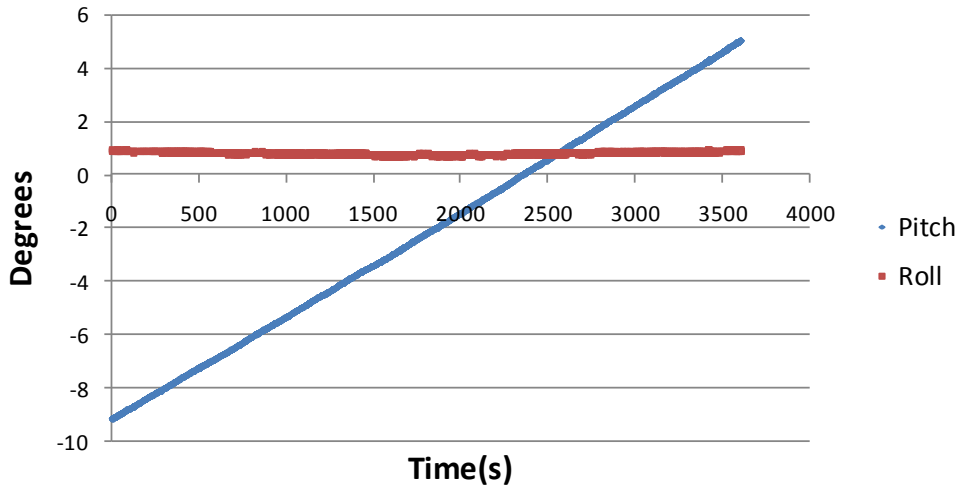

Figure 46: Hexapod Sun Tracking Path

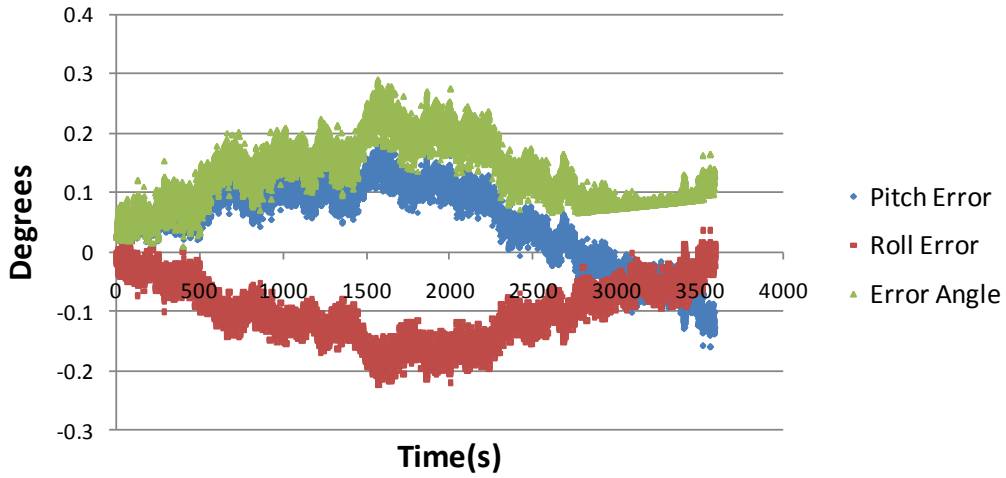

Figure 47: Hexapod Sun Tracking Errors

The sun tracking simulation shows the hexapod is able to track an object continuously as it passes close to the vertical.

Table 13: Hexapod Accuracy and Speed

	Speed	Error Angle
Tracking	0.014°/s	0.3˚ ± 0.1˚
Positioning	0.03°/s	0.21˚ ± 0.1˚

The physical tests have shown that the hexapod satisfies the stationary positioning accuracy of 0.5° and dynamic accuracy of 1° and load capacity of 1 kg.

6 DESIGN OF HEXAPOD FOR PED

When designing a full scale hexapod there are a number of factors which need to be taken into account since there is a large difference between a protected laboratory and an exposed environment such as the PED. These differences require the consideration of corrosion protection as well as protection against external influences such wind and rain.

Experience gained from the construction of the model was implemented in order to improve the design of the hexapod for the PED.

6.1 Engineering Requirements

The engineering requirements from SKA for the system are:

- Position Comstar ST-12 Antennae (Diameter 3.7 m)
- Accuracy of 0.13°
- Ability to move between any two coordinates in the viewing angle of 120° within 1 minute

6.2 Considerations due to Larger Scale

For the full scale design there are a number of factors that must be taken into account.

- Since it is an exposed environment the hexapod should be protected against the elements by the use of corrosion resistant materials, and bearings with suitable seals.
- The hexapod should survive a wind speed of 110km/h which is the same rating of the Antennae (calculation shown in appendix G).
- The current array of six 2.4 m alt-az mounted antennae utilize 36 V DC, this should be maintained so that controllers and power supplies which are currently utilized can be used throughout the array. This will enable easier integration of the hexapod into the current array.
- The hexapod should interface with the existing 3.7 m antennae, requiring little or no adjustments to the current antennae.

6.3 RF Considerations

The following are key points[3] that should be addressed during the design of the hexapod system of the PED:

[3] Professor H. Reader of Stellenbosch University, who is also a researcher for SKA was consulted on the design steps to reduce radio interference.

- Keep switching times as low as possible, as the rising edge is especially problematic.
- All cables should be shielded.
- Twist wire pairs together to decrease amount of interference.
- Ground plates when entering control room.
- DC motors produce less interference than AC motors.

6.4 Knowledge Gained from Hexapod Model

- Laser cutting components is a cost-effective method to machine parts.
- The connection between the legs and the joint blocks had some play. For the full-scale hexapod a longer thread must be used to decrease the play.
- Reusable connections such as threaded connections and circlips, allow quick modifications, these are recommended to be maintained in the design.
- The accuracy of the platform joints is critical to the performance of the hexapod, and their accuracy should be tested before installation.

6.5 Parameter Identification and Model Validation

A CAD model was constructed with a platform that bolted to the current antennae's structure, requiring no antennae modification. Datasheets of a local linear drive supplier were obtained and drives selected which were estimated to be suitable. Autodesk Inventor was used to obtain the inertia as well as the mass of the various components after definition of each component's density. This information was added to the dynamics model and a simulation was performed to determine the force requirements of each linear drive.

The parameters used in the dynamic model are presented in Table 14. The definition of e1 and e2 were presented previously in chapter 3, Figure 18.

Table 14: Parameters Used in Dynamic Model

Part	Mass	Inertia	Centre of Gravity
Platform	45.0 kg	$\begin{bmatrix} 34.15108 & -0.000148 & 0.003599 \\ -0.000148 & 34.150204 & -0.000208 \\ 0.003599 & -0.000208 & 65.242879 \end{bmatrix}$	height = 2.30 m
Linear drives cylinder	9.4 kg	$\begin{bmatrix} 1.417471 & -0.000237 & -0.073221 \\ -0.000237 & 1.443684 & -0.030376 \\ -0.073221 & -0.030376 & 0.038853 \end{bmatrix}$	e1 = 0.32 m
Linear drives piston	10.1 kg	$\begin{bmatrix} 1.834018 & 0.003964 & 0.025103 \\ 0.003964 & 1.822508 & 0.029766 \\ 0.025103 & 0.029766 & 0.021269 \end{bmatrix}$	e2 = 0.54 m

Using the updated parameters for the PED hexapod, simulations were performed to determine the force requirements of the linear actuators. The static force required by each of the legs to support the antennae mounted on the platform is 183 N. The dynamic forces are illustrated in Figure 48 for an acceleration of 1 m/s in the x-direction.

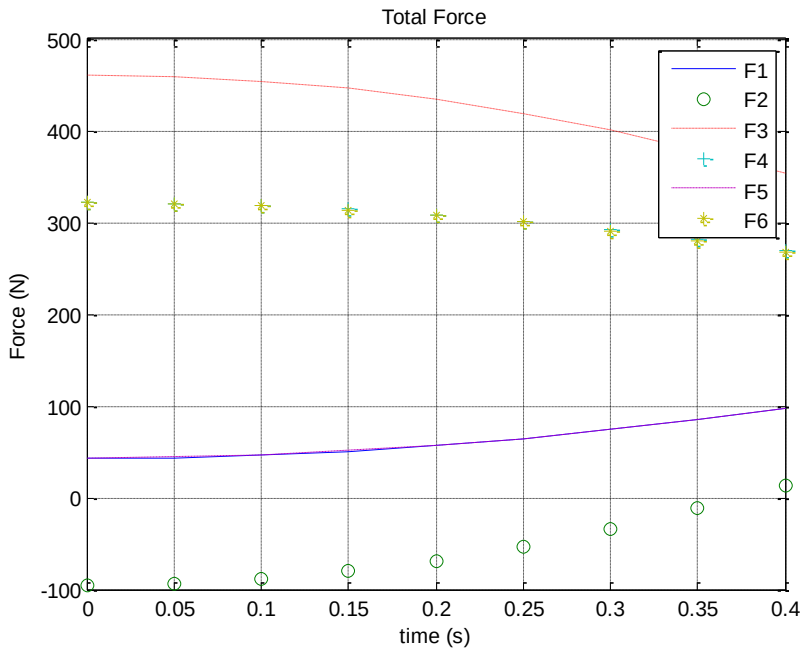

Figure 48: Leg Forces for an Acceleration of 1m/s in *x*-Direction

F*i* denotes the dynamic force acting on the *i*th leg. Of course, the hexapod's speed requirements are miniscule, with an acceleration of 1m/s far exceeding the requirements of the hexapod performance.

6.6 Predicted Performance

From the force requirements discussed previously a linear actuator was specified which is able to lift 200 kg. With the gear ratio required to lift 200 kg, the speed of 16 mm/s will allow the hexapod to change its viewing angle by 3.7°/s. This however does not take into account any switching times, but it will be able to slew rapidly. If no switching times are considered the hexapod will be able to view an angle of 120° in 33 seconds.

The various encoder options for the linear drive were considered, although there is an increase in the price of encoders relative to their accuracy, the price of the encoders is small relative to the total price of the hexapod. It was therefore decided to choose an encoder which would give a resolution of 10 pulses per mm. With the designed hexapod configuration this leads to an error angle of 0.028°. Although it is relatively easy to quantify the error angle due to encoder resolution, it was seen in the hexapod model that the machining variations provided the majority of the error angle.

Although the linear actuators were custom made for the model, standard linear actuators are suggested for the full-scale hexapod as the budget will be significantly larger than for the model. The lifetime of the PED hexapod will also exceed the model hexapod. Linear drives can be ordered with encoders that are able to integrate well into the system, so linear actuators and encoders will be ordered together.

6.7 Base Joint Design

The base joints on the model worked particularly well. They had very little play in comparison to the platform joints. The length of the connection to the linear drive in the model was originally made adjustable. This feature is not required for the full scale model. The linear drives connected directly to the base joint by adding a M16 thread to the bottom of the linear drive.

6.8 Platform Joint Design

After analysing the performance of the platform joints of the model it was seen that there was a bit of play in the interface between the side of the joints and the joint block. In order to remove this, three bolts connect each side of the joint to the joint block as opposed to two.

Tight machining tolerances should be implemented and the platform joints should be tested separately, using a dial gauge, before integration into the PED hexapod system. The amount of play in the joint can further be decreased by spring-loading the joint.

6.9 Complete Design of Hexapod for PED

The full scale CAD design was drawn of the hexapod in Figure 49, with the Comstar-ST12 mounted onto the platform.

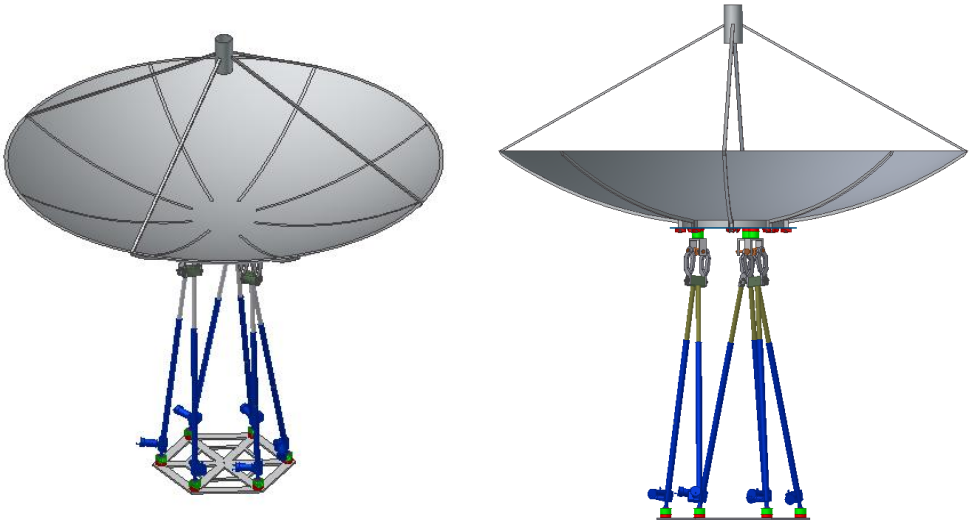

Figure 49: Designed PED Hexapod

Quotes obtained for each of the components is summarised in Table 15.

Table 15: Cost of PED Hexapod

Component	Number	Supplier	Cost
Linear actuators & encoders	6	Bircraft Quote #13988	R102 668.40
Base joints	6	Leading Edge 70	R7 286.00
Platform joints	3	Leading Edge 70	R10 842.00
Platform	1	Fabrinox	R1 300.00
Base	1	Fabrinox	R2 700.00
Commissioning			R35 000.00
		Total	R159 796.40

The cost of a full scale hexapod is estimated at R160 000. It has been claimed that the hexapod will be a more economic structure than an el-azimuth mount (Kingsley *et al.*, 1997) for the 12 m antennae. This is in contrast to this design presented for the PED hexapod.

6.10 Calibration Procedure

A more robust calibration procedure is required for the PED hexapod. A suggested calibration procedure will require limit switches to be installed at the minimum range of each linear drives' stroke length. The calibration procedure will then be:

1. Decrease all six legs in length till they reach their minimum length limit switches.
2. Reset the encoder values and adjust each leg to the required length.

This brief procedure will enable the encoders to be absolute instead of relative encoders and will then provide the repeatability required to implement a more detailed error model as discussed in Chapter 2.5.

6.11 PED Hexapod

After extensive computer simulations, the specifications of the PED hexapod were estimated and summarised in Table 16.

Table 16: Specifications of PED Hexapod.

Parameter	Value
Error Angle Due to Encoder Resolution	>0.028°
Maximum Speed	3.7°/s
Maximum Viewing Angle	120° (Az 0 to 360° El 40°-90°)
Cost	R160 000

The designed PED hexapod will have a viewing angle of 120°, an error angle greater than 0.028°, and have a maximum slewing speed of 3.7°/s.The total cost of the PED hexapod will be R 160 000.

7 CONCLUSIONS

An overview of the project is presented in the following chapter. Firstly the project results are discussed, hereafter the conclusions are presented and possible future work suggested.

7.1 Overview of the Project Outcomes

A complete hexapod system, shown in Figure 50, has been systematically developed through the application of engineering methodology.

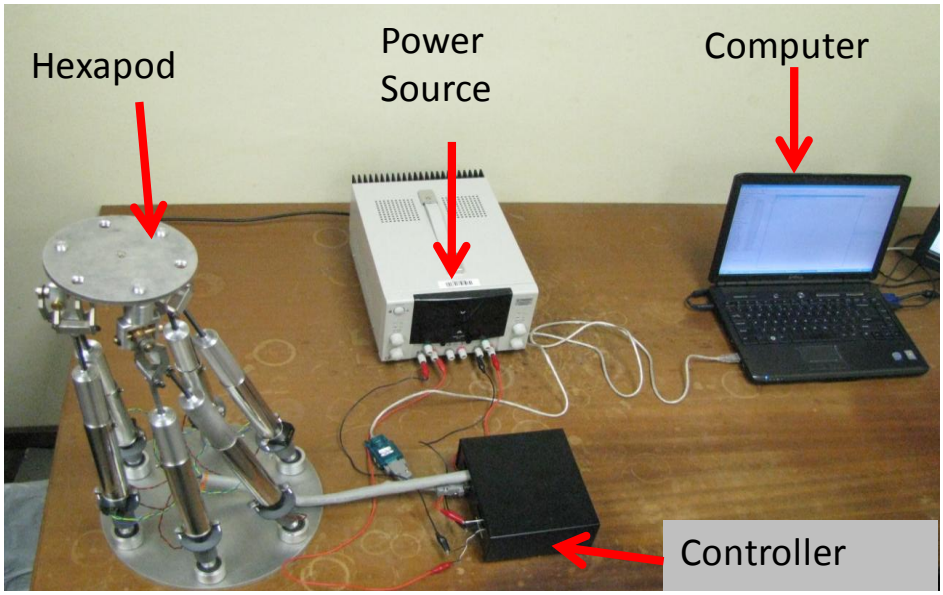

Figure 50: Complete Hexapod System

7.1.1 Mathematical Modelling

Firstly various forward kinematic models were researched and the model most suitable for computation was selected. Together the forward and inverse kinematic models of the hexapod were modelled and tested in Matlab. During the design process the kinematic models were used to determine the stroke length required by the linear drives.

Thereafter various dynamics models were investigated. Resulting in the model by (Tsai, 1999) being selected, modelled in Matlab and verified with a numerical example from literature. The dynamics are used to determine the forces required in each of the legs in response to accelerations, loading and orientaion of the hexapod's platform. Once the force requirements of the linear drives were known they were designed.

A hexapod scale model was built to illustrate the suitable performance of the mathematical models. Various hexapod layouts were considered, before selecting

the 6-3 layout. Once the hexapod model was selected, the effect of the encoder resolution was considered. A programme was developed to determine the error angle given the hexapod parameters and the encoder resolution. This programme made use of both the forward and inverse kinematic equations. Using this programme, errors which the hexapod will have at different orientations due to the discrete leg resolution was calculated. This aided in determining the required encoder resolution.

While calculating the path that the hexapod was to track, the condition number of the Jacobian was used to ensure that the hexapod does not reach a singular position, where control of the hexapod would be lost.

7.1.2 Mechanical Design

The mechanical design of the hexapod posed three challenges, the base (1-1) joint, the platform (2-1) joint and the linear actuators. The base joints developed could achieve a larger angle than the standard ball joint sourced, the linear drives were able to lift the desired load of 1 kg and the 2-1 joints were able to reach the desired angles.

The hexapod model was manufactured and assembled. After some initial testing of the system, improvements were made to ensure that all the legs were of uniform length by the addition of spacers.

7.1.3 Electronic Design

A PCB was laid out with a microcontroller that has serial communication ability, is able to read six encoders, an orientation sensor and control six motors. Additionally a tilt sensor was built and mounted on the platform.

The microcontroller was programmed with a number of commands which it receives from the computer interface and then executes. Reading the encoders with a change notification interrupt on the microcontroller was critical to ensure accurate performance of the hexapod and that no changes in the encoders went undetected.

7.1.4 Interface Design

A simple GUI was developed and used to calibrate and test the hexapod model. Once desired initial and final orientations of the hexapod’s platform were input as well as the step size of the leg increments, a singularity free path was calculated and transmitted to the controller which would move the hexapod model between the two points. An emergency stop was added to the system to allow the platform to be stopped immediately in case of malfunction.

7.1.5 Hexapod Model Testing

Initial testing showed that the hexapod was not repeatable. Adjustments were made and the tests were repeated.

The hexapod's positioning and dynamic accuracy was tested. A sun tracking simulation was used to determine the accuracy with which the hexapod could track a desired path. The engineering requirements compared to the measured results of the hexapod are shown in Table 17.

Table 17: Engineering Requirements compared to Results

	Engineering Requirements	Measured Results
Positional accuracy	0.5°	0.21˚ ± 0.1˚
Dynamic accuracy	1°	0.3˚ ± 0.1˚
Load capacity	1 kg	1 kg

Additional requirements which were also met in order to achieve the results of Table 17 are: *a graphical user interface that allows easy input of the hexapod's orientation* and *a control system to accurately track objects and position the hexapod.*

All the engineering requirements of the model were satisfied.

7.1.6 PED Hexapod – Full Scale Hexapod

After the scale model was designed, built, tested and analyzed a design for the full-scale model was performed. A complete CAD model has been developed in Autodesk Inventor, using the datasheets of the ST-12 antennae, as well as the MecVel linear actuators. After defining the materials of the various components the mass and inertia of the components were obtained from Autodesk Inventor and used to update the dynamic model. Once the dynamic model was updated simulations were performed to determine the force requirements of the linear actuators.

The rest of the hexapod parameters were used to update the forward and inverse kinematic models. These were then used to determine the required stroke length as well as the encoder resolution and calculate the maximum possible error due to encoder resolution.

The simulation tools developed which incorporate the kinematic and dynamic models were used to determine the required stroke length, encoder resolution and linear drive forces.

The basic design of the model was scaled up to position the Comstar ST-12 antennae. Additional factors were considered due to the external environment such as corrosion protection, water proof seals and resistance to high speed winds. 36 V DC motors were specified for the linear drives as this is currently used by the smaller el-azimuth antennae of the PED array.

Quotes were obtained for the linear actuators and the total cost of the full-scale hexapod was estimated at R160 000, with the major cost component being the linear actuators. The total time that it will take to have the PED hexapod operational is four months.

7.2 Concluding Remarks

A hexapod positioning device has a number of advantages over the traditional el-azimuth mount. It has a high load carrying capacity, stiffness and precise positioning accuracy. However the major disadvantage of the hexapod as a positioning device is that it has a smaller workspace than the traditional el-azimuth mount. It does however have a continuous viewing angle directly overhead, unlike the el-azimuth mount, and will be ideal for studies for which this will be desirable.

A model hexapod was designed, built and tested. The test results showed that the hexapod model was able to achieve the required performance specifications, even though there were considerable machining variations. Although some adjustments were required after the initial tests, lessons were learnt and documented which will be valuable during the commissioning of the PED hexapod.

Components designed for the PED hexapod include a full mechanical design, a user interface and software which is able to solve the forward and inverse kinematic equations as well as the dynamic equations of the system.

After an investment of R160 000 the 3.7 m antennae will be equipped with an accurate hexapod positioning mount. It can then be used to further investigate the feasibility of being utilized as the positioning mechanism of the SKA.

7.3 Recommendations

The PED hexapod can be used as a tool to develop further tracking algorithms, as well as educate students as to alternative positioning mechanisms to el-azimuth mounts.

Although the issue of discrete path planning was raised in this thesis there are many alternative schemes which could be developed and weighed against each other. There is a possibility to perform original research in this area.

REFERENCES

ADS International s.r.l. (May 2001). MMTO International Technical Memorandum #01-2 *Secondary Mirrors Support M2/F5 Hexapod Design Kinematics Support*. Smithsonian Institutions & University of Arizona.

Alemzadeh, K., Hyde, R. A., & Gao, J. 2007. *Prototyping a robotic dental testing simulator*. Proc. IMechE.

Balda, Miroslav. 11 February 2008 *Levenberg-Marquardt-Fletcher algorithm for nonlinear least squares problems.* Available at: http://www.mathworks/matlabcentral/fileexchange.com. [2008, May 23]

Blanchard, B. S., & Fabrycky, W. J. 2006. *Systems Engineering and Analysis*. New Jersey: Pearson Prentice Hall.

Bonev. (2009, March 16). *The Parallel Mechanisms Information Center*. (ParalleMIC) http://www.parallemic.org. Retrieved: [2009, June 23].

Cappel, K. L. 1967. Patent No. 3295224. US.

Chen, C.-T., & Liao, T.-T. 2008. Optimal Path Programming of the Stewart Platform. *Advanced Robotics*. 22:705–730.

Chiu, Y.-J., & Perng, M.-H. 2003. *Self-calibration of a general hexapod manipulator using cylinder*. International Journal of Machine Tools and Manufacture (43):1051-1066.

Chiu, Y.-J., & Perng, M.-H. 2004. Self-calibration of a general hexapod manipulator with enhanced precision in 5-DOF motions. *Mechanism and Machine Theory*. 39: 1-23.

Dasgupta, B., & Mruthyunjaya, T. S. 1998. *A Newton-Euler Formulation for the inverse dynamics of the Stewart platform manipulator* . Mechanism and Machine Theory , (33):1135-1152.

Dydal, R., 2009. *Communication Sattelite Antennas: System Architecture, Technology and evaluation*. U.S.A: McGraw Hill.

Fichter, E. 1986. A Stewart Platform Based Manipulator: General Theory and Practical Construction. *International Journal of Robotics Research*. (5):157-181.

Guo, H., & Li, H. 2006. Dynamic Analysis and Simulation of a Six Degree of Freedom Stewart Platform Manipulator. *Proceedings of the Institution of Mechanical Engineers*. 61-72.

Hanselman, D.C. *Modified Newton's Method.* 2006. Available at: http://www.mathworks.com/matlabcentral/fileexchange. [2008, May 23]

Horrel, J. *PED dish first light.2007.* Available at: http://www.ska.ac.za/newsletter/issues/06/07.html Retrieved: [2008, March 26]

Jangan, M. 2005, January 20. *Servo system for GMRT Antenna*. Available at: http://www.gmrt.ncra Retrieved: [June 18, 2008]

Kingsley, J. S., Martin, R. N., & Gasho, V. L. 1997. A Hexapod 12 m Antenna Design Concept for the MMA. Taipei.

Koekebakker, S. H. 2001. *Model based control of a flight simulator motion.* Delft: Delft University, PhD Thesis.

Ku, D.-M. 2000. Forward kinematic Analysis of a 6-3 type Stewart Platform Mechanism. 214 (K):233-241..

Knöchel, F., & Fritzsche, B. 2003. Radio Astronomy at Schools. *Contract: 18369/04/NL/CP*. Germany, Fraunhofer Institut.

Kurfess, T. R. (Ed.). 2000. *Robotics and Automation Handbook*. Florida: CRC Press.

Liu, K., Lewis, F., & Fitzgerald, M. 1994. *Solution of Nonlinear Kinematics of a Parallel-Link Constrained Stewart Platform Manipulator*. Circuits Systems Signal

Nguyen, C., & Antrazi, S. 1990. *Trajectory Planning and Control of a 6 DOF Manipulator with Stewart Platform-Based Mechanism*. Maryland: NASA. Process 13, 167-183.

McInroy, J. E., O'Brien, J. F., & Neat, G. W. 1999. Precise, Fault-Tolerant Pointing Using a Stewart Platform. *IEEE/ ASME Transacations of Mechatronics*, 4 (1):91-95.

Meirovitch, L. 2001. Fundamentals of Vibrations. Singapore: Mc Graw Hill.

Meng, Y., & Zhuang, H. 2007. Autonomous robot calibration using vision technology. *Robotics and Computer-Integrated Manufacturing*, 23:436-446.

Merlet, J-P. 2002. Still a Long Way to Go For Parallel Mechanisms. Presentation. Sophia-Antipolis.

Patel, A., & Ehmann, K. 2000 Calibration of a hexapod machine tool using a redundant leg. *International Journal of Machine Tools and Manufacture*, (40):489-512.

Pugazhenthi, S., Nagarajan, T., & Singaperumal, M. 2002. Optimal trajectory planning for a hexapod machine. *Proceedings of the Institution of Mechanical Engineers* , C(216):1247-1257.

Ren, X.-D., & Su, Z.-R. F.-P. 2009. *A new calibration method for parallel kinematics machine tools using orientation constraint*. International Journal of Machine Tools and Manufacture. 49 (708-721).

Rothbart, H.A. 1985. *Mechanical Design and Systems Handbook* (2nd ed.). New York: McGraw-Hill.

Roy, Vincent. 20 October 2010 *Sun_position.m.* Available at: http://www.mathworks/matlabcentral/fileexchange.com. Retrieved: [2010, October 20]

Shigley, J. E., Mischke, C., & Budyanas, R. G. 2004. *Mechanical Engineering Design* (Vol. 7). New York: Mc Graw Hill.

SKA. 2009. Meerkat Site Specifications. Cape Town: Square Kilometer Array South Africa.

SKA. 2009. Square Kilometer Array. from The International Radio Telescope for the 21st Century: Available at: http://www.skatelescope.org/pages/page_skares.htm [2009, August 25]

Stewart, D. 1965. *A Platform With Six Degrees of Freedom*. Proceedings of the Institute of Mechanical Engineering , 180 (1):371-385

Tsai, L.-W. 1999. *Robot Analysis: the mechanics of serial and parallel manipulators.* NY: John Wiley & Sons.

Ulacay, Ö. 2006. *Design and Control of a Stewart Platform*. MSC Thesis. Sabanci University.

Youssef, H. A., & El-Hofy, H. 2008. *Machining Technology: machine tools and operations.* CRC Press.

Yuriy, T. 2006. *Control system for parallel manipulator with six degrees of freedom*. Donetsk National Technical University, Masters Thesis

Zhang, C., & Song, S. 1994. *Displacement analysis of the 6-6 stewart platform mechanisms*, Mechanism and Machine Theory (29):547-557.

Zhuang, H., & Roth, Z. S. 1993. Method for Kinematic Calibration of Stewart Platforms. *Journal of Robotic Systems* , (10): 391-405.

Zhuang, H., Yan, J., & Masory, O. 1998. Calibration of Stewart Platforms and Other Parallel Manipulators by Minimizing Inverse Kinematic Residuals. *Journal of Robotic Systems*, 395-404

APPENDIX A: MATHEMATICAL DETAIL

As the mathematical models used in this thesis were not developed by the author, but their detail is necessarily to fully understand the thesis, they are presented here in detail.

It should be noted that by rewriting equation (3-1) the definition of the unit vector along each leg is obtained as:

$$s_i = \frac{m + t_j - b_i}{d_i} \qquad \textbf{(0-1)}$$

for $i = 1,2, \ldots 6$ and $j = \lceil i/2 \rceil$.

This is useful for the derivation of the dynamic equations of the hexapod.

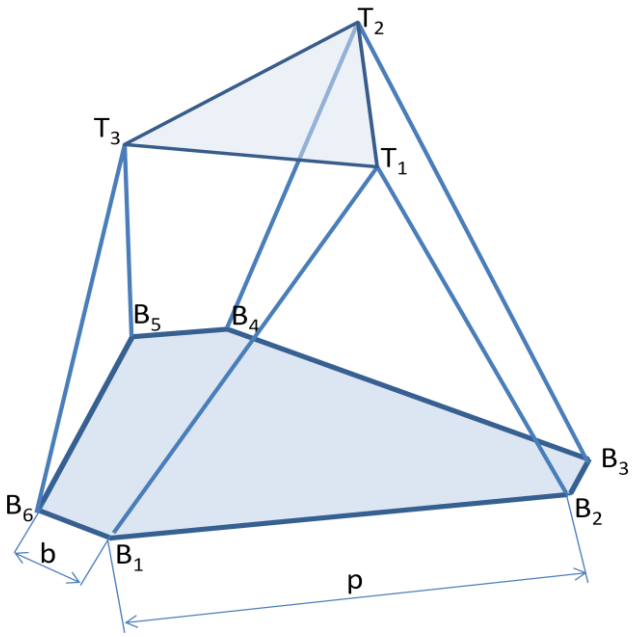

Hexapod with Base with Two Different Side Lengths

A top view of the base, illustrated below, is used to gain expressions for the base coordinates.

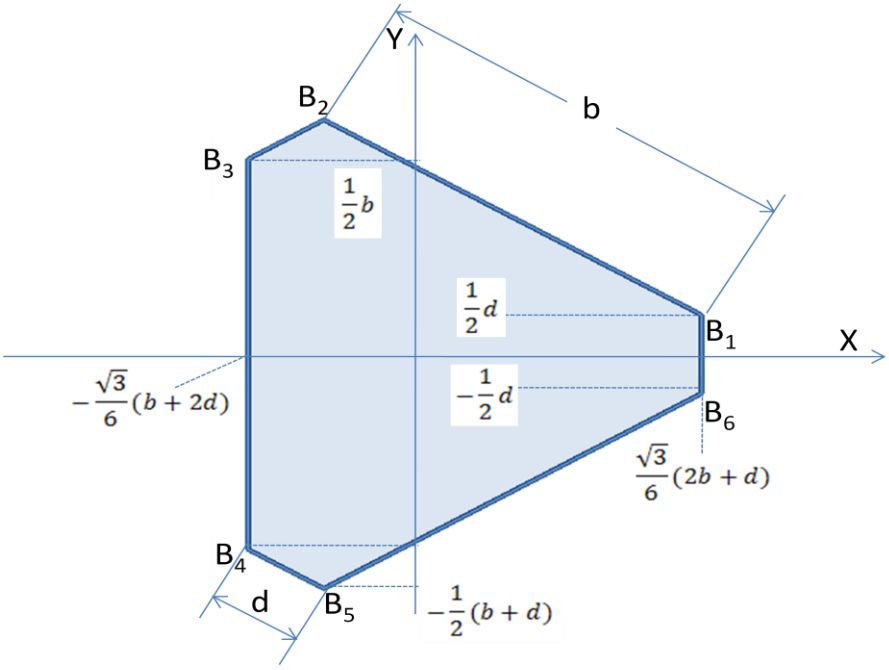

Base of Platform with Dimensions

All the points are spaced equi-distant from the centre of the base, where the origin of the coordinate system is defined. Taking the gradients of the lines into account, the base coordinates are given as:

$$X_{B1} = \frac{\sqrt{3}}{6}(2b + d), \qquad Y_{B1} = \frac{1}{2}d, \qquad \mathrm{Z_{B1}} = 0, \tag{0-2}$$

$$X_{B2} = -\frac{\sqrt{3}}{6}(b - d), \qquad Y_{B2} = \frac{1}{2}(b + d), \qquad \mathrm{Z_{B2}} = 0, \tag{0-3}$$

$$X_{B3} = -\frac{\sqrt{3}}{6}(b + 2d), \qquad Y_{B3} = \frac{1}{2}b, \qquad \mathrm{Z_{B3}} = 0, \tag{0-4}$$

$$X_{B4} = -\frac{\sqrt{3}}{6}(b + 2d), \qquad Y_{B4} = -\frac{1}{2}b, \qquad \mathrm{Z_{B4}} = 0, \tag{0-5}$$

$$X_{B5} = -\frac{\sqrt{3}}{6}(b - d), \qquad Y_{B5} = -\frac{1}{2}(b + d), \qquad \mathrm{Z_{B5}} = 0, \tag{0-6}$$

$$X_{B6} = \frac{\sqrt{3}}{6}(2b + d), \qquad Y_{B6} = -\frac{1}{2}d \text{ and} \qquad \mathrm{Z_{B6}} = 0. \tag{0-7}$$

After determination of the base coordinates, a representation of the platform is required. Unfortunately this is not as simple as the base coordinates, and some new parameters need to be defined to make this representation easier.

The movement of the platform is constrained by the leg lengths. With reference to the following figure, a new parameter h_i is defined as the height of the triangle. The point where h_1 meets the base of the triangle is denoted by (X_{P1}, Y_{P1}).

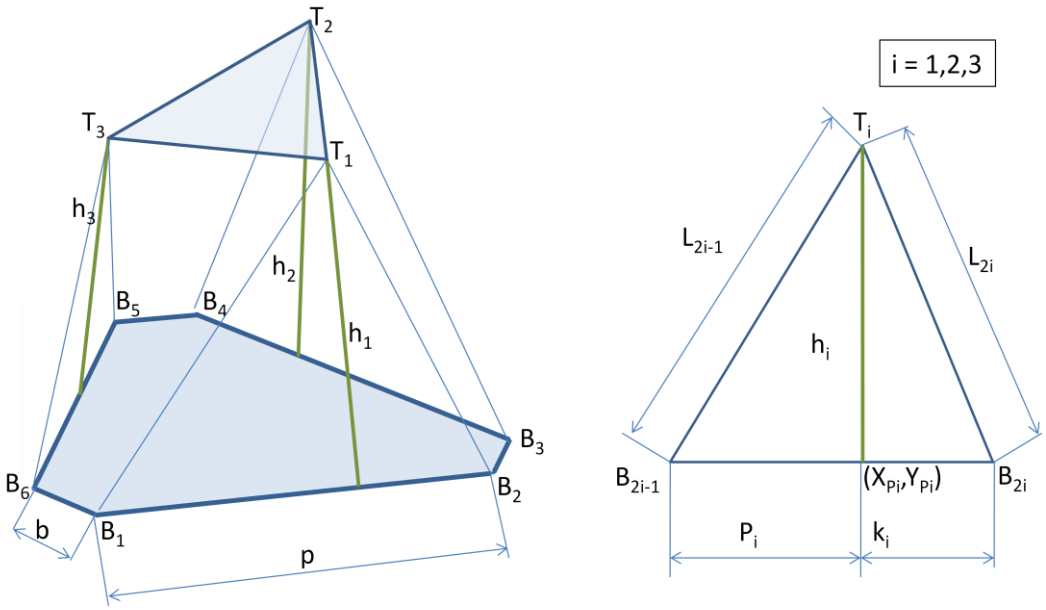

Hexapod Coordinates

Pythagoras's theorem gives the following:

$$h_i = \sqrt{{L_{2-i}}^2 - {P_i}^2} \quad i = 1,2,3. \tag{0-8}$$

Considering the case where $i = 1$:

$${h_1}^2 = {L_1}^2 - {P_1}^2, \text{and} \tag{0-9}$$

$${h_1}^2 = {L_2}^2 - {k_1}^2. \tag{0-10}$$

At the base of the triangle, the following is valid:

$$k_1 = p - P_1. \tag{0-11}$$

Equating (0-9) and (0-10) leads to:

$${L_1}^2 - {P_1}^2 = {L_2}^2 - {k_1}^2. \tag{0-12}$$

Substituting (0-11) into (0-12) gives:

$${L_1}^2 - {P_1}^2 = {L_2}^2 - (p - P_1)^2. \tag{0-13}$$

The resultant general expression for the base is:

$$P_i = \frac{1}{2b}(b^2 + L_{2i-1}^2 - L_{2i}^2) \quad i = 1,2,3. \tag{0-14}$$

After establishing an expression of the location of the base coordinates (X_{Pi}, Y_{Pi}), it is necessary to determine the location of the platform. The edges of the platform are located along the green lines shown in the following Figure.

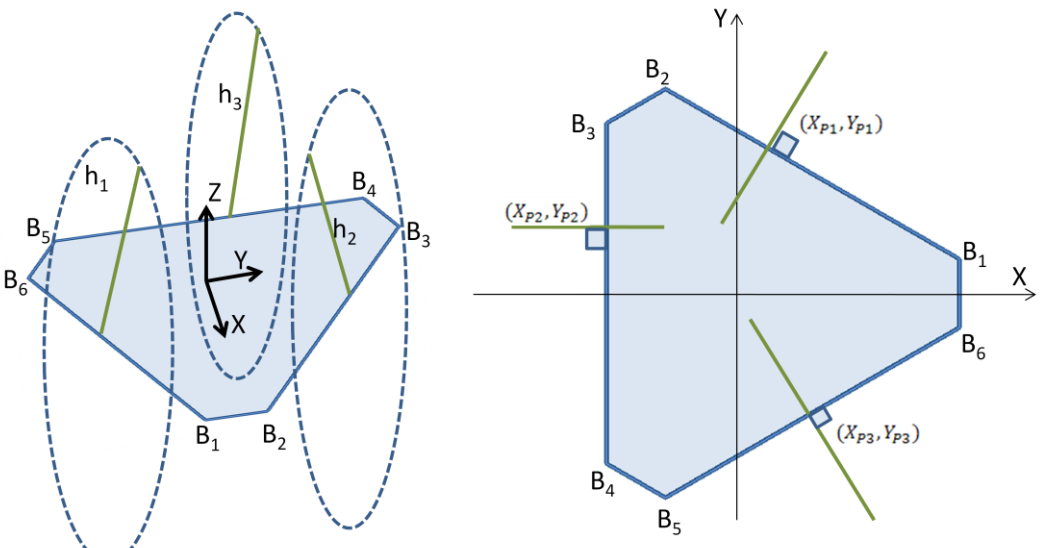

Top View of Base

These lines are generated by the rotation of h_i (where $i = 1,2,3$) about the base of the triangles for which they are defined.

The points of intersection are:

$$X_{P1} = \frac{\sqrt{3}}{6}(2b + d - 3P_1), \tag{0-15}$$

$$X_{P2} = -\frac{\sqrt{3}}{6}(b + 2d), \tag{0-16}$$

$$X_{P3} = -\frac{\sqrt{3}}{6}(b - d - 3P_3), \tag{0-17}$$

$$Y_{P1} = \frac{1}{2}(d + P_1), \tag{0-18}$$

$$Y_{P2} = \frac{1}{2}(b - 2P_2) \text{ and} \tag{0-19}$$

$$Y_{P3} = -\frac{1}{2}(b + d - P_3). \tag{0-20}$$

By utilising the gradients of each of the lines shown in the previous Figure, the following equations are defined:

$$Y_{T1} = \sqrt{3}X_{T1} - \left(\sqrt{3}X_{P1} - Y_{P1}\right) = \sqrt{3}X_{T1} + \frac{1}{b}(L_1^2 - L_2^2), \quad \textbf{(0-21)}$$

$$Y_{T2} = Y_{P2} = \frac{1}{2b}(L_4^2 - L_3^2) \text{ and} \quad \textbf{(0-22)}$$

$$Y_{T3} = -\sqrt{3}X_{T3} + \left(\sqrt{3}X_{P3} + Y_{P3}\right) = -\sqrt{3}X_{T3} + \frac{1}{b}(L_5^2 - L_6^2). \quad \textbf{(0-23)}$$

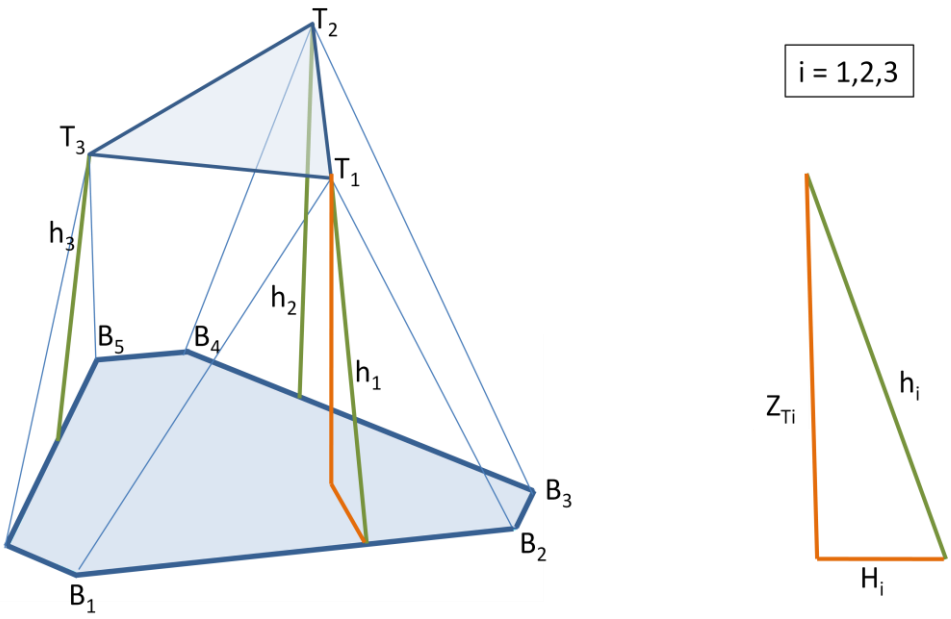

Definition of H_i

Continuing to describe the position of the platform, a further parameter H_i is defined as the projection of h_i on the X-Y plane:

$$H_i = \sqrt{(X_{Ti} - X_{Pi})^2 + (Y_{Ti} - Y_{Pi})^2} \text{ and} \quad \textbf{(0-24)}$$

$$Z_{Ti} = \sqrt{h_i^2 - H_i^2}. \quad \textbf{(0-25)}$$

Utilizing equations (0-15) to (0-23), the z-coordinates of the top platform are expressed as:

$$Z_{T1} = \sqrt{h_1^2 - 4(X_{T1} - X_{P1})^2}, \quad \textbf{(0-26)}$$

$$Z_{T2} = \sqrt{h_2^2 - (X_{T2} - X_{P2})^2} \text{ and} \quad \textbf{(0-27)}$$

$$Z_{T3} = \sqrt{h_3^2 - 4(X_{T3} - X_{P3})^2}. \quad \textbf{(0-28)}$$

The final step in the derivation of the forward kinematic equations entails the derivation of three equations with three variables. The platform parameters required in this step are illustrated below.

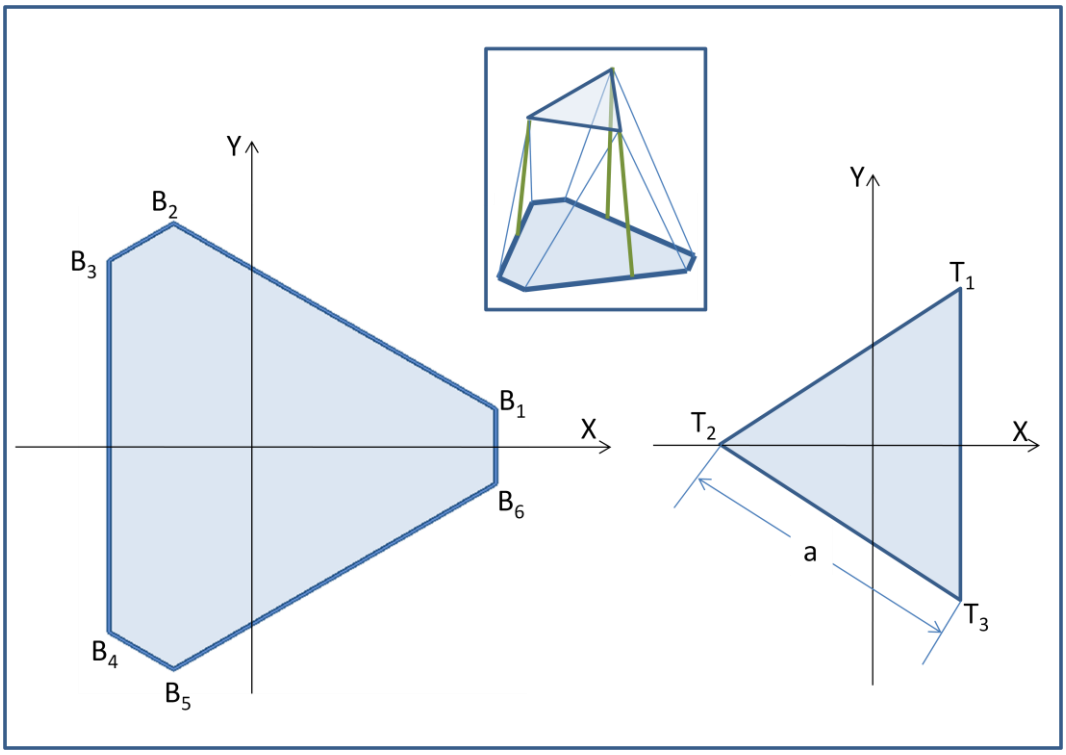

Platform Parameters

The top platform's sides have a fixed length of a. This is the distance between the corners of the platform and can be expressed as:

$$|T_1 - T_2| = |T_2 - T_3| = |T_3 - T_1| = a. \quad \textbf{(0-29)}$$

Substituting the platform coordinates into the first constraint, $|T_1 - T_2| = a$, yields:

$$\sqrt{(X_{T1} - X_{T2})^2 + (Y_{T1} - Y_{T2})^2 + (Z_{T1} - Z_{T2})^2} = a. \quad \textbf{(0-30)}$$

This can be simplified with substitution to:

$$a^2 + 2X_{T1}X_{T2} - 2X_{T1}\left(X_{P1} + \sqrt{3}(Y_{P1} - Y_{P2})\right) - 2X_{P2}X_{T2}$$
$$-((\sqrt{3}X_{P1} - Y_{P1} + Y_{P2})^2 + (h_1^2 + h_2^2) - 4X_{P1}^2 - X_{P2}^2) \quad \textbf{(0-31)}$$
$$+2\sqrt{(h_1^2 - 4(X_{T1} - X_{P1})^2)(h_2^2 - (X_{T2} - X_{P2})^2)} = 0.$$

In a similar fashion, the following two equations are also derived:

$$a^2 - 4X_{T1}X_{T3} - 2X_{T1}\left(X_{P1} + 3X_{P3} + \sqrt{3}(Y_{P1} - Y_{P2})\right)$$
$$-2X_{T3}\left(-3X_{P1} + X_{P3} + \sqrt{3}(Y_{P1} - Y_{P3}\right)$$
$$-((\left(\sqrt{3}(X_{P1} + X_{P3}\right) - Y_{P1} + Y_{P3})^2 + (h_1^2 + h_3^2) - 4X_{P1}^2 \quad \textbf{(0-32)}$$
$$- 4X_{P3}^2)$$
$$+2\sqrt{(h_1^2 - 4(X_{T1} - X_{P1})^2)(h_3^2 - 4(X_{T3} - X_{P3})^2)} = 0 \; and$$

$$a^2 + 2X_{T2}X_{T3} - 2X_{T3}\left(X_{P3} + \sqrt{3}(Y_{P2} - Y_{P3})\right) - 2X_{P2}X_{T2}$$
$$-((\sqrt{3}X_{P3} - Y_{P2} + Y_{P3})^2 + (h_2^2 + h_3^2) - X_{P2}^2 - 4X_{P3}^2) \quad \textbf{(0-33)}$$
$$+2\sqrt{(h_2^2 - (X_{T2} - X_{P2})^2)(h_3^2 - (X_{T3} - X_{P3})^2)} = 0.$$

The previous three equations have only three unknowns: X_{T1}, X_{T2} and X_{T3}. Solving the equations for these unknowns is the key step in the derivation of the forward kinematics equations

Once equations (0-31), (0-32) and (0-33) are solved, it is necessary to obtain the platform's *y* and *z* coordinates. This is done by simply substituting the X values into equations (0-21), (0-22) and (0-23) to obtain the Y values and (0-26), (0-27) and (0-28) to obtain the Z values. The platform's position and orientation can now be completely described and the forward kinematics is complete.

Proof of Equation (3-6) also (0-31):

We want to derive:

$$a^2 + 2X_{T1}X_{T2} - 2X_{T1}\left(X_{P1} + \sqrt{3}(Y_{P1} - Y_{P2})\right) - 2X_{P2}X_{T2}$$

$$-((\sqrt{3}X_{P1} - Y_{P1} + Y_{P2})^2 + (h_1^2 + h_2^2) - 4X_{P1}^2 - X_{P2}^2)$$

$$+2\sqrt{(h_1^2 - 4(X_{T1} - X_{P1})^2)(h_2^2 - (X_{T2} - X_{P2})^2)} = 0.$$

Since all the sides of the platform are equal to a:

$$|T_1 - T_2| = |T_2 - T_3| = |T_3 - T_1| = a. \quad \textbf{(0-34)}$$

Taking the first part of the equation above:

$$|T_1 - T_2| = a, \quad \textbf{(0-35)}$$

$$\sqrt{(X_{T1} - X_{T2})^2 + (Y_{T1} - Y_{T2})^2 + (Z_{T1} - Z_{T2})^2} = a. \quad \textbf{(0-36)}$$

This simplifies to:

$$\sqrt{(X_{T1} - X_{T2})^2 + (Y_{T1} - Y_{T2})^2 + (Z_{T1} - Z_{T2})^2} = a, \text{or} \quad \textbf{(0-37)}$$

$$(X_{T1} - X_{T2})^2 + (Y_{T1} - Y_{T2})^2 + (Z_{T1} - Z_{T2})^2 - a^2 = 0. \quad \textbf{(0-38)}$$

Multiplying out leads to:

$$X_{T1}{}^2 - 2X_{T1}X_{T2} + X_{T2}{}^2 + Y_{T1}{}^2 - 2Y_{T1}Y_{T2} + Y_{T2}{}^2 + Z_{T1}{}^2 - 2Z_{T1}Z_{T2} + Z_{T2}{}^2 - a^2 = 0. \quad \textbf{(0-39)}$$

Substituting in equations (0-21), (0-22), (0-26) and (0-27) into (0-39) produces:

$$X_{T1}{}^2 - 2X_{T1}X_{T2} + X_{T2}{}^2 + (\sqrt{3}X_{T1} - (\sqrt{3}X_{P1} - Y_{P1}))^2 - 2\left(\sqrt{3}X_{T1} - (\sqrt{3}X_{P1} - Y_{P1})\right)Y_{P2} + Y_{P2}{}^2 + h_1^2 - 4(X_{T1} - X_{P1})^2 - 2\left(\sqrt{h_1^2 - 4(X_{T1} - X_{P1})^2}\right)\sqrt{h_2^2 - (X_{T2} - X_{P2})^2} + h_2^2 - (X_{T2} - X_{P2})^2 - a^2 = 0. \quad \textbf{(0-40)}$$

Equation (3.6) is multiplied with -1, giving:

$$-a^2 - 2X_{T1}X_{T2} + 2X_{T1}\left(X_{P1} + \sqrt{3}(Y_{P1} - Y_{P2})\right) + 2X_{P2}X_{T2} + (\sqrt{3}X_{P1} - Y_{P1} + Y_{P2})^2 + h_1^2 + h_2^2 - 4X_{P1}^2 - X_{P2}^2 - 2\sqrt{(h_1^2 - 4(X_{T1} - X_{P1})^2)(h_2^2 - (X_{T2} - X_{P2})^2)} = 0. \quad \textbf{(0-41)}$$

Equation (0-40) is now further simplified. It will be reduced to the form of (0-41). Once parts of the proof are in the same form as equation (0-41) they are written in bold, to highlight the changes made in the equation.

$$\mathbf{-a^2 - 2X_{T1}X_{T2}} + X_{T1}{}^2 + X_{T2}{}^2 + (\sqrt{3}X_{T1} - (\sqrt{3}X_{P1} - Y_{P1}))^2 - 2\left(\sqrt{3}X_{T1} - (\sqrt{3}X_{P1} - Y_{P1})\right)Y_{P2} + Y_{P2}{}^2 + \mathbf{h_1^2} + \mathbf{h_2^2} - 4(X_{T1} - X_{P1})^2 - (X_{T2} - X_{P2})^2 - \mathbf{2\sqrt{(h_1^2 - 4(X_{T1} - X_{P1})^2)(h_2^2 - (X_{T2} - X_{P2})^2)}} = 0 \quad \textbf{(0-42)}$$

when expanded gives

$$-\boldsymbol{a^2} - \boldsymbol{2X_{T1}X_{T2}} + {X_{T1}}^2 + {X_{T2}}^2 + 3{X_{T1}}^2 - 2\sqrt{3}X_{T1}\left(\sqrt{3}X_{P1} - Y_{P1}\right) + \left(\sqrt{3}X_{P1} - Y_{P1}\right)^2 - 2\sqrt{3}X_{T1}Y_{P2} + 2\left(\sqrt{3}X_{P1} - Y_{P1}\right)Y_{P2} + {Y_{P2}}^2 + \boldsymbol{h_1^2 + h_2^2} - 4(X_{T1} - X_{P1})^2 - (X_{T2} - X_{P2})^2 - \boldsymbol{2\sqrt{(h_1^2 - 4(X_{T1} - X_{P1})^2)(h_2^2 - (X_{T2} - X_{P2})^2)}} = 0. \quad \textbf{(0-43)}$$

The ${X_{T1}}^2$ terms now cancel out:

$$-\boldsymbol{a^2} - \boldsymbol{2X_{T1}X_{T2}} + 4{X_{T1}}^2 + {X_{T2}}^2 - 2\sqrt{3}X_{T1}\left(\sqrt{3}X_{P1} - Y_{P1}\right) + 3{X_{P1}}^2 - 2\sqrt{3}X_{P1}Y_{P1} + {Y_{P1}}^2 - 2\sqrt{3}X_{T1}Y_{P2} + 2\left(\sqrt{3}X_{P1} - Y_{P1}\right)Y_{P2} + {Y_{P2}}^2 + \boldsymbol{h_1^2 + h_2^2} - 4{X_{T1}}^2 + 8X_{T1}X_{P1} - {X_{P1}}^2 - {X_{T2}}^2 + 2X_{P2}X_{T2} - {X_{P2}}^2 - \boldsymbol{2\sqrt{(h_1^2 - 4(X_{T1} - X_{P1})^2)(h_2^2 - (X_{T2} - X_{P2})^2)}} = 0. \quad \textbf{(0-44)}$$

Further expansion of terms gives us:

$$-\boldsymbol{a^2} - \boldsymbol{2X_{T1}X_{T2}} + 4{X_{T1}}^2 + {X_{T2}}^2 - 6X_{T1}X_{P1} + 2\sqrt{3}X_{T1}Y_{P1} + 3{X_{P1}}^2 - 2\sqrt{3}X_{P1}Y_{P1} + {Y_{P1}}^2 - 2\sqrt{3}X_{T1}Y_{P2} + 2\sqrt{3}X_{P1}Y_{P2} - 2Y_{P1}Y_{P2} + {Y_{P2}}^2 + \boldsymbol{h_1^2 + h_2^2} - 4{X_{T1}}^2 + 8X_{T1}X_{P1} - \boldsymbol{4{X_{P1}}^2} - {X_{T2}}^2 + 2X_{P2}X_{T2} - {X_{P2}}^2 - \boldsymbol{2\sqrt{(h_1^2 - 4(X_{T1} - X_{P1})^2)(h_2^2 - (X_{T2} - X_{P2})^2)}} = 0. \quad \textbf{(0-45)}$$

Rearrangement and cancellation of the ${X_{T1}}^2$ terms leads to:

$$-\boldsymbol{a^2 - 2X_{T1}X_{T2}} - 6X_{T1}X_{P1} + 2\sqrt{3}X_{T1}Y_{P1} + [3{X_{P1}}^2 + {Y_{P2}}^2 + {Y_{P1}}^2 - 2\sqrt{3}X_{P1}Y_{P1} + 2\sqrt{3}X_{P1}Y_{P2} - 2Y_{P1}Y_{P2}]$$
$$- 2\sqrt{3}X_{T1}Y_{P2} + \boldsymbol{h_1^2 + h_2^2} + 8X_{T1}X_{P1} - \boldsymbol{4{X_{P1}}^2} + 2X_{P2}X_{T2} - {X_{P2}}^2$$
$$- \boldsymbol{2\sqrt{(h_1^2 - 4(X_{T1} - X_{P1})^2)(h_2^2 - (X_{T2} - X_{P2})^2)}} = 0. \quad \textbf{(0-46)}$$

Using the substitution $(\sqrt{3}X_{P1} - Y_{P1} + Y_{P2})^2 = 3{X_{P1}}^2 + {Y_{P2}}^2 + {Y_{P1}}^2 - 2\sqrt{3}X_{P1}Y_{P1} + 2\sqrt{3}X_{P1}Y_{P2} - 2Y_{P1}Y_{P2}$ leads to:

$$-\boldsymbol{a^2 - 2X_{T1}X_{T2}} + 2X_{T1}X_{P1} + 2\sqrt{3}X_{T1}Y_{P1} + \boldsymbol{(\sqrt{3}X_{P1} - Y_{P1} + Y_{P2})^2} - 2\sqrt{3}X_{T1}Y_{P2} + \boldsymbol{h_1^2 + h_2^2 - 4{X_{P1}}^2}$$
$$+ 2X_{P2}X_{T2} - {X_{P2}}^2 - \boldsymbol{2\sqrt{(h_1^2 - 4(X_{T1} - X_{P1})^2)(h_2^2 - (X_{T2} - X_{P2})^2)}} = 0. \quad \textbf{(0-47)}$$

Rearranging the terms gives (0-48) gives the equation:

$$-\boldsymbol{a^2 - 2X_{T1}X_{T2}} + 2X_{T1}X_{P1} + 2\sqrt{3}X_{T1}Y_{P1} - 2\sqrt{3}X_{T1}Y_{P2} + \boldsymbol{(\sqrt{3}X_{P1} - Y_{P1} + Y_{P2})^2} + \boldsymbol{h_1^2 + h_2^2 - 4{X_{P1}}^2}$$
$$+ 2X_{P2}X_{T2} - {X_{P2}}^2 - \boldsymbol{2\sqrt{(h_1^2 - 4(X_{T1} - X_{P1})^2)(h_2^2 - (X_{T2} - X_{P2})^2)}} = 0. \quad \textbf{(0-48)}$$

A final simplification leads to:

$$\boldsymbol{-a^2 - 2X_{T1}X_{T2} + 2X_{T1}\left(X_{P1} + \sqrt{3}(Y_{P1} - Y_{P2})\right) + (\sqrt{3}X_{P1} - Y_{P1} + Y_{P2})^2 + h_1^2 + h_2^2 - 4{X_{P1}}^2 + 2X_{P2}X_{T2}}$$
$$\boldsymbol{- {X_{P2}}^2 - 2\sqrt{(h_1^2 - 4(X_{T1} - X_{P1})^2)(h_2^2 - (X_{T2} - X_{P2})^2)} = 0,} \quad \textbf{(0-49)}$$

which is the equal to (0-41).

Therefore equation (3-6), or (0-31), is correct. Equations (3-7), or (0-32), and (3-8), or (0-33), can be proven in a similar fashion.

Dynamics

D'Alemberts principle can be expressed as:

$$\sum_{i=1}^{N}(F_i - m_i\ddot{r}_i)\delta r_i = 0 \qquad i = 1,2 \ldots N \tag{0-50}$$

F_i = applied force

m_i= mass of particle

$m_i\ddot{r}_i$ = inertia force

The advantage of D'Alemberts procedure over Newton-Euler's method is that all the reaction forces do not need to be calculated.

Derivation of Dynamics Equations

The derivation of the dynamics is presented in order to show how the forces in the legs were calculated for given angular and displacement accelerations.

The inertia of the platform is expressed in terms of the base coordinates:

$${}^{B}I_P = {}^{B}R_T\,{}^{T}I_P\,{}^{T}R_B. \tag{0-51}$$

In order to convert coordinates from the top platform coordinate system to the base coordinates, a rotation matrix (${}^{B}R_T$) is used,

$$t_i = {}^{B}R_T\,{}^{T}t_i. \tag{0-52}$$

Where t_i are the vectors of the platform coordinates referenced to the platform

One assumption made during the formulation of the dynamics, is that each leg is connected to the base by a universal joint. This prohibits the rotation about the longitudinal axis and leads to the rotation sequence, shown below.

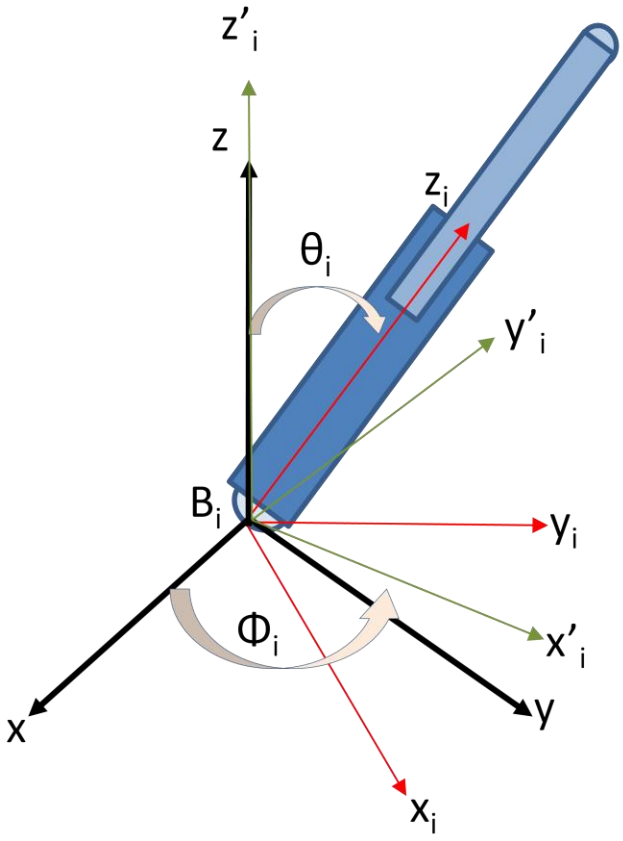

Leg Detail Illustrating Rotation Sequenc

The rotation sequence consists of:

1. a rotation φ_i about the *z*-axis which creates a (x'_i, y'_i, z'_i) system.
2. followed by a rotation θ_i about the rotated y'_i-axis.

The rotation matrix uses the following definitions:

$$cos\theta_i = s_{iz}, \quad \textbf{(0-53)}$$

$$\sin\theta_i = \sqrt{{s_{ix}}^2 + {s_{iy}}^2}, \quad \textbf{(0-54)}$$

$$sin\emptyset_i = \frac{s_{iy}}{sin\theta_i} \text{ and} \quad \textbf{(0-55)}$$

$$cos\emptyset_i = \frac{s_{iy}}{sin\theta}. \quad \textbf{(0-56)}$$

The rotation matrix is described by two Euler Angles. (There is a rotation $\emptyset$ about the z-axis, then a second rotation θabout the rotated y-axis.) An assumption is

made that each limb is connected to the base with a universal joint and cannot rotate about its longitudinal axis.

$$ {}^{B}R_i = \begin{bmatrix} \cos\emptyset_i cos\theta_i & -\sin\emptyset_i & \cos\emptyset_i \sin\theta_i \\ sin\emptyset_i cos\theta_i & \cos\emptyset_i & sin\emptyset_i \sin\theta_i \\ -\sin\theta_i & 0 & cos\theta_i \end{bmatrix} \quad \textbf{(0-57)} $$

The velocity of each leg is calculated using the displacement velocity and angular velocity:

$$ v_{ti} = v_m + \omega_m \times t_i \text{ and} \quad \textbf{(0-58)} $$

$$ {}^{i}v_{ti} = {}^{i}R_B v_{ti}. \quad \textbf{(0-59)} $$

Angular velocity of each leg is calculated by:

$$ {}^{i}\omega_i = \frac{1}{d_i}({}^{i}s_i \times {}^{i}v_{ti}) = \frac{1}{d_i}\begin{bmatrix} -{}^{i}v_{tiy} \\ {}^{i}v_{tix} \\ 0 \end{bmatrix}. \quad \textbf{(0-60)} $$

Angular acceleration of each leg:

$$ {}^{i}\dot{\omega}_i = \frac{1}{d_i}\begin{bmatrix} -{}^{i}\dot{v}_{tiy} + \frac{2^{i}v_{tiz}\ {}^{i}v_{tiy}}{d_i} \\ {}^{i}\dot{v}_{tix} - \frac{2^{i}v_{tiz}\ {}^{i}v_{tix}}{d_i} \\ 0 \end{bmatrix}. \quad \textbf{(0-61)} $$

As shown in Figure 18, the legs are split into two different components called the piston and the cylinder. The cylinder is connected to the base. The distance from the base joint to the cylinders centre of mass is a constant e_1.

$$ {}^{i}\dot{v}_{1i} = \frac{e_1}{d_i}\begin{bmatrix} -{}^{i}\dot{v}_{tix} + \frac{2^{i}v_{tiz}\ {}^{i}v_{tix}}{d_i} \\ {}^{i}\dot{v}_{tix} - \frac{2^{i}v_{tiz}\ {}^{i}v_{tiy}}{d_i} \\ -\frac{{}^{i}v_{tix}^2 + {}^{i}v_{tiy}^2}{d_i} \end{bmatrix} \quad \textbf{(0-62)} $$

The piston is connected to the platform. The distance from the top platform joint to the centre of mass of the piston is a constant e_2.

$$ {}^{i}\dot{v}_{2i} = \frac{1}{d_i}\begin{bmatrix} (d_i - e_2)\ {}^{i}\dot{v}_{bix} + \dfrac{2e_2\,{}^{i}v_{tiz}\ {}^{i}v_{tix}}{d_i} \\ (d_i - e_2)\ {}^{i}\dot{v}_{tiy} - \dfrac{2e_2\,{}^{i}v_{tiz}\ {}^{i}v_{tiy}}{d_i} \\ d_i\ {}^{i}\dot{v}_{tiz} - \dfrac{e_2({}^{i}v_{tix}^2 + {}^{i}v_{tiy}^2)}{d_i} \end{bmatrix} \quad \textbf{(0-63)} $$

Link Jacobian Matrices (first order partial derivatives):

$$ J_{ti} = \begin{bmatrix} 1 & 0 & 0 & 0 & t_{iz} & -t_{iy} \\ 0 & 1 & 0 & -t_{iz} & 0 & -t_{iy} \\ 0 & 0 & 1 & t_{iy} & -t_{iy} & 0 \end{bmatrix}, \quad \textbf{(0-64)} $$

$$ \begin{aligned} {}^{i}J_{tix} = [&c\emptyset_i c\theta_i, \quad s\emptyset_i c\theta_i, \quad -s\theta_i, \\ &-b_{iz}s\emptyset_i c\theta_i - b_{iy}s\theta_i, \quad b_{iz}c\emptyset_i c\theta_i + b_{ix}s\theta_i, \\ &-b_{iy}c\emptyset_i c\theta_i + b_{ix}s\emptyset_i c\theta_i], \end{aligned} \quad \textbf{(0-65)} $$

$$ {}^{i}J_{tiy} = [-s\emptyset_i, c\emptyset_i, 0, -b_{iz}c\emptyset_i, -b_{iz}s\emptyset_i, -b_{iy}s\emptyset_i + -b_{ix}c\emptyset_i] \quad \textbf{(0-66)} $$

and

$$ \begin{aligned} {}^{i}J_{tiz} = [&c\emptyset_i s\theta_i, \quad s\emptyset_i s\theta_i, \quad -c\theta_i, \\ &-b_{iz}s\emptyset_i s\theta_i + b_{iy}c\theta_i, \quad b_{iz}c\emptyset_i s\theta_i - b_{ix}c\theta_i, \\ &-b_{iy}c\emptyset_i s\theta_i + b_{ix}s\emptyset_i s\theta_i]. \end{aligned} \quad \textbf{(0-67)} $$

Platform Jacobian matrix:

$$ J_m = \begin{bmatrix} {}^{1}J_{t1z} \\ {}^{2}J_{t2z} \\ \vdots \\ {}^{6}J_{t6z} \end{bmatrix}. \quad \textbf{(0-68)} $$

Platform forces due to applied and inertia wrenches:

$$ \hat{F}_m = \begin{bmatrix} m_{top}g - m_{top}\dot{v}_m \\ -{}^{A}I_m\dot{\omega}_m - \omega_m \times ({}^{A}I_m\omega_m) \end{bmatrix}. \quad \textbf{(0-69)} $$

Forces on cylinder attached to base:

$$ {}^{i}\hat{F}_{1i} = \begin{bmatrix} m_{1i}\ {}^{i}R_B g - m_{1i}\ {}^{i}v_{1i} \\ -\ {}^{i}I_{1i}\ {}^{i}\omega_i - \ {}^{i}\omega_i \times ({}^{B}I_{1i}\ {}^{i}\omega_i) \end{bmatrix}. \quad \textbf{(0-70)} $$

Forces on piston attached to platform:

$$ {}^{i}\hat{F}_{2i} = \begin{bmatrix} m_{2i}\ {}^{i}R_B g - m_{2i}\ {}^{i}v_{1i} \\ -\ {}^{i}I_{2i}\ {}^{i}\omega_i - \ {}^{i}\omega_i \times ({}^{B}I_{2i}\ {}^{i}\omega_i) \end{bmatrix}. \quad \textbf{(0-71)} $$

$$ J_x = \begin{bmatrix} {}^{1}J_{1x} \\ {}^{2}J_{2x} \\ \vdots \\ {}^{6}J_{6x} \end{bmatrix} \quad \textbf{(0-72)} $$

$$ J_y = \begin{bmatrix} {}^{1}J_{1y} \\ {}^{2}J_{2y} \\ \vdots \\ {}^{6}J_{6y} \end{bmatrix} \quad \textbf{(0-73)} $$

$$ \hat{F}_x = \begin{bmatrix} \dfrac{e_1\hat{f}_{11x} + (d_1 - e_2)\hat{f}_{21x} + \hat{n}_{11x} + \hat{n}_{21x}}{d_1} \\ \dfrac{e_1\hat{f}_{12x} + (d_2 - e_2)\hat{f}_{22x} + \hat{n}_{12x} + \hat{n}_{22x}}{d_2} \\ \vdots \\ \dfrac{e_1\hat{f}_{16x} + (d_6 - e_2)\hat{f}_{26x} + \hat{n}_{16x} + \hat{n}_{26x}}{d_6} \end{bmatrix} \quad \textbf{(0-74)} $$

$$ \hat{F}_y = \begin{bmatrix} \dfrac{e_1\hat{f}_{11y} + (d_1 - e_2)\hat{f}_{21y} + \hat{n}_{11y} + \hat{n}_{21y}}{d_1} \\ \dfrac{e_1\hat{f}_{12y} + (d_2 - e_2)\hat{f}_{22y} + \hat{n}_{12y} + \hat{n}_{22y}}{d_2} \\ \vdots \\ \dfrac{e_1\hat{f}_{16y} + (d_6 - e_2)\hat{f}_{26y} + \hat{n}_{16y} + \hat{n}_{26y}}{d_6} \end{bmatrix} \quad \textbf{(0-75)} $$

$$\hat{F}_z = \begin{bmatrix} \hat{f}_{21y} \\ \hat{f}_{22y} \\ \vdots \\ \hat{f}_{26y} \end{bmatrix} \quad \textbf{(0-76)}$$

The principle of virtual work leads to:

$$J_m^T\left(\tau + \hat{F}_z\right) + \hat{F}_m + J_x^T\hat{F}_x + J_y^T\hat{F}_y = 0. \quad \textbf{(0-77)}$$

Simplifying:

$$\tau = (J_m^T)^{-1}\left(-\hat{F}_m - J_x^T\hat{F}_x - J_y^T\hat{F}_y\right) - \hat{F}_z. \quad \textbf{(0-78)}$$

Where τ is the force in the legs.

APPENDIX B: SCHEMATICS OF PRINTED CIRCUIT BOARD

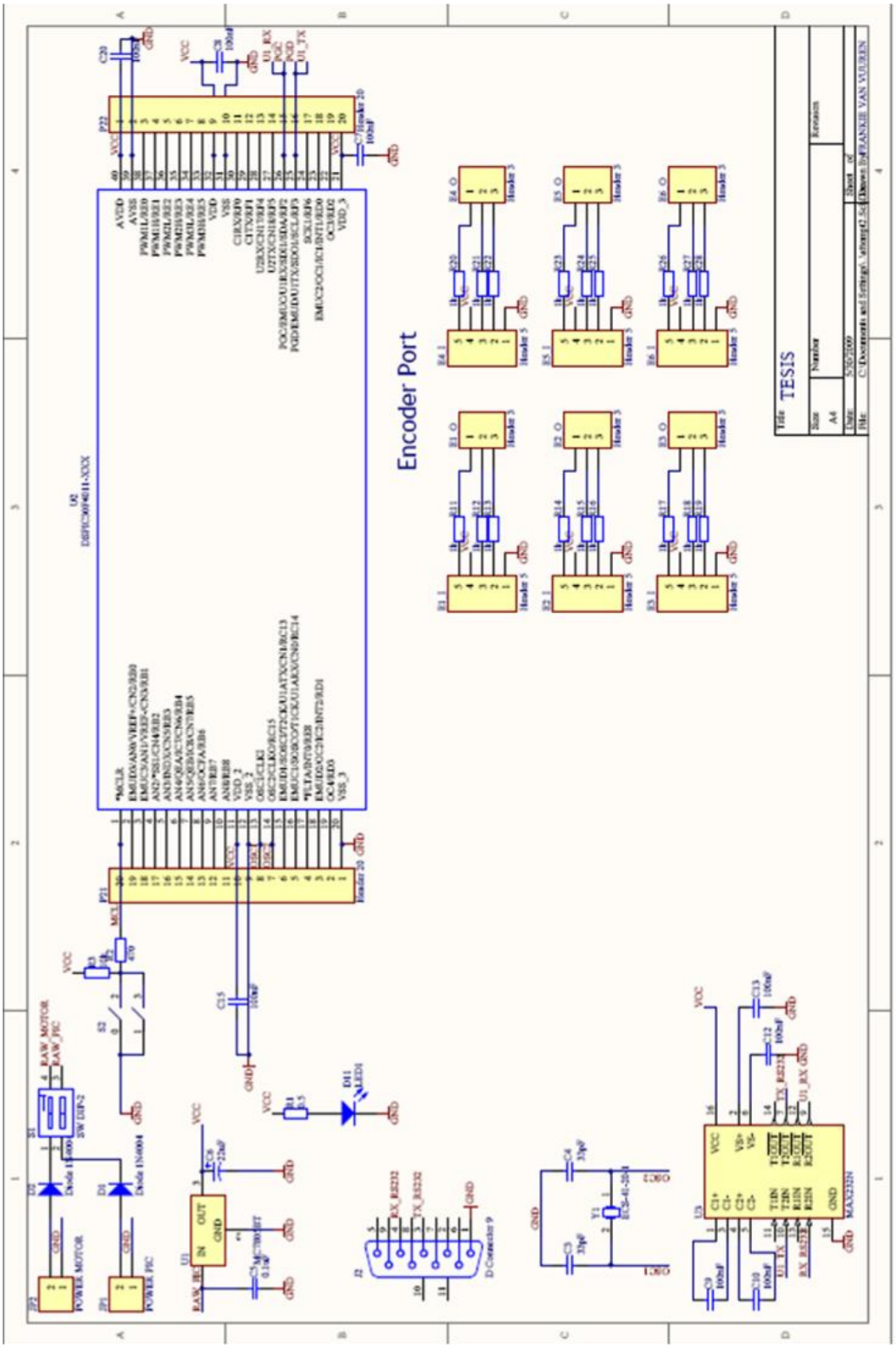

Appendix B: Schematics of Printed Circuit Board

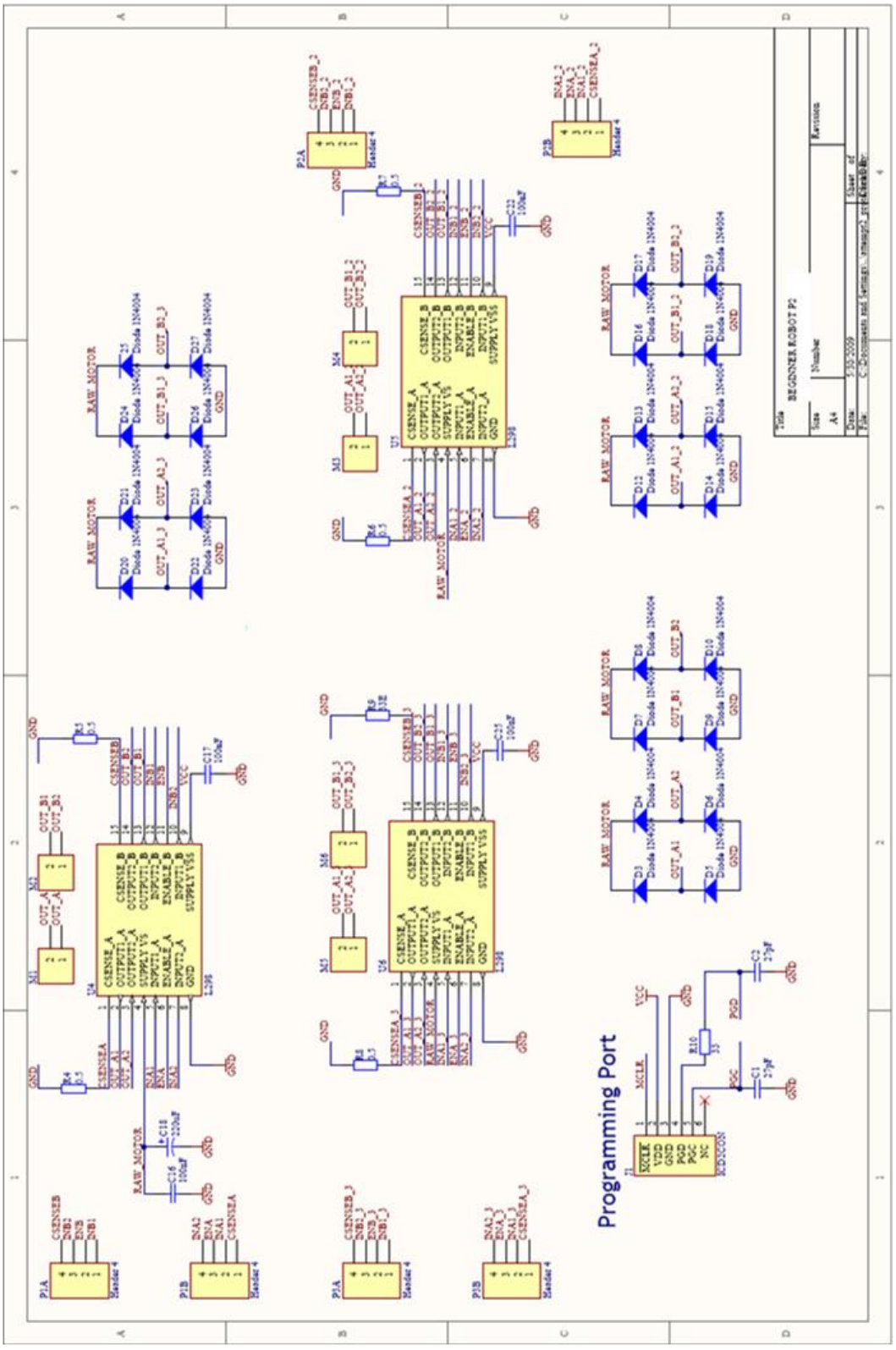

APPENDIX C: DATASHEETS

Excerpts from the most important parameters of components used are presented from their datasheets.

The datasheet below shows the motors selected. The 6 V, 47 rpm motor was selected. As seen from the dimensions this is a very small motor.

QJT-12JS 直齿轮

Spur Gear Type

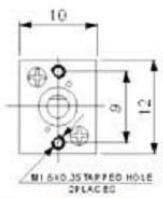

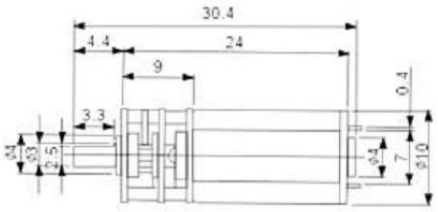

WEIGHT: 9.0g(APPROX)

MODEL	VOLTAGE RATED	NO LOAD		AT MAXIMUM EFFICIENCY				STALL		
		SPEED	CURRENT	SPEED	CURRENT	TORQUE		OUTPUT	TORQUE		CURRENT
	V	rpm	A	rpm	A	g·cm	mN·m	W	g·cm	mN·m	A
QJT-12JS	5	250	0.045	187	0.134	82	8	0.16	330	32.3	0.4
	6	62	0.07	47	0.22	500	49	0.24	2100	205.8	0.7

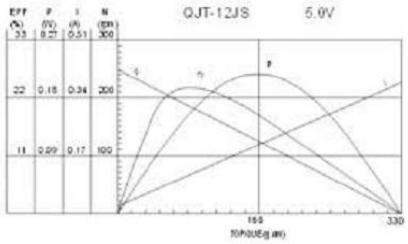

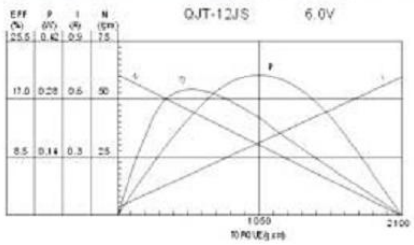

The rotary encoder which was used to measure the leg lengths.

Mechanical Characteristics

Parameter	Symbol	Dimension	Tolerance[1]	Units
Codewheel Fits These Standard Shaft Diameters		2 3 4 5 6 8	+0.000 -0.015	mm
		5/32 1/8 3/16 1/4	+0.0000 -0.0007	in
Moment of Inertia	J	0.6 (8.0 x 10^{-6})		g-cm^2 (oz-in-s^2)
Required Shaft Length[2]		14.0 (0.55)	± 0.5 (± 0.02)	mm (in.)
Bolt Circle[3]	2 screw mounting	19.05 (0.750)	± 0.13 (± 0.005)	mm (in.)
	3 screw mounting	20.90 (0.823)	± 0.13 (± 0.005)	mm (in.)
	external mounting ears	46.0 (1.811)	± 0.13 (± 0.005)	mm (in.)
Mounting Screw Size[4]	2 screw mounting	M 2.5 or (2-56)		mm (in.)
	3 screw mounting	M 1.6 or (0-80)		mm (in.)
	external mounting ears	M 2.5 or (2-56)		mm (in.)
Encoder Base Plate Thickness		0.33 (0.130)		mm (in.)
Hub Set Screw		(2-56)		(in.)

Notes:
1. These are tolerances required of the user.
2. The HEDS-55X5 and 56X5, HEDM-5505, 5605 provide an 8.9 mm (0.35 inch) diameter hole through the housing for longer motor shafts. See Ordering Information.
3. The HEDS-5540 and 5640 must be aligned using the aligning pins as specified in Figure 3, or using the alignment tool as shown in "Encoder Mounting and Assembly". See also "Mounting Considerations."
4. The recommended mounting screw torque for 2 screw and external ear mounting is 1.0 kg-cm (0.88 in-lbs). The recommended mounting screw torque for 3 screw mounting is 0.50 kg-cm (0.43 in-lbs).

Electrical Interface

To insure reliable encodingperformance, the HEDS-5540/5640 and HEDM-5540 three channel encoders require 2.7 kΩ (± 10%) pull-up resistors on output pins 2, 3, and 5 (Channels I, A, and B) as shown in Figure 1. These pull-up resistors should be located as close to the encoder as possible (within 4 feet). Each of the three encoder outputs can drive a single TTL load in this configuration. The HEDS-5500, 5600, and HEDM-5500, 5600 two channel encoders do not normally require pull-up resistors. However, 3.2 kΩ pull-up resistors on output pins 3 and 5 (Channels A and B) are recommended to improve rise times, especially when operating above 100 kHz frequencies.

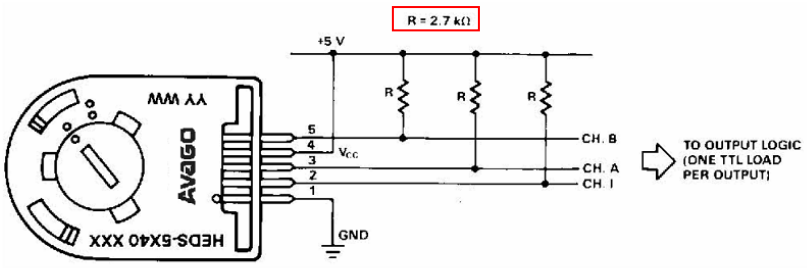

Figure 1. Pull-up Resistors on HEDS-5X40 and HEDM-5540 Encoder Outputs.

Encoder Mounting and Assembly

1a. For HEDS-5500 and 5600: Mount encoder base plate onto motor. Tighten screws. Go on to step 2.

1b. For HEDS-5540, 5640 and HEDM-5500, 5600, 5540 : Slip alignment tool onto motor shaft. With alignment tool in place, mount encoder baseplate onto motor as shown above. Tighten screws. Remove alignment tool.

1c. It is recommended that adhesive* is applied to the screw-baseplate interface to prevent screw loosening due to effect of high temperature on plastic

2. Snap encoder body onto base plate locking all 4 snaps.

3a. Push the hex wrench into the body of the encoder to ensure that it is properly seated into the code wheel hub set screws. Then apply a downward force on the end of the hex wrench. This sets the code wheel gap by levering the code wheel hub to its upper position.

3b. While continuing to apply a downward force, rotate the hex wrench in the clockwise direction until the hub set screw is tight against the motor shaft (The recommended torque to tighten the setscrew is 15-18 ozf.inch). The hub set screw attaches the code wheel to the motor's shaft.

3c. Remove the hex wrench by pulling it straight out of the encoder body.

4. Use the center screwdriver slot, or either of the two side slots, to rotate the encoder cap dot clockwise from the one dot position to the two dot position. Do not rotate the encoder cap counterclockwise beyond the one dot position.

The encoder is ready for use!

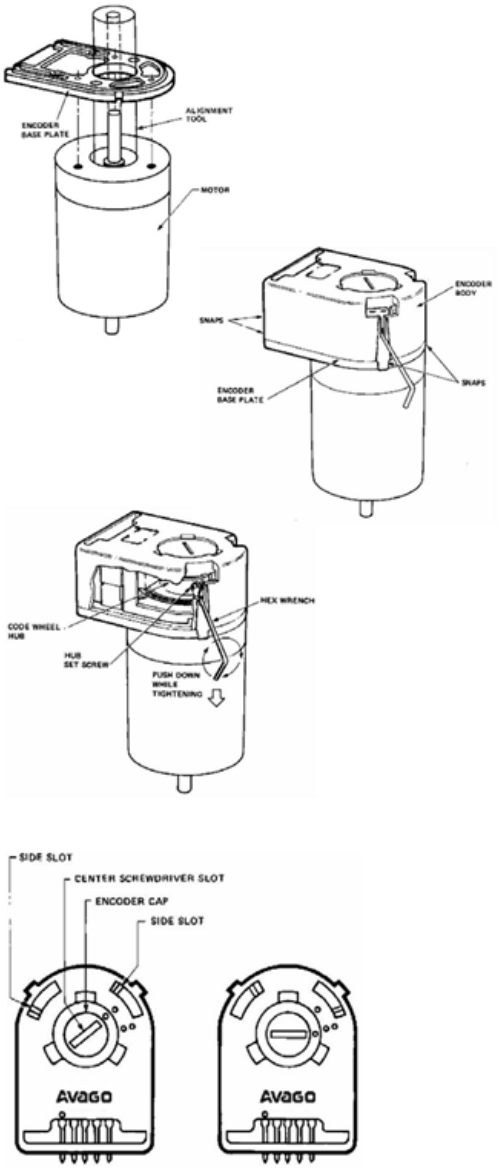

The Dual bridge driver was used to control the speed and direction of the motors and interfaced with the microcontroller.

L298

DUAL FULL-BRIDGE DRIVER

- OPERATING SUPPLY VOLTAGE UP TO 46 V
- TOTAL DC CURRENT UP TO 4 A
- LOW SATURATION VOLTAGE
- OVERTEMPERATURE PROTECTION
- LOGICAL "0" INPUT VOLTAGE UP TO 1.5 V (HIGH NOISE IMMUNITY)

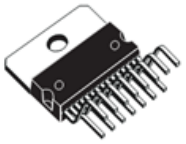

Multiwatt15

PowerSO20

ORDERING NUMBERS : L298N (Multiwatt Vert.)
L298HN (Multiwatt Horiz.)
L298P (PowerSO20)

DESCRIPTION

The L298 is an integrated monolithic circuit in a 15-lead Multiwatt and PowerSO20 packages. It is a high voltage, high current dual full-bridge driver designed to accept standard TTL logic levels and drive inductive loads such as relays, solenoids, DC and stepping motors. Two enable inputs are provided to enable or disable the device independently of the input signals. The emitters of the lower transistors of each bridge are connected together and the corresponding external terminal can be used for the connection of an external sensing resistor. An additional supply input is provided so that the logic works at a lower voltage.

BLOCK DIAGRAM

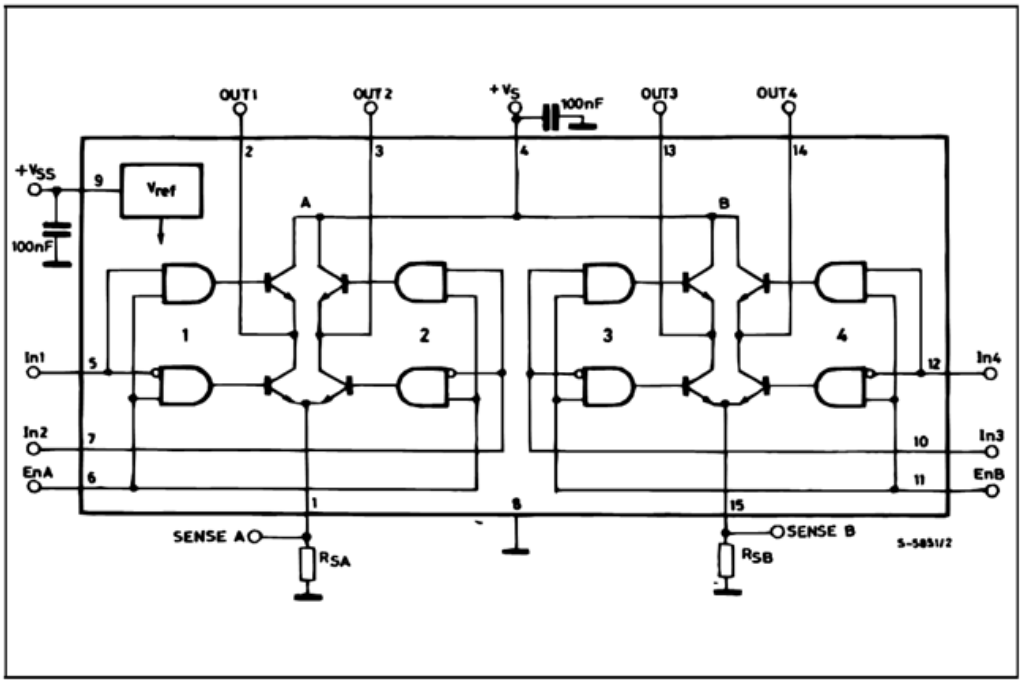

L298

ABSOLUTE MAXIMUM RATINGS

Symbol	Parameter	Value	Unit
V_S	Power Supply	50	V
V_{SS}	Logic Supply Voltage	7	V
V_i,V_{en}	Input and Enable Voltage	–0.3 to 7	V
I_O	Peak Output Current (each Channel) – Non Repetitive (t = 100µs) –Repetitive (80% on –20% off; t_{on} = 10ms) –DC Operation	 3 2.5 2	 A A A
V_{sens}	Sensing Voltage	–1 to 2.3	V
P_{tot}	Total Power Dissipation (T_{case} = 75°C)	25	W
T_{op}	Junction Operating Temperature	–25 to 130	°C
T_{stg}, T_j	Storage and Junction Temperature	–40 to 150	°C

PIN CONNECTIONS (top view)

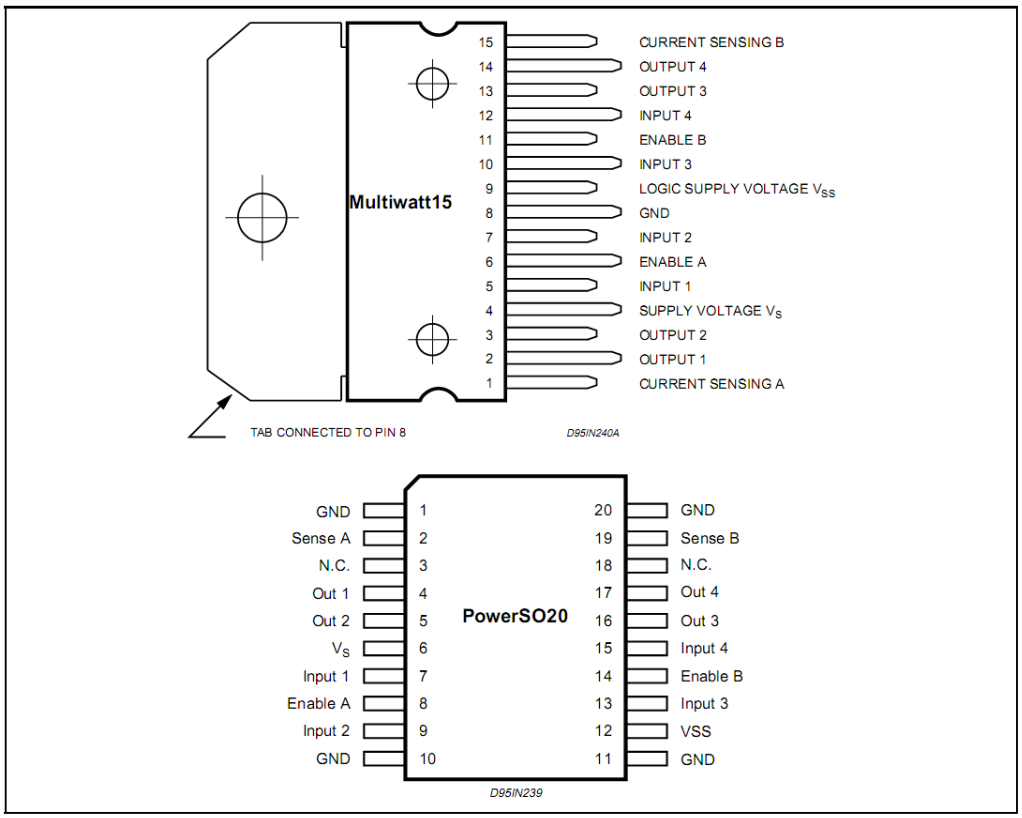

THERMAL DATA

Symbol	Parameter		PowerSO20	Multiwatt15	Unit
$R_{th\ j\text{-}case}$	Thermal Resistance Junction-case	Max.	–	3	°C/W
$R_{th\ j\text{-}amb}$	Thermal Resistance Junction-ambient	Max.	13 (*)	35	°C/W

(*) Mounted on aluminum substrate

Two pages summarizing the layout as well as the functionality of the microcontroller are shown below.

Pin Diagrams

40-Pin PDIP

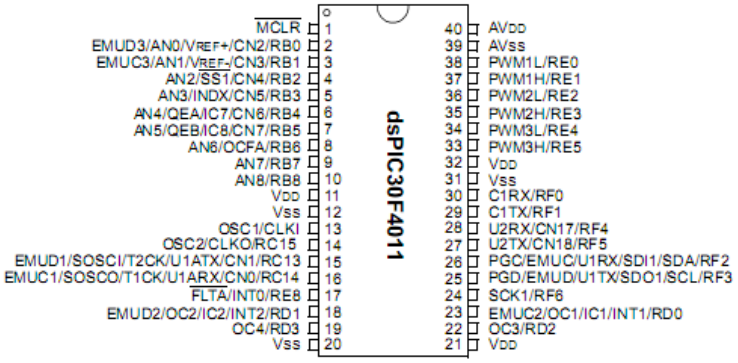

MICROCHIP

dsPIC30F4011/4012

High-Performance, 16-bit Digital Signal Controllers

Note: This data sheet summarizes features of this group of dsPIC30F devices and is not intended to be a complete reference source. For more information on the CPU, peripherals, register descriptions and general device functionality, refer to the "*dsPIC30F Family Reference Manual*" (DS70046). For more information on the device instruction set and programming, refer to the "*dsPIC30F/33F Programmer's Reference Manual*" (DS70157).

High-Performance, Modified RISC CPU:

- Modified Harvard architecture
- C compiler optimized instruction set architecture with flexible addressing modes
- 83 base instructions
- 24-bit wide instructions, 16-bit wide data path
- 48 Kbytes on-chip Flash program space (16K instruction words)
- 2 Kbytes of on-chip data RAM
- 1 Kbyte of nonvolatile data EEPROM
- Up to 30 MIPS operation:
  - DC to 40 MHz external clock input
  - 4 MHz-10 MHz oscillator input with PLL active (4x, 8x, 16x)
- 30 interrupt sources:
  - 3 external interrupt sources
  - 8 user-selectable priority levels for each interrupt source
  - 4 processor trap sources
- 16 x 16-bit working register array

DSP Engine Features:

- Dual data fetch
- Accumulator write-back for DSP operations
- Modulo and Bit-Reversed Addressing modes
- Two, 40-bit wide accumulators with optional saturation logic
- 17-bit x 17-bit single-cycle hardware fractional/integer multiplier
- All DSP instructions are single cycle
- ±16-bit, single-cycle shift

Peripheral Features:

- High-current sink/source I/O pins: 25 mA/25 mA
- Timer module with programmable prescaler:
  - Five 16-bit timers/counters; optionally pair 16-bit timers into 32-bit timer modules
- 16-bit Capture input functions
- 16-bit Compare/PWM output functions
- 3-wire SPI modules (supports 4 Frame modes)
- I^2C™ module supports Multi-Master/Slave mode and 7-bit/10-bit addressing
- 2 UART modules with FIFO Buffers
- 1 CAN module, 2.0B compliant

Motor Control PWM Module Features:

- 6 PWM output channels:
  - Complementary or Independent Output modes
  - Edge and Center-Aligned modes
- 3 duty cycle generators
- Dedicated time base
- Programmable output polarity
- Dead-time control for Complementary mode
- Manual output control
- Trigger for A/D conversions

Quadrature Encoder Interface Module Features:

- Phase A, Phase B and Index Pulse input
- 16-bit up/down position counter
- Count direction status
- Position Measurement (x2 and x4) mode
- Programmable digital noise filters on inputs
- Alternate 16-Bit Timer/Counter mode
- Interrupt on position counter rollover/underflow

Analog Features:

- 10-Bit Analog-to-Digital Converter (A/D) with 4 S/H inputs:
  - 1 Msps conversion rate
  - 9 input channels
  - Conversion available during Sleep and Idle
- Programmable Brown-out Reset

PACIFIC SATELLITE
Room 1101, China Merchant Tower, Shun Tak Centre, 168 Connaught Road Centra
Hong Kong. Tel: 852-29653121 Fax: 852-25580406
Email: albert@pacificsatellite.com www.pacificsatellite.com

COMSTAR® Antennas

COMSTAR MESH DISH

Specification	ST-7	ST-10	ST-12	ST-14.5	PSF-16	PSF-20
Type :	4 section	8 section	8 section	12 section	16 section	20 section
Operating Freq. :	1 to 13 GHz	1 to 13 GHz	1 to 13 GHz	1 to 13 GHz	1 to 13 GHz	1 to 13 GHz
Diameter :	2.3m (90")	3.0m (120")	3.69m (145")	4.5m (177")	4.9m (192")	6.1m (240")
Reflective Material :	Aluminium	Aluminium	Aluminium	Aluminium	Aluminium	Aluminium
Mesh Thickness :	C / Ku Mesh 0.7mm ±0.05mm	C / Ku Mesh 0.7mm ±0.05mm	C / Ku Mesh 0.7mm ±0.05mm	C / Ku Mesh 0.7mm ±0.05mm	C / Ku Mesh 0.7mm ±0.05mm	C / Ku Mesh 0.7mm ±0.05mm
Mounting :	Polar Mount	Polar Mount	Polar Mount	Polar Mount	Fixed Mount	Fixed Mount
F/D Ratio :	0.4	0.38	0.4	0.4	0.4	0.4
Feed :	Prime focus Quad Feed Support	Prime focus Quad Feed Support	Prime focus Quad Feed Support	Prime focus Quad Feed Support	Prime focus Quad Feed Support	Prime focus Quad Feed Support
Pole Size (O.D) :	89mm (3.5")	89mm (3.5")	89mm (3.5")	127 mm (5")	140mm (5.5")	140mm (5.5")
Focal Length :	915mm (36")	1160mm (45 7/8")	1460mm (57 1/2")	1800mm (70 7/8")	1960mm (77")	2440mm (96")
Gain at 4.2 GHz :	38.3 dBi	40.3 dBi	42.3 dBi	43.9 dBi	44.5 dBi	46.0 dBi
Gain at 12.2 GHz :	46.5 dBi	47.8 dBi	49.8 dBi	50.8 dBi	52 dBi	53.1 dBi
First Side Lobe (dB) :	≤-16	≤-18	≤-18	≤-16	≤-16	≤-16
EL Travel Range :	0~90°	0~90°	0~90°	0~90°	0~90°	0~90°
AL Travel Range	0~360°	0~360°	0~360°	0~360°	0~360°	0~360°
Withstand Wind (Operational) :	110km/h	110km/h	110km/h	110km/h	110km/h	110km/h
Weight :						
Reflector - Net Weight	11.5kg	20.5kg	32kg	39kg	55 kg	110 kg
Reflector - Gross Weight	13.5kg	23.5kg	37kg	45kg	136 kg	206 kg
Mount - Net Weight	21kg	28.5kg	29kg	70kg	88 kg	115kg
Mount - Gross Weight	25kg	32kg	36kg	80kg	113kg	135kg
Feedsupport - Net Weight	1.8kg	2.5kg	3kg	21kg		
Feedsupport - Gross Weight	2kg	3kg	3.5kg	23kg		
Packing Size: :						
Reflector	1.17 x 1.17 x 0.13	(1.26+0.065)/2 x 1.53 x 0.25	(1.5+0.09)/2 x 1.9 x 0.23	(1.2+0.07)/2 x 2.53 x 0.5	2.75 x 1.12 x 0.34 m	3.4 x 1.12 x 0.46 m
Mount	0.66 x 0.62 x 0.23	0.88 x 0.88 x 0.18	0.88 x 0.88 x 0.24	1.2 x 1.2 x 0.35	1.24 x 0.77 x 0.53 m	1.24 x 0.77 x 0.53 m
Support	1.3 x 0.05 x 0.05	1.7 x 0.05 x 0.05	2.07 x 0.05 x 0.06	2.45 x 0.10 x 0.14		
Total Volume: :						
Reflector	0.203m^3	0.25m^3	0.453m^3	0.714m^3	1.05m^3	1.75m^3
Mount	0.094m^3	0.139m^3	0.186m^3	0.5m^3	0.51m^3	0.51m^3
Support	0.003m^3	0.004m^3	0.047m^3	0.034m^3		

Beam width[4]	**1.3°**

[4] Specifications of comstar ST12 from http://www.joysky.com.au/DyProducts_1.aspx

APPENDIX D: CAD DRAWINGS

The following are the main assembly drawings of the hexapod.

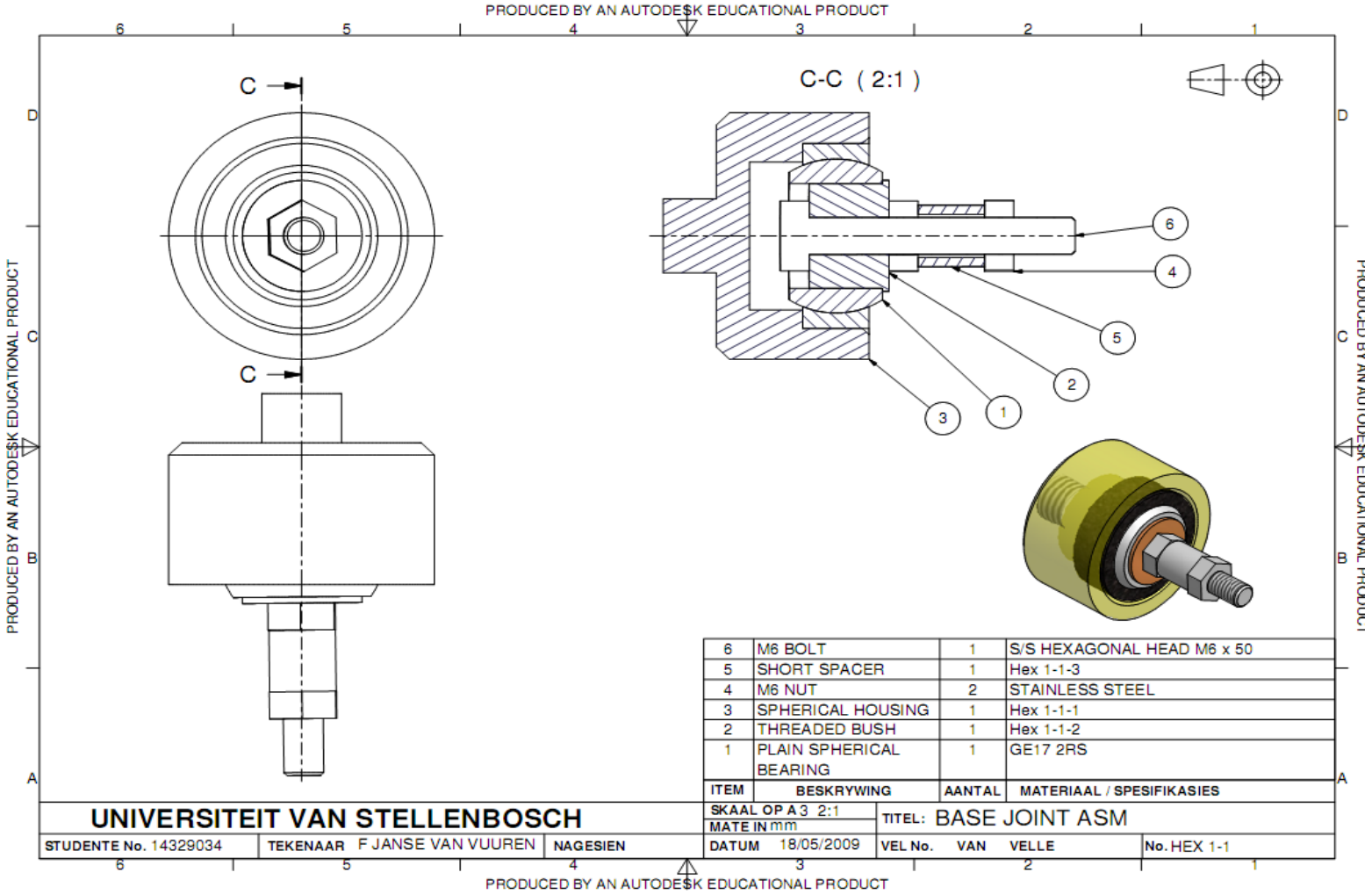

ITEM	BESKRYWING	AANTAL	MATERIAAL / SPESIFIKASIES
6	M6 BOLT	1	S/S HEXAGONAL HEAD M6 x 50
5	SHORT SPACER	1	Hex 1-1-3
4	M6 NUT	2	STAINLESS STEEL
3	SPHERICAL HOUSING	1	Hex 1-1-1
2	THREADED BUSH	1	Hex 1-1-2
1	PLAIN SPHERICAL BEARING	1	GE17 2RS

UNIVERSITEIT VAN STELLENBOSCH

STUDENTE No. 14329034	TEKENAAR F JANSE VAN VUUREN	NAGESIEN	SKAAL OP A3 2:1
			MATE IN mm
			DATUM 18/05/2009

TITEL: BASE JOINT ASM

VEL No. VAN VELLE No. HEX 1-1

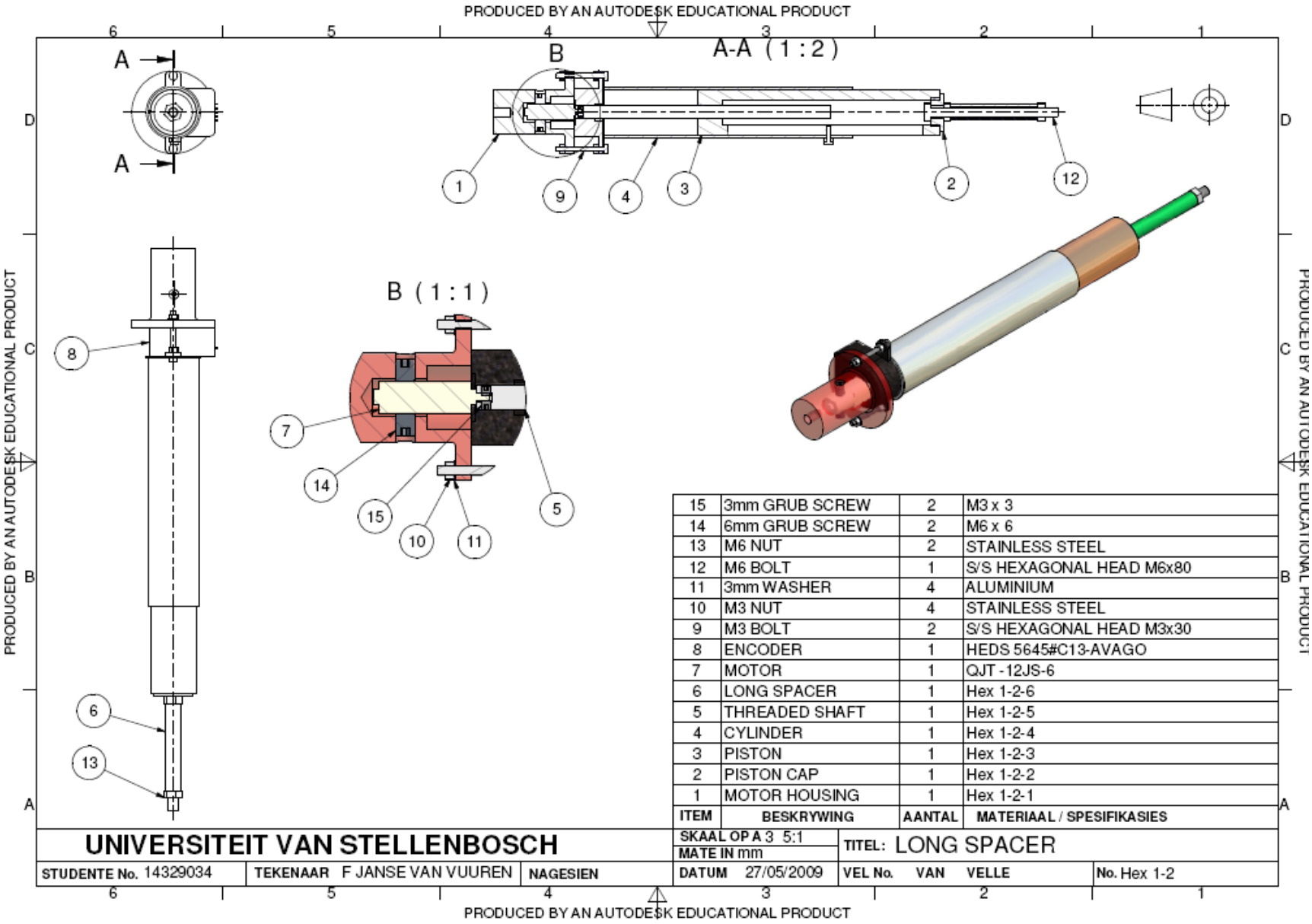
PRODUCED BY AN AUTODESK EDUCATIONAL PRODUCT
A
A
B
A-A (1 : 2)
B (1 : 1)
1
9
4
3
2
12
8
7
14
15
10
11
5
6
13
15 3mm GRUB SCREW 2 M3 x 3
14 6mm GRUB SCREW 2 M6 x 6
13 M6 NUT 2 STAINLESS STEEL
12 M6 BOLT 1 S/S HEXAGONAL HEAD M6x80
11 3mm WASHER 4 ALUMINIUM
10 M3 NUT 4 STAINLESS STEEL
9 M3 BOLT 2 S/S HEXAGONAL HEAD M3x30
8 ENCODER 1 HEDS 5645#C13-AVAGO
7 MOTOR 1 QJT -12JS-6
6 LONG SPACER 1 Hex 1-2-6
5 THREADED SHAFT 1 Hex 1-2-5
4 CYLINDER 1 Hex 1-2-4
3 PISTON 1 Hex 1-2-3
2 PISTON CAP 1 Hex 1-2-2
1 MOTOR HOUSING 1 Hex 1-2-1
ITEM BESKRYWING AANTAL MATERIAAL / SPESIFIKASIES
UNIVERSITEIT VAN STELLENBOSCH
SKAAL OP A 3 5:1
MATE IN mm
TITEL: LONG SPACER
STUDENTE No. 14329034
TEKENAAR F JANSE VAN VUUREN
NAGESIEN
DATUM 27/05/2009
VEL No. VAN VELLE
No. Hex 1-2
PRODUCED BY AN AUTODESK EDUCATIONAL PRODUCT

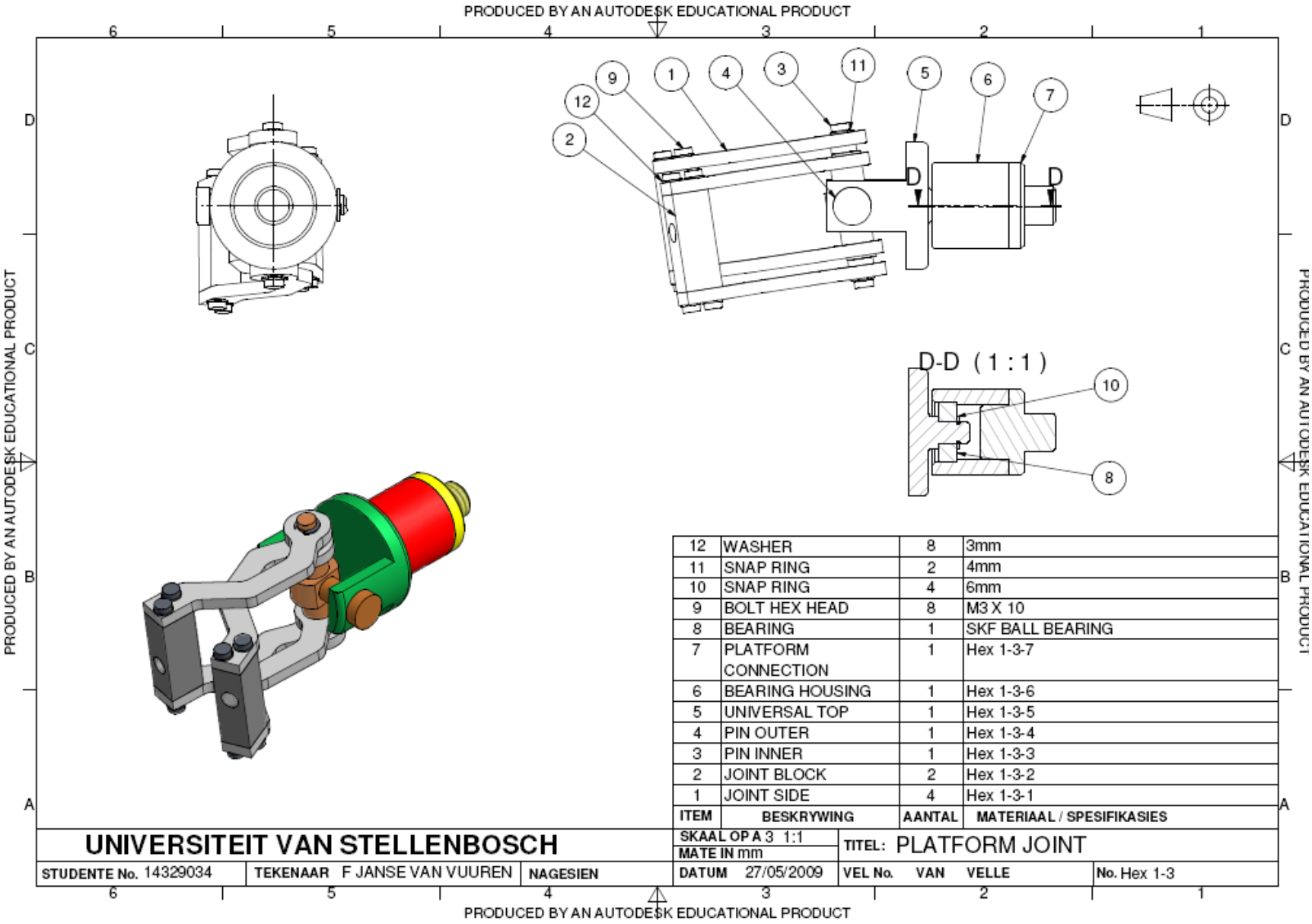

ITEM	BESKRYWING	AANTAL	MATERIAAL / SPESIFIKASIES
12	WASHER	8	3mm
11	SNAP RING	2	4mm
10	SNAP RING	4	6mm
9	BOLT HEX HEAD	8	M3 X 10
8	BEARING	1	SKF BALL BEARING
7	PLATFORM CONNECTION	1	Hex 1-3-7
6	BEARING HOUSING	1	Hex 1-3-6
5	UNIVERSAL TOP	1	Hex 1-3-5
4	PIN OUTER	1	Hex 1-3-4
3	PIN INNER	1	Hex 1-3-3
2	JOINT BLOCK	2	Hex 1-3-2
1	JOINT SIDE	4	Hex 1-3-1

UNIVERSITEIT VAN STELLENBOSCH

SKAAL OP A 3 1:1
MATE IN mm
TITEL: PLATFORM JOINT

STUDENTE No. 14329034 | TEKENAAR F JANSE VAN VUUREN | NAGESIEN | DATUM 27/05/2009 | VEL No. VAN VELLE | No. Hex 1-3

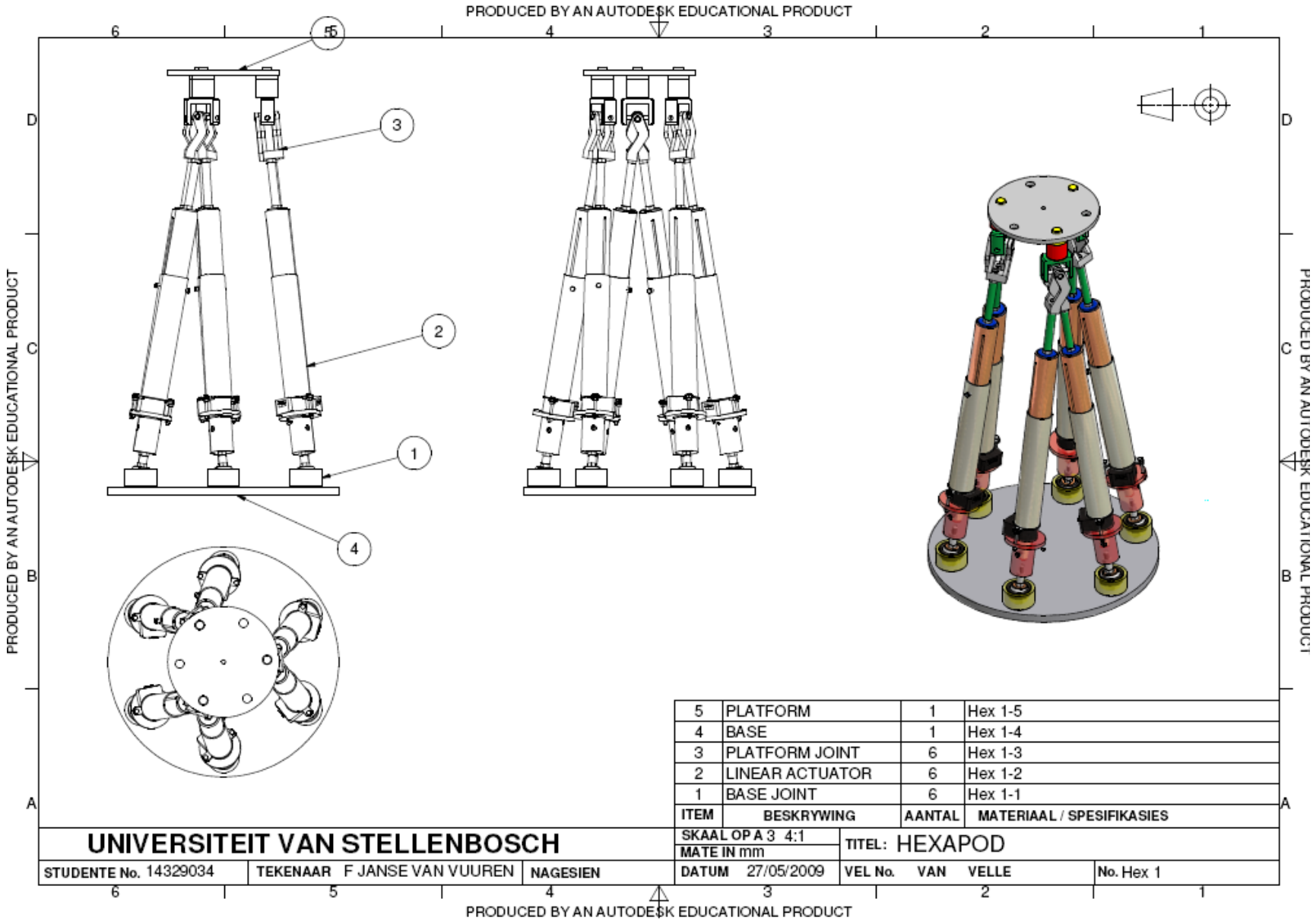
PRODUCED BY AN AUTODESK EDUCATIONAL PRODUCT
5
3
2
1
4
PRODUCED BY AN AUTODESK EDUCATIONAL PRODUCT
PRODUCED BY AN AUTODESK EDUCATIONAL PRODUCT
5 PLATFORM 1 Hex 1-5
4 BASE 1 Hex 1-4
3 PLATFORM JOINT 6 Hex 1-3
2 LINEAR ACTUATOR 6 Hex 1-2
1 BASE JOINT 6 Hex 1-1
ITEM BESKRYWING AANTAL MATERIAAL / SPESIFIKASIES
UNIVERSITEIT VAN STELLENBOSCH
SKAAL OP A 3 4:1
MATE IN mm
TITEL: HEXAPOD
STUDENTE No. 14329034
TEKENAAR F JANSE VAN VUUREN
NAGESIEN
DATUM 27/05/2009
VEL No. VAN VELLE
No. Hex 1
PRODUCED BY AN AUTODESK EDUCATIONAL PRODUCT

APPENDIX E: SYSTEM COMMANDS

The following are commands and the corresponding actions that the controller will perform. The commands must be sent to the controller via the serial port at a Baud Rate of 9600 bps.

Commands and Actions of Microcontroller

Command	Action
S	Stop and disable all leg motors
R	Reads and sends all leg lengths
L	Reads set lengths
C	Calibrate, resets encoders
A	Send all leg length data
Z	Send all leg lengths constantly
N	Send North South tilt sensor data
W	Send East West tilt sensor data
Y	Checks if previous leg lengths reached
E	Enable all leg motors
T=n	Test legs n = 1,2,3..6
U(n)=(direction)	Sets leg direction n = 1,2,3..6 direction = u or d

APPENDIX F: COST OF PROJECT

ITEM	DESCRIPTION	COST
Aluminium Round Bar	D30 x 1200 mm	R200
	D10 x 100 mm	R30
Aluminium Square Bar	20 x 20 x 300 mm	R30
PVC	D50 x 400 mm	R100
Phosphor bronze	D16 x 300 mm	R50
Stainless Steel Tubing	D32 x 1 m	R80
Encoders	6 HEDS 5645#C13-AVAGO	R4000
PCB Manufacturing		R400
Electronic Components	L298N x 3	R95
	Max 232	R4
	DsPic30F4011	R60
	Voltage Regulator	R7.55
	Heatsink	R7.54
	Connections (YYC09 series)	R8.00
	Headers	R6.00
Laser Cutting	Joint Sides	R50
	Tube Ears	R39.12
	Platform	R50
	Base	R80
Machining Costs		R12 000
Plain Spherical Bearings	6 x GE17ES DYZV	R150
Roller Ball Bearings	3 x SKF	R75
	Total	R17 522.21

Machining costs accounted for the majority of the project costs while the encoders were the next most expensive item.

For the full scale design to position the 3.4 m antennae at the PED the mechanical design can be scaled.

The electronics will not need to be scaled at all; however alternative H bridges might be required depending on the amount of current which the motors will draw.

APPENDIX G: WIND FORCE CALCULATIONS

Mesh dishes have [5]40% force of solid dishes.

The Comstar ST-12 can withstand wind of 110km/h. So the base should hopefully be able to do the same.

Pressure due to wind:

$$\begin{aligned} Pressure &= \frac{1}{2}\rho v^2 C_d \\ &= \frac{1}{2} \times 1.2 \times 30.55^2 \times 0.8 \\ &= 448\ Pa. \end{aligned} \quad \textbf{(0-81)}$$

Force on the antennae dish:

$$Force_{on\ dish} = Pressure \times Area \quad \textbf{(0-84)}$$

Drag Coefficient 0.8 for meshed dishes

$$\begin{aligned} Force_{on\ dish} &= 448\ Pa \times \frac{\pi}{4}(3.69\ m)^2 \\ Force_{on\ dish} &= 4\,792\ N \end{aligned} \quad \textbf{(0-85)}$$

Assuming the forces are equally distributed amongst the six legs:

$$\begin{aligned} Force_{per\_leg} &= \frac{Force_{on\ dish}}{6} \\ &= 798\ N. \end{aligned} \quad \textbf{(0-87)}$$

Force rating of each leg since each leg can lift 200 kg:

$$Force_{rating} = 200 \times 9.81 = 1962\ N. \quad \textbf{(0-88)}$$

$$Force_{rating} > Force_{per\_leg}. \quad \textbf{(0-89)}$$

Therefore the hexapod will be able to survive the windspeed of 110 km/h

[5] According to table on http://www.geo-orbit.org/sizepgs/grndpole.html

APPENDIX H: HEXAPOD MODEL ACCURACY TEST RESULTS

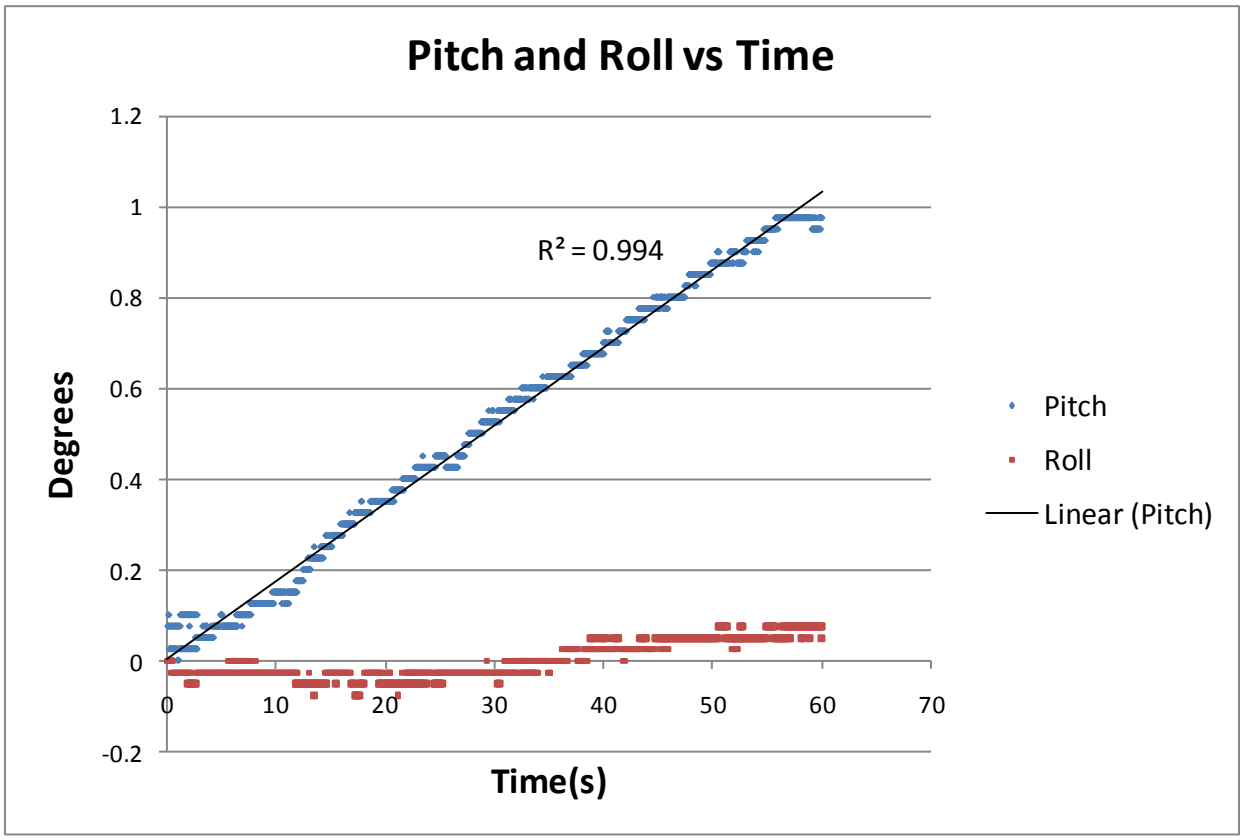

Algorithm 1: Azimuth 0° Elevation 90° to 89°

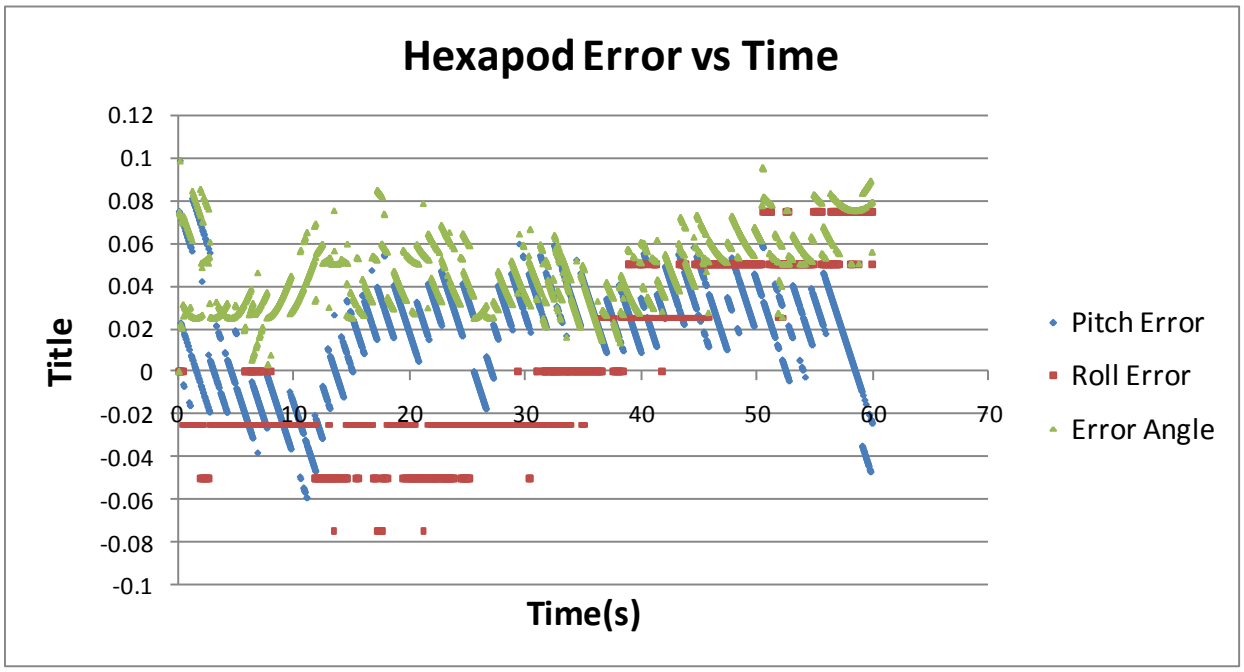

Algorithm 1: Errors Azimuth 0° Elevation 90° to 89°

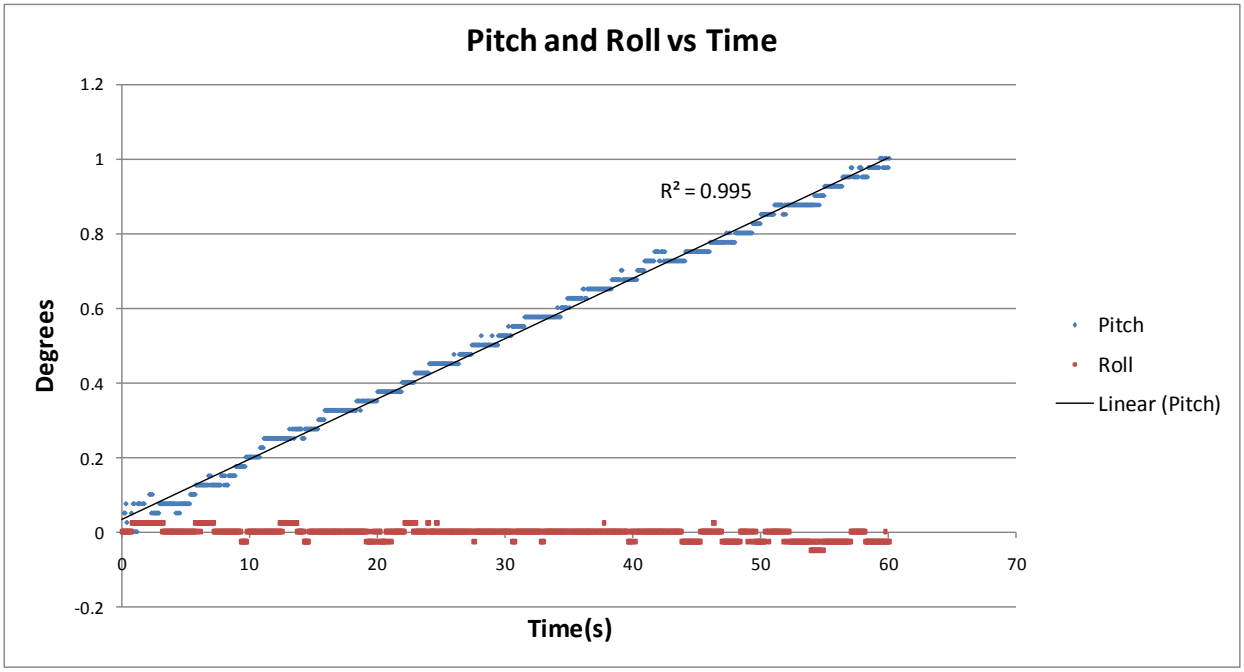

Algorithm 2: Azimuth 0° Elevation 90° to 89°

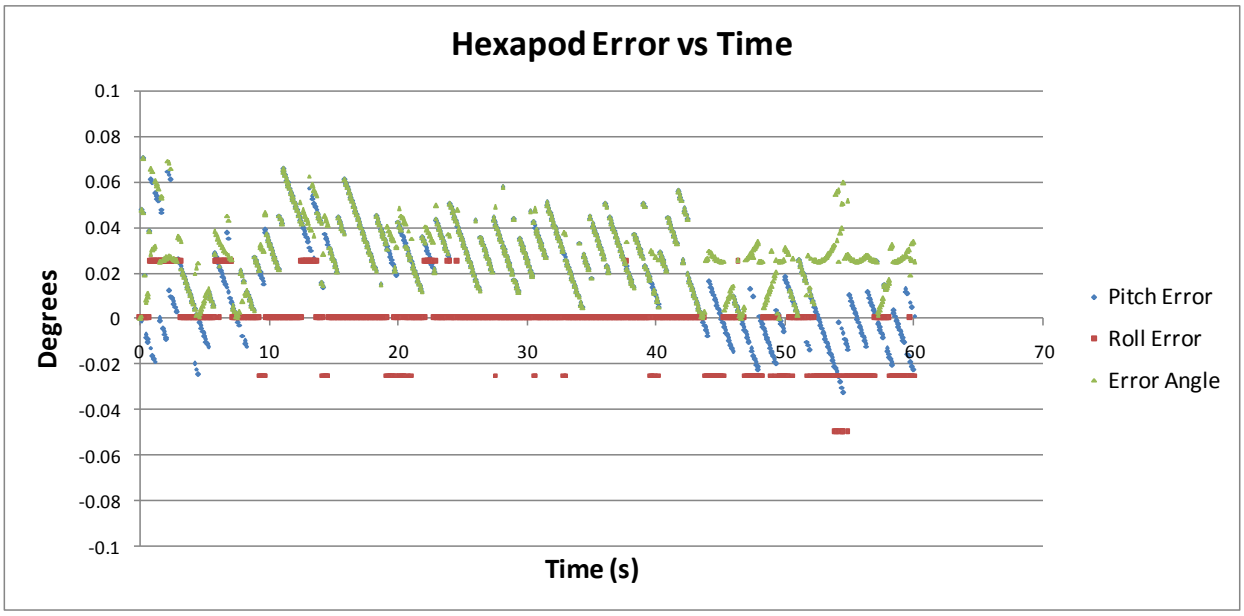

Algorithm 2: Errors Azimuth 0° Elevation 90°to 89°